NOAA ERLTM-OD 6

A UNITED STATES DEPARTMENT OF COMMERCE PUBLICATION

NOAA Technical Memorandum OD 6

U.S. DEPARTMENT OF COMMERCE
NATIONAL OCEANIC AND ATMOSPHERIC ADMINISTRATION
Research Laboratories

Development of a System for Remote Sensing of Ionospheric Motions and Microstructure:

The Kinesonde in France, 1970

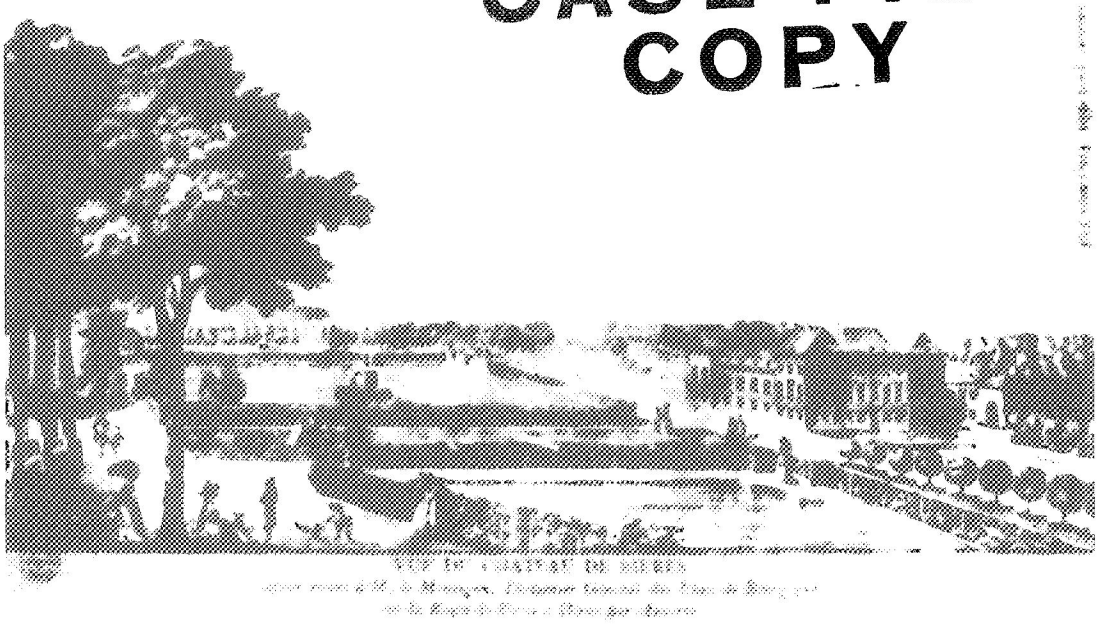

Office of the Director
BOULDER, COLORADO
January 1971

Report Through Nov. 1970
NASA Order No. W-13039
NATO GRANT NO. 413
NOAA Project No. 251405630

ENVIRONMENTAL RESEARCH LABORATORIES

OFFICE OF THE DIRECTOR

IMPORTANT NOTICE

Technical Memoranda are used to insure prompt dissemination of special studies which, though of interest to the scientific community, may not be ready for formal publication. Since these papers may later be published in a modified form to include more recent information or research results, abstracting, citing, or reproducing this paper in the open literature is not encouraged. Contact the author for additional information on the subject matter discussed in this Memorandum.

NATIONAL OCEANIC AND ATMOSPHERIC ADMINISTRATION

BOULDER, COLORADO

U.S. DEPARTMENT OF COMMERCE
National Oceanic and Atmospheric Administration
Environmental Research Laboratories

NOAA Technical Memorandum ERLTM-OD 6

DEVELOPMENT OF A SYSTEM FOR REMOTE SENSING OF IONOSPHERIC MOTIONS AND MICROSTRUCTURE: The Kinesonde in France, 1970

J. W. Wright
W. Plywaski
L. S. Fedor

Report of Activities Conducted
Jointly Under the Sponsorship of
National Aeronautics and Space Administration Order No. W-13039
North Atlantic Treaty Organization Research Grant No. 413
and Project No. 251405630 of the
National Oceanic and Atmospheric Administration
Environmental Research Laboratories
Boulder, Colorado 80302

Office of the Director
Boulder, Colorado
January 1971

Contents

		Page
List of Illustrations		iv
Abstract		vii
Part 1.	The Kinesonde in France, 1970	1
	Motivation, Objectives, Planning and Preparation	1-9
	The Kinesonde and Examples of Data	9-16
	Meteor Radar Comparisons	17-22
	Thomson Scatter Comparisons	23-30
	Other Experiments	31-32
	Early Results	33-38
Acknowledgments		39
References		41-43
Appendix I.	Kinesonde Technical Description	45
	Description of Principal Functions	45-49
	Technical Details of Principal Sub-units	51-63
Appendix II.	Antenna System	65
Appendix III.	Data Processing	75
Appendix IV.	Considerations Regarding Applicable Theory	95
Appendix V.	List of European Workers in D- and E-Region Winds	103

List of Illustrations and Tables

Chateau Bierre-lés-Semur about 1750 ..... front cover
Outline map of France showing principal experimental sites .. back cover

Figure		Page
1	Kinesonde Tractor, diesel generator and Laboratory Trailer	5
2	Kinesonde Trailer interior	6
3	Sample ionogram from Kinesonde	8
4	Model of vertex down log periodic antenna	10
5	Vertex-down log periodic antenna.	11
6	Kinesonde functional diagram	12
	Kinesonde commutation diagram	13
7	Examples of Kinesonde amplitude and phase 'raw data' plotted on microfilm by computer	14
8	Schematic diagram of the Meteor Radar-Kinesonde deployment	15
9	Scaled ground plan of Kinesonde installation at chateau Bierre-lés-Semur	16
10	View of chateau Bierre-lés-Semur site	18
11	Detail of North receiving antenna construction	20
(Table 1)	Coordinates of chateau Bierre antennas	21
12	Graphic timetable of Kinesonde recordings	22
13	Schematic diagram of CNET Thomson scatter sounder	24
14	View of Kinesonde installation at St. Santin	25
15	Surveyed layout of Kinesonde installation at St. Santin de Maurs (Cantal)	26
(Table 2)	Coordinates of St. Santin antennas	27
(Table 3)	Dates of Kinesonde campaigns at St. Santin	28
(Table 4)	Types of Thomson scatter observation programs	29
16	Kinesonde results, 30 January 1970	34
17	Height profiles, U_E, compared with Kinesonde V_E/Z	36
18	Height profiles, U_E, compared with Kinesonde V_E/Z	38
(Table I-1)	Kinesonde Frequency Synthesis	46
I-1	Variable Frequency Synthesizer	50
I-2	Original Steering Oscillator	52
I-3	New Steering Oscillator	53
(Table I-2)	Kinesonde RF and IF Frequencies	56
I-4	Receiver Dynamic Response	57
I-5	Receiver Transient Response	58
(Table I-3)	Receiver Amplitude Calibration	59
I-6	Phase Digitization	60
I-7	Amplitude Digitization	61
I-8	Transmitter Pulse Amplifier	63

Figure		Page
II-1	Power Gain Comparison, VULPA-VDLPA	67
II-2	E-Plane Power Gain Patterns	68
II-3	H-Plane Power Gain Patterns	69
II-4	Receiving Antenna Detail	70
II-5	Receiving Antenna Isolation	72
II-6	Antenna Commutation Isolation	73
III-1	Kinesonde Data Editing Notes	76
III-2	Digital Amplitude, Phase Graphs	77
	Antenna Array "Box"	79
III-3	Complex Amplitude Spectra	81
III-4	Complex Cross Correlations	82
III-5	Correloid Crossections	83
III-6	Correloid Analysis Tabulation	86
III-7	Key to Fig. III-6	87
III-8	The Spatial Correloid	90
III-9	Filter Response Curves	91
III-10	Results of Fading Simulation Tests	93
	Scattered Power Dependence on Angle of Incidence	98
	Histogram of Correloid Mean Square Residuals	100

ABSTRACT

For more than two decades, observations of ionospheric radar echoes at closely-spaced antennas have provided quantitative measures of motions in the upper atmosphere. Perhaps unintentionally, the theoretical structure justifying this technique was developed backward, starting with a powerful correlation description of the random echo amplitude (and phase) variations observable at the ground, from which, by a series of definitions, mean and random velocities and anisometric structure parameters are obtained. The random structure of the pattern was rigorously related to that near the ionosphere by the theory of diffraction, but the next links in this chain are less definite. The radio scattering process, which occurs in a plasma resonance condition, yet has no satisfactory description. Of more popular current significance is the question of wave-or-turbulence identification of the ionospheric irregularities themselves, and of the relationship of their motion to that of the neutral and ionized media in which they occur.

The initiative for progress in this field has devolved upon experiment, and new light should be shed on the questions by direct comparisons of spaced antenna measurements against some techniques free of these particular interpretive problems.

The program of investigations reported here includes activity on three major components of the experimental problem: (a) development of what we judge to be a suitably competent measurement system, the digitized multifrequency complex-amplitude Kinesonde; (b) refinement of a statistically-rigorous procedure for correlation analysis of spaced-sensor measurements; and (c) completion of several series of simulated and actual experiments. In particular we report on an experimental program conducted during the past year to compare E-region Kinesonde measurements with time-dependent neutral wind profiles obtained by the meteor wind technique and again, over a broader range of altitudes extending into the F region, to compare the Kinesonde results against Thomson scatter measurements of meridional ion drift. These two experimental efforts were conducted during 1970 in cooperation with the Centre National D'Etudes Des Telecommunications near their Meteor Radar and Thomson Scatter sites of Sens Beaujeau and St. Santin, France, respectively. A few early comparisons with meteor winds suggest that the Kinesonde technique, applied within the daytime E-region, observes the neutral wind profile directly; the standard 'point source' correction appears valid.

Development of a System for Remote Sensing of Ionospheric Motions and Microstructure: The Kinesonde in France, 1970

J. W. Wright, W. Plywaski and L. S. Fedor
National Oceanic and Atmospheric Administration
Boulder, Colorado

Motivation and Objectives

Our present problem concerns the verification of a ground-based radio method for measuring turbulence and motions in the high atmosphere, between about 60 and 300 km altitude. The basic technique is widely known among ionospheric radio physicists and has been applied in a simple form for over 20 years; it involves comparisons of the randomly-varying amplitudes of ionospherically-reflected radio pulses, among closely-spaced receiving antennas. By choosing the radio frequency appropriately, the height range mentioned above may be examined. Over the past years only a very few comparisons have been made of this technique with other sources of upper atmospheric wind data, and, unfortunately, limitations of data handling have forced most experimenters to use relatively primitive versions of the radio spaced antenna experiment.

About two years ago we began observations with a much elaborated version of this experiment, which we now call the "Kinesonde". This instrument is fully digitized, observes at six freely-chosen frequencies (hence altitudes) simultaneously, measures vertical as well as horizontal motions, is mobile for field use, and is supported by new and improved methods of data analysis.

The large number of upper atmosphere workers who are familiar with this technique are in common agreement that, despite its economy, long history, versatility, and other advantages, too many uncertainties

of interpretation exist to permit considering its wider use until they are resolved (Hines, 1964). The existence of such uncertainties is not surprising in itself, because neither the nature of the ionospheric irregularities (which serve as tracers of the atmospheric motions), nor many aspects of the radio scattering and diffraction processes (by which the moving pattern is produced at the ground), are well understood. In recent years a number of international bodies have recognized the need for an objective comparison of this technique with other sources of atmospheric wind data and have recommended that such experiments be performed. We have undertaken comparisons with certain rocket experiments with encouraging results but these opportunities are too intermittent and too limited in altitude to settle the matter decisively (Wright, 1968).

Decisive tests of the various interpretations which may be made of Kinesonde measurements require comparisons with techniques which are not only more direct, but which offer height and time continuity, and resolution, comparable to the Kinesonde. The meteor radar technique is recognized as satisfying each of these criteria for direct measurements of the neutral winds in the 80 - 120 km region, while the Thomson scatter method has recently been used successfully to measure ion drifts between 120 - 400 km. In each of these techniques the most advanced work is being done at two experimental sites (see map, rear cover) in France by investigators associated with the Groupe de Recherches Ionosphériques (Spizzichino, et al. 1965; Spizzichino, 1967; Vasseur, 1969. For an independent assessment see Lindzen, 1969). A comparison of the French Meteor Radar Winds and of their Thomson Scatter ion drifts, with Kinesonde measurements at the two French experimental sites, was our specific experimental objective of the past year reported here.

Comparative measurements by the Kinesonde are attractive from the standpoint of the French experiments as well. Although developments are underway in the Meteor and Thomson Scatter programs to

prepare additional sites from which the total wind (or drift) vector can be measured, at present these experiments are limited to observing motions in one vertical plane only. Thus, series' of colocated Kinesonde measurements in three spatial dimensions could supply valuable additional data to the studies now underway in the French programs, as well as information useful in planning the expansion of each facility. Of course it is recognized that the utility of these results to the French programs strongly depends upon establishing first the interpretation of the Kinesonde measurements.

Origin and Support of the Experiment

At the 1967 Assembly of the International Union of Geodesy and Geophysics in St. Gallen, Switzerland, a Symposium was held on the topic "Upper Atmospheric Winds, Waves, and Ionospheric Drifts". The International Scientific Radio Union (URSI) took advantage of the wide representation of workers in this field attending the Symposium, to organize a working party on Ionospheric Drift Analysis. This was the first organized attempt in recent years to confront old versions of the technique with new and to review possibilities of interpretation in the light of more direct observations of winds and waves at high altitudes. The principal collaborators in the present experiment agreed at the meeting that the intercomparison of techniques urged at the symposium, and later by the working party, was a timely and worthwhile objective for their respective experimental systems. The only practical alternative involved transporting the Kinesonde to the experimental site of the French Meteor Radar and again to the French Thomson Scatter facility; the initiative was therefore ours to obtain the necessary program support and endorsements.

The National Aeronautics and Space Administration, since 1965, has supported our development of the Kinesonde and its associated data processing methods. The present experiment was set as a prime goal for the continuation of that program during the past year.

The North Atlantic Treaty Organization's Scientific Affairs Division provided a Research Grant specifically to support the international collaborative aspects of the experiment, following endorsement of our objectives by Prof. C. O. Hines (University of Toronto) and Prof. B. R. Briggs (University of Adelaide).

The U. S. Army Ballistic Research Laboratories, which has engaged the Kinesonde in support of chemiluminescent trail and Cesium ion cloud releases at high altitudes from gun-launched vehicles, arranged military sea transport for the experimental equipment.

The U. S. Department of Commerce provided the vehicles, diesel generator and secondary experimental equipment, and supported the two American collaborators.

Other European Cooperation

Other programs for the measurement of atmospheric motions have been underway in Europe for many years, with organized coordination since a Regional Meeting on Ionospheric Research at Lindau (Harz), June 1969. A preliminary list of participants is reprinted as Appendix V. We consider it an additional benefit of the timing chosen for our experiment that it could thus participate in a well-coordinated program of wind and drift measurements over the entire European continent. It is explicit in our plans for analyzing our results, that they be shared with the other participants of the program.

Planning and Preparation

The period 1967 - 1969 was one of 'shakedown' and continuing development of the Kinesonde; several tasks important to our objectives are detailed in the Appendices I - III of this report. An early but limited series of observations with the system (Wright and Fedor, 1969) demonstrated the compatability of Fedor's (1967) 'statistically-rigorous' correlation analysis with Kinesonde measurements, providing evidence that meaningful height profiles of ionospheric movements, in 3 dimensions, could be obtained.

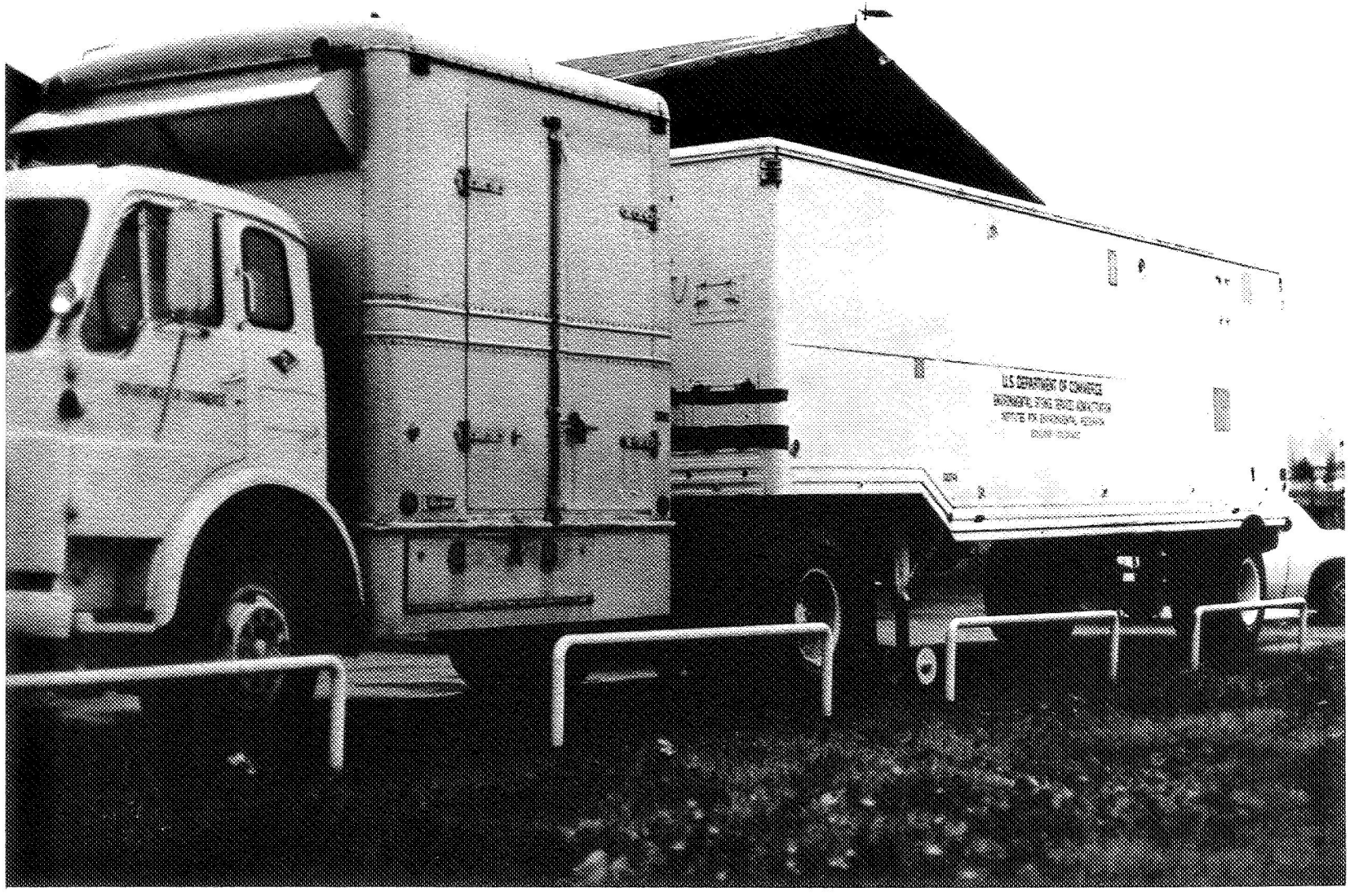

Fig. 1. Kinesonde Tractor, Diesel Generator, and Laboratory Trailer. Diesel generator develops 32.8 KVA 3 φ 220 V, with changeover for external power if available. Tractor and trailer contain all materials, including antennas and 45_m sectional tower.

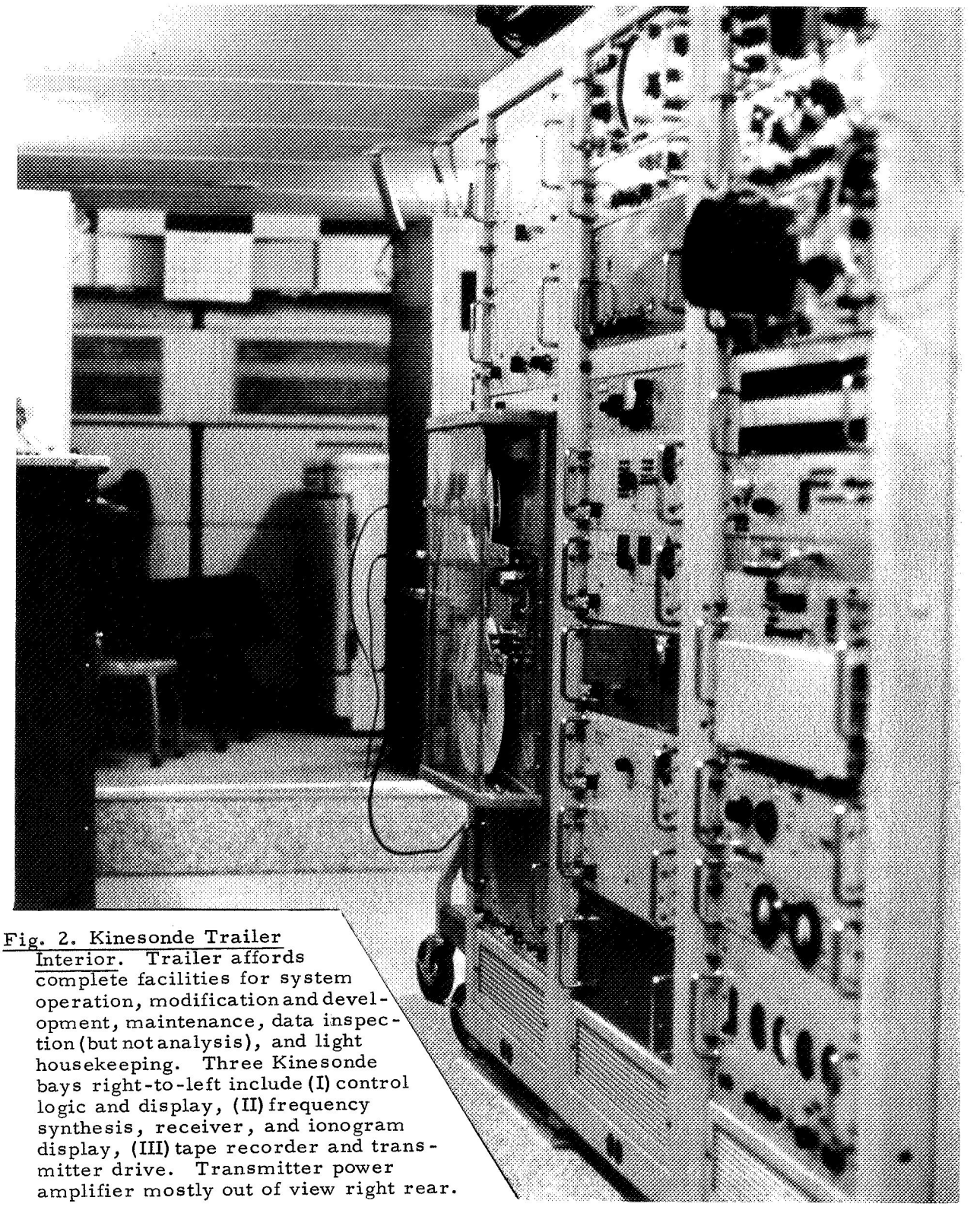

Fig. 2. Kinesonde Trailer Interior. Trailer affords complete facilities for system operation, modification and development, maintenance, data inspection (but not analysis), and light housekeeping. Three Kinesonde bays right-to-left include (I) control logic and display, (II) frequency synthesis, receiver, and ionogram display, (III) tape recorder and transmitter drive. Transmitter power amplifier mostly out of view right rear.

Our determination to optimize the possibilities for comparing the Kinesonde measurements with the French Meteor Radar and Thomson Scatter results implied, of course, that the Kinesonde be located to observe the same ionospheric region in each case; in particular, the meteor system employs inclined beams, so that no existing field site would be available in the desired region. Furthermore, uncertainties of electrical power compatability and stability required that the Kinesonde travel as an independent, self-sufficient system. Our laboratory made available a climatized laboratory trailer, tractor, and 32 Kw diesel generator (figs. 1, 2). In 1968/1969 the Kinesonde, tractor, and generator were used in support of rocket and gun-launched experiments at Wallops Island and Eglin AFB, giving some confidence in the dependability of the system. During these exercises, initial developments were undertaken to obtain an ionosonde capability within the Kinesonde, since this provides, via simple film recordings, data from which the ionospheric electron density distribution is obtained. This, in turn, is necessary to determine the effective altitudes and height intervals of the Kinesonde measurements. An example of an analog virtual height v. frequency recording (ionogram) obtained by the Kinesonde is shown in fig. 3. While recordings of this quality were not achieved until the second half of the experiment in France, the E-region observations of the first half can be fully analyzed with controlled model profiles of the E-region.

By far the greatest problem in field deployment of the Kinesonde, as with any HF sounding device, is the antenna system. The receiving antennas (described in Appendix II) are simple spaced probes, and except for the large quantities of transmission line and terrain required, they give only minor difficulties. The transmitting antenna, on the other hand, is always a compromise among conflicting requirements of size, ease of construction, economy, efficiency, performance 'flatness', and low-frequency cutoff. In preparation for this program, we undertook the design of a vertex-down, single-plane log-periodic dipole antenna; theoretical calculations (by our colleague Dr. M. T. Ma)

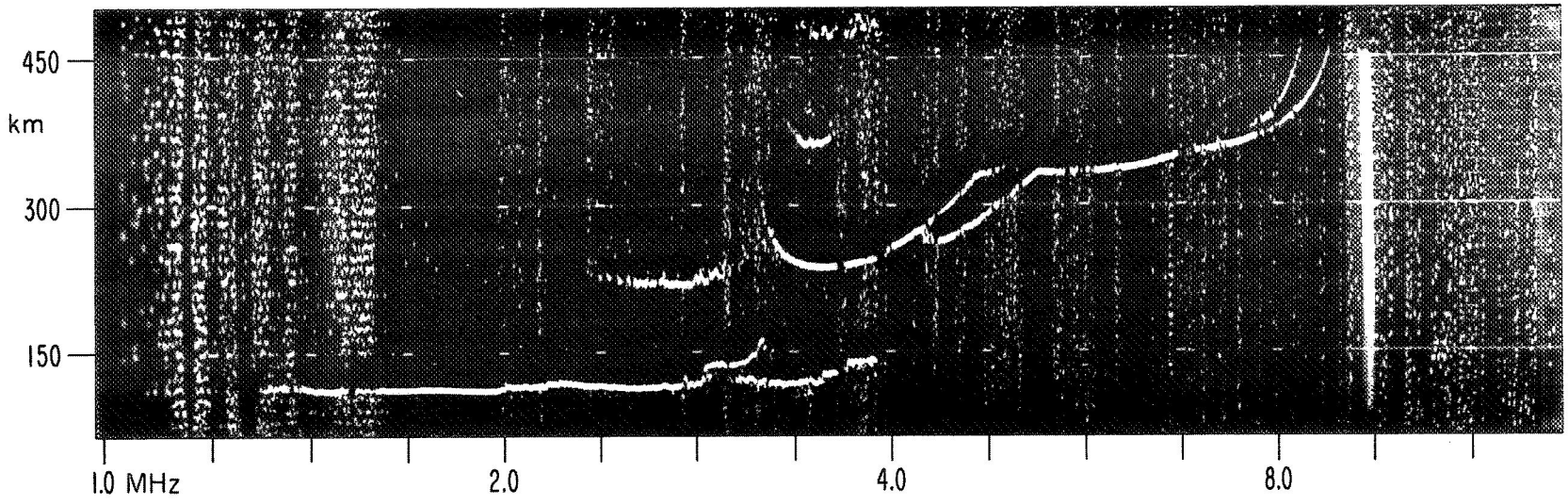

Fig. 3. Sample Ionogram from Kinesonde. Analog film recording, in which Kinesonde steps, in Ionosonde mode, from 1 - 16 MHz in 4 bands, 400 steps/band, 2 pulses/step (horizontal scale). Vertical scale registers echo arrival time and hence apparent (virtual) height. Because the group (radio pulse) velocity is reduced in the ionosphere, ultimately to zero at two critical electron densities dependent on the radio frequency and geomagnetic field, the virtual height always exceeds the true height. The echoes from the frequency series therefore trace out two curves on the ionogram which are related to the vertical structure of the underside of the ionosphere. More closely, the curves resemble a graph of dh/dN, the slope (or inverse height gradient) of the electron density profile, and they therefore sensitively indicate details of the vertical structure. In this example, the lowest echoes are reflected from an electron density of about $10^4/cm^3$ at 95 km, while the highest penetrate the F-region peak density of about $10^6/cm^3$ near 280 km. The complete profile can be recovered by computation. At the Kinesonde, a storage-oscilloscope display of the ionogram guides selection of 6 frequencies freely chosen in the 1-16 MHz range for digital recordings of echo amplitude and phase at spaced antennas.

and model measurements (with P. Arnold) proved to agree favorably with measurements made later on the full-scale antenna (Appendix II). A photograph of the model appears in fig. 4. The design was based upon use of a central antenna tower of 45-meter height. With the assurance that experienced workers could be engaged for its erection in France, we obtained an inexpensive tower which was transported in 15 3-meter sections, inside the laboratory trailer. The antenna was about two-thirds prefabricated in Boulder, and only a final assembly was required during its initial erection (fig. 5).

The Kinesonde (Technical Description, Appendix I; Functional Diagram, Fig. 6)

The Kinesonde has been designed to provide most of the capabilities we believe essential to the spaced antenna experiment. It is curious that many of these features appear combined in this instrument for the first time, considering that the experimental concepts are by no means new, and that they are clearly required by even the 'classical' theoretical description of the experiment. Of these, perhaps the most obvious, most important, and until recently most difficult requirement is for digitized recording of the measurements, for without this capability it is impractical to satisfy the inherently statistically overdetermination of the wanted parameters. Theory likewise demands measurement of the complex amplitude (amplitude and phase) of the received echo. The remaining significant capabilities of the Kinesonde are related to its multifrequency design: it affords the frequency range sufficient to perform measurements throughout the bottomside ionosphere, and provides sufficiently fine-frequency resolution to permit tests of the idea that vertical motions can be extracted from comparisons of echoes at closely-spaced frequencies.

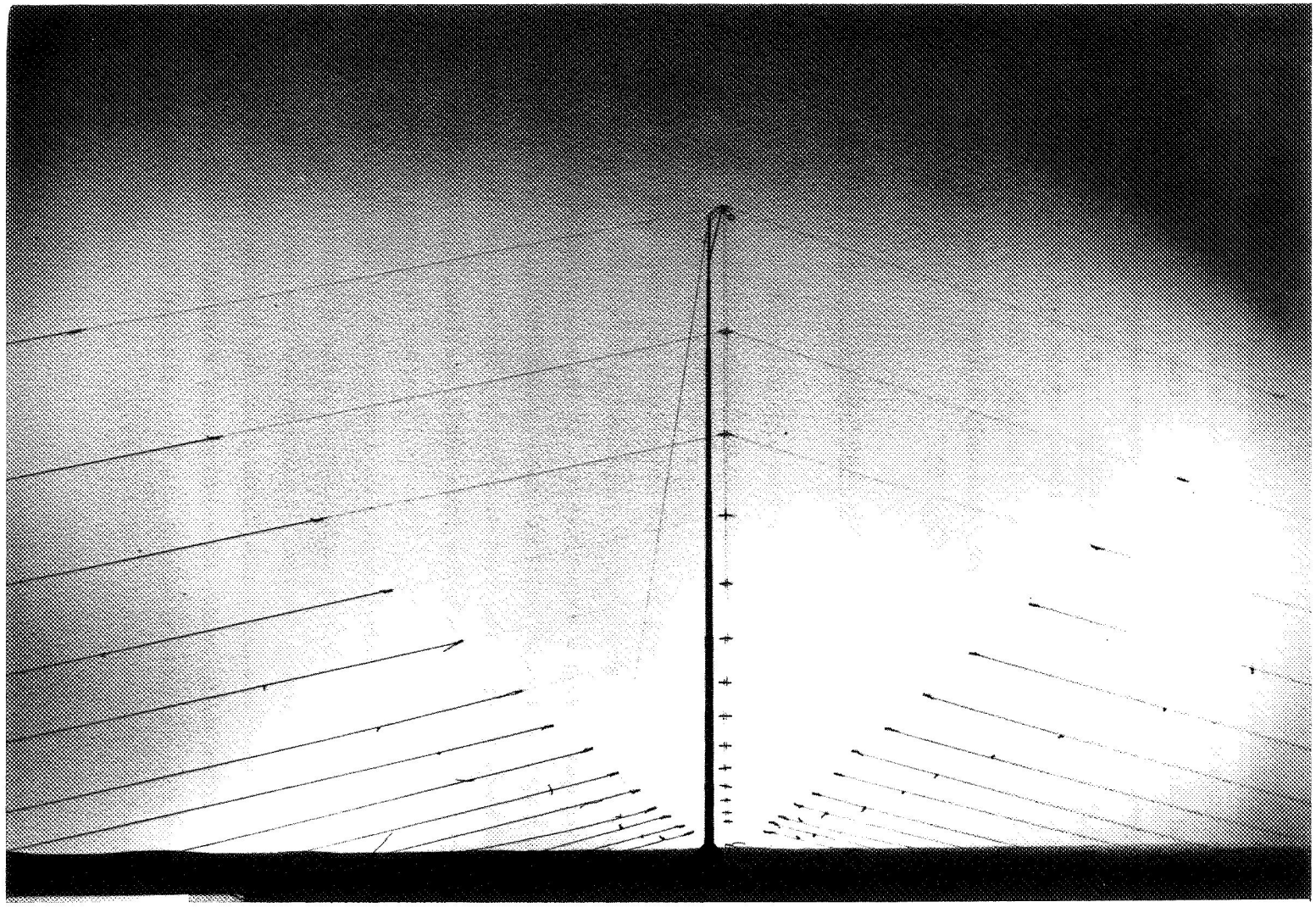

Fig. 4. Model of Vertex Down Log Periodic Antenna. Transmitting antenna (see Appendix II). Radiating elements are alternately connected to opposite sides of balanced transmission line which extends vertically from feed-point at bottom. Radiating elements extend (at 30° droop below horizontal) to linearly decreasing distances, and at logarithmic spacings.

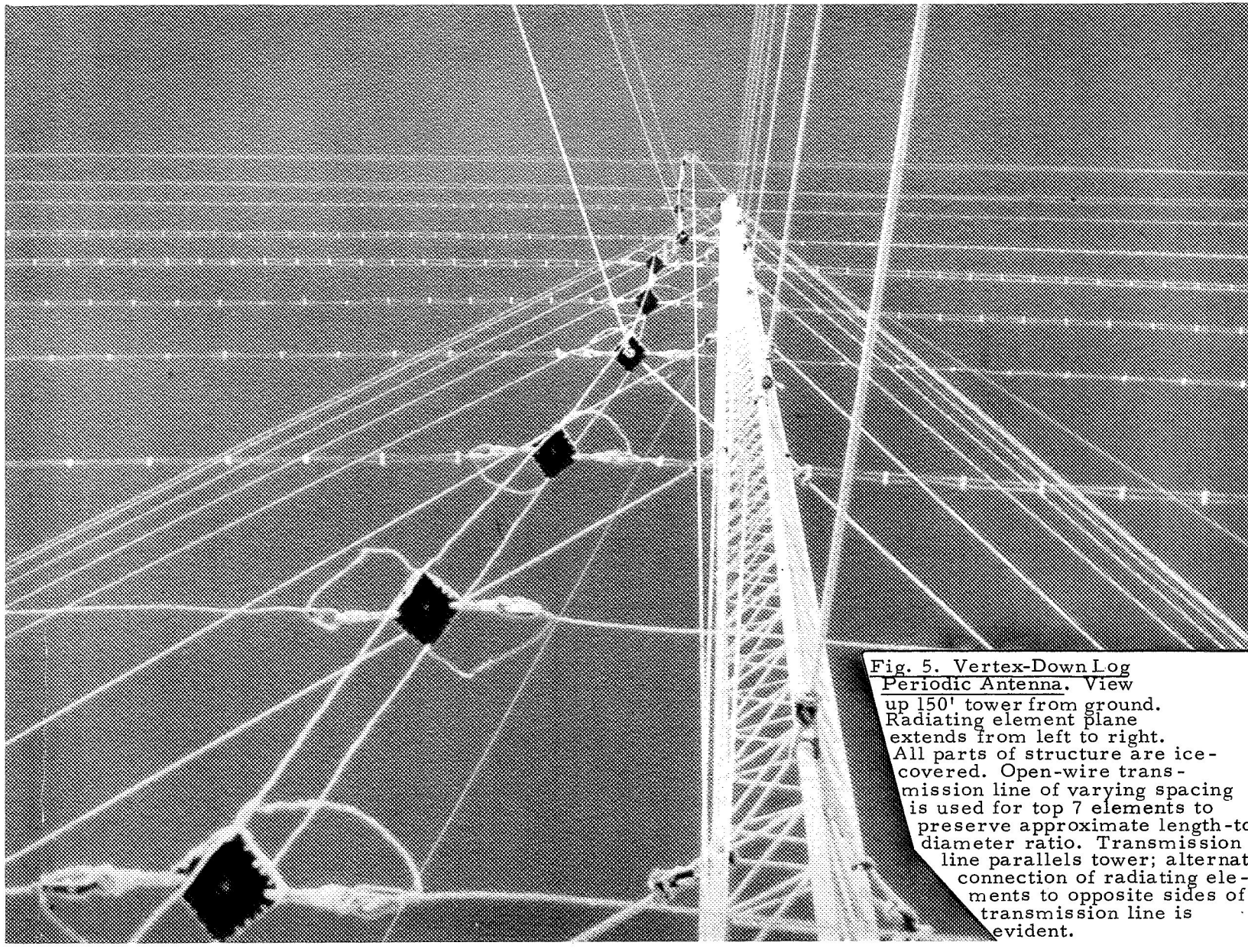

Fig. 5. Vertex-Down Log Periodic Antenna. View up 150' tower from ground. Radiating element plane extends from left to right. All parts of structure are ice-covered. Open-wire transmission line of varying spacing is used for top 7 elements to preserve approximate length-to-diameter ratio. Transmission line parallels tower; alternate connection of radiating elements to opposite sides of transmission line is evident.

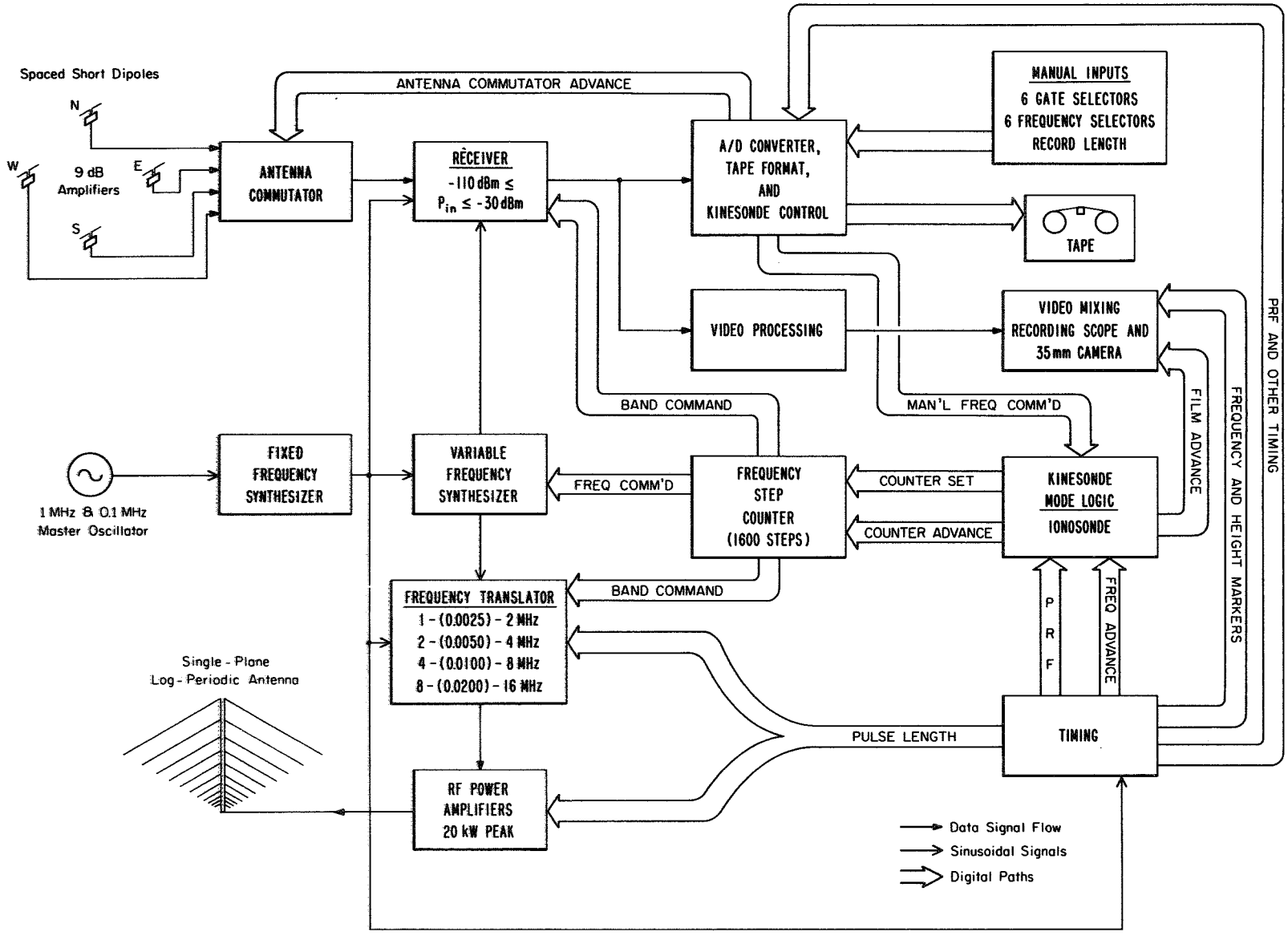

Fig. 6. Kinesonde Functional Diagram. Detailed description in Appendix I.

Kinesonde Data: (See Technical Details, Appendix III)

The Kinesonde records in two modes. Analog film recordings (fig. 3) scan the total frequency range available (1 - 16 MHz) and provide ionograms describing the structure of the ionosphere during experimental sequences. We have developed special methods of analysis (Paul, 1967; Howe and McKinnis, 1967; Wright, 1967) to extract detailed height profiles of electron density from ionograms, and this capability is fully used in analyzing the Kinesonde's second (and principal) mode of recording.

In this second mode, computer-compatible digital tape recordings of the time variation of the amplitude and phase of selected ionospheric echoes are made at six chosen frequencies and at 4 spaced antennas. Measurements are made on these 24 channels at an overall commutation rate of 100/second, or about 4/second on each channel, as shown in the diagram below.

COMMUTATION PATTERN; 100 pulses/sec

Pulse, Cycle No	1	2	3	4	5	6	7	Cycle One	14	15	16	17	18	19	20	21	22	23	24	25	26	Cycle Two		
Antenna	North							East						South						West						North					
Frequency	1	2	3	4	5	6	1	2	3	4	5	6	1	2	3	4	5	6	1	2	3	4	5	6	1	2	3	4	5			

Kinesonde Channel Commutation Diagram

When decommutated and plotted by a computer, single channels of the data typically resemble the examples of figure 7.

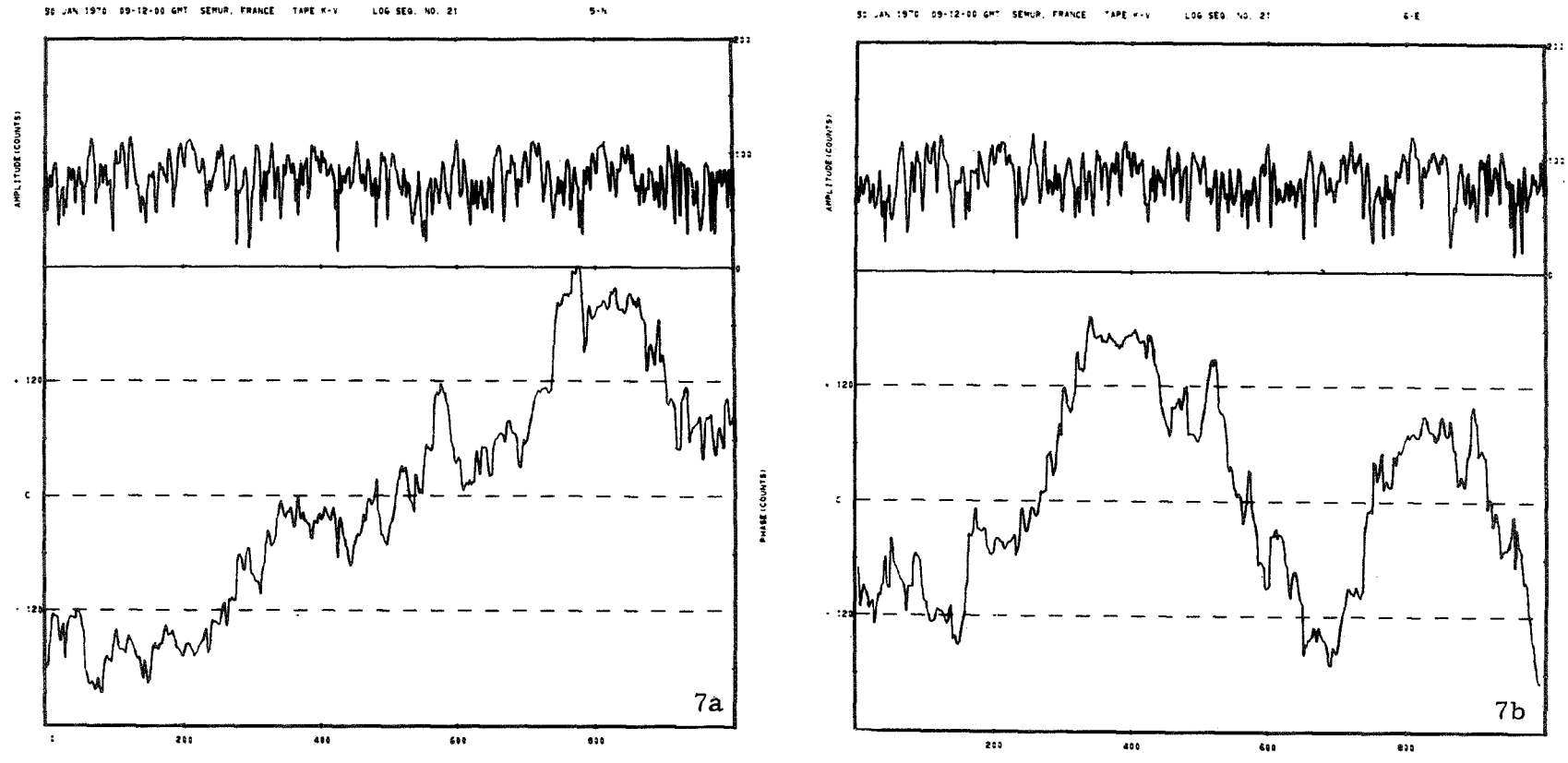

Fig. 7. Examples of Kinesonde Amplitude and Phase 'Raw Data' Plotted on Microfilm by Computer. Amplitude (upper part of each frame) and phase (lower part) comprising the time variation of complex amplitude of selected ionospheric echoes over 4-minute periods (horizontal scale). Measurements of complex amplitude in each channel are made each 24/100 seconds; of the 1000 recorded values in each channel, only alternate points are plotted here for clarity. Amplitude vertical scale 0-200 counts corresponds to about 70 db dynamic range. Phase resolution is always 80 counts/rotation, but phase scale range is adjusted in plotting to accommodate the full phase excursion sensed by computer from sign of successive phase differences. The two channels plotted here are observed at spaced frequencies and spaced antennas: 2.4025 MHz, North antenna (left) and 2.4075 MHz, East antenna (right). 24 independent amplitude - phase channels are contained in each digital tape record.

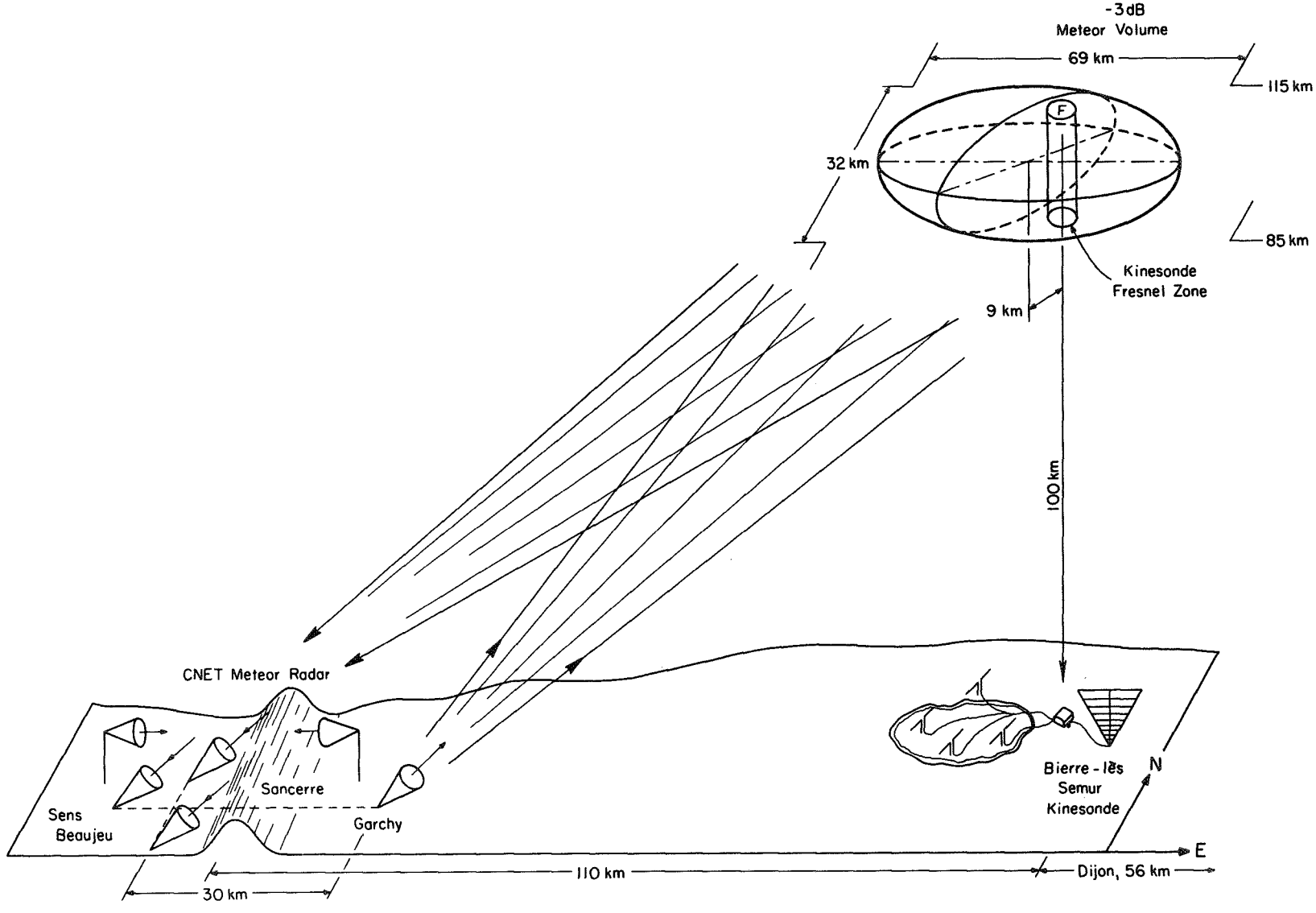

Fig. 8. Schematic diagram of the Meteor Radar-Kinesonde Deployment. Inclined beams of the 50 MHz CW Meteor Radar of the Centre National D'Etudes Des Telecommunications at its Garchy and Sens Beaujeu stations observe meteors within the volume located about 110 km to the east. The Kinesonde was located about 9 km North of the center of the 69 (EW) x 32 (NS) ellipse. For the frequencies used typically by the Kinesonde (1.6 - 5 MHz) for E-region observations, the radii of the first Fresnel zone vary from 4.8 to 2.8 km.

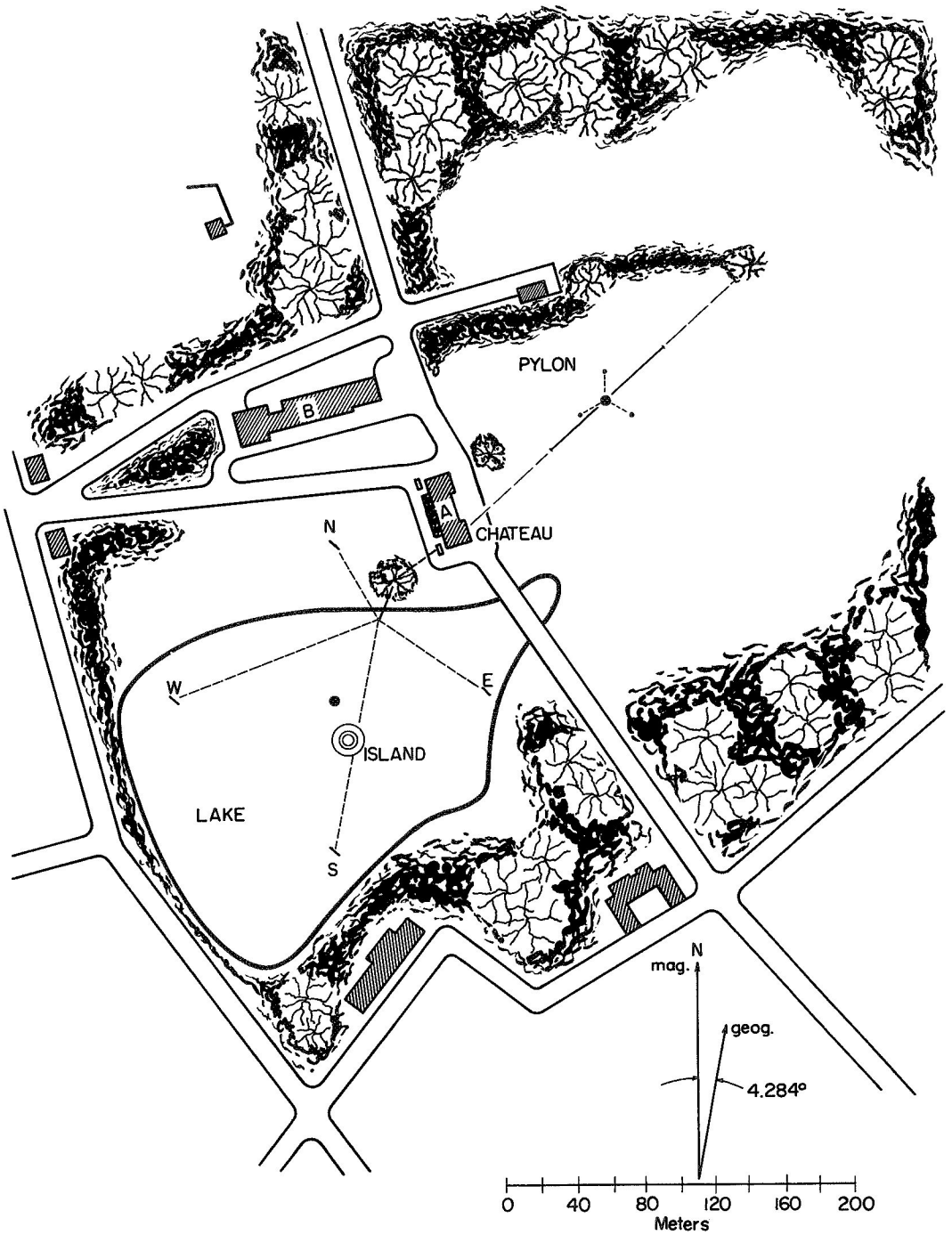

Fig. 9. Scaled ground plan of Kinesonde installation at chateau Bierre-lés-Semur. Variations of elevation less than 2 meters over entire plan. The log-periodic transmitting antenna was suspended on the 45^{m} pylon, and stretched between the chateau and a large spruce tree. The receiving array, except for the North antenna, was placed near the surface of the lake.

The Kinesonde in France: Meteor Radar Comparisons

Site Selection and Installation: The Meteor Radar of the Centre National D'Etudes des Telecommunications employs beams inclined about 45° toward the east (fig. 8), and their pattern, together with the statistics of meteor occurrence define the "3 db" volume within which most of the observed meteors occur. This region is centered about 110 km east of Sancerre and about 56 km west of Dijon; the horizontal projection of the region is about 69 km (EW) by 32 km (NS). We sought a field site anywhere within the 3 db area, and finally selected, in the center of its northern half, the park of a chateau* in the village of Bierre-lés-Semur, used in the summer as a children's vacation colony by the Archdiocese of Dijon. The site (fig. 9) proved ideal for our purposes: The enclosed, nearly flat area 300 x 600 meters included a small lake which we selected for the antenna array when it conveniently froze over during our initial surveys of the site. The flat surface of the lake aided an accurate layout of the receiving antenna array (fig. 10) and perhaps contributed slightly to its performance.

The North antenna of the 130-meter square array was located on land at the front of the chateau, and provided easy access for special experiments undertaken on antenna performance and inter-antenna coupling. A detail of the North antenna is shown in fig. 11. The RF transmission lines were four equal 204.8 meter lengths of RG9/U(50 Ω) cable. Despite varying distances to the Kinesonde, we have learned that equal cable lengths simplify phase and amplitude calibrations of the system. Variable lengths of RG 58/U cable are used to supply 20 VDC to broadband RF preamplifiers at each antenna. Table 1 (page 10) gives the measured locations of antenna locations, etc. at Bierre-lés-Semur.

---

* The chateau, originally about twice its present size (front cover) was constructed in 1749 by the Marquis de Montigny, Treasurer for the Ducs de Bourgorgne.

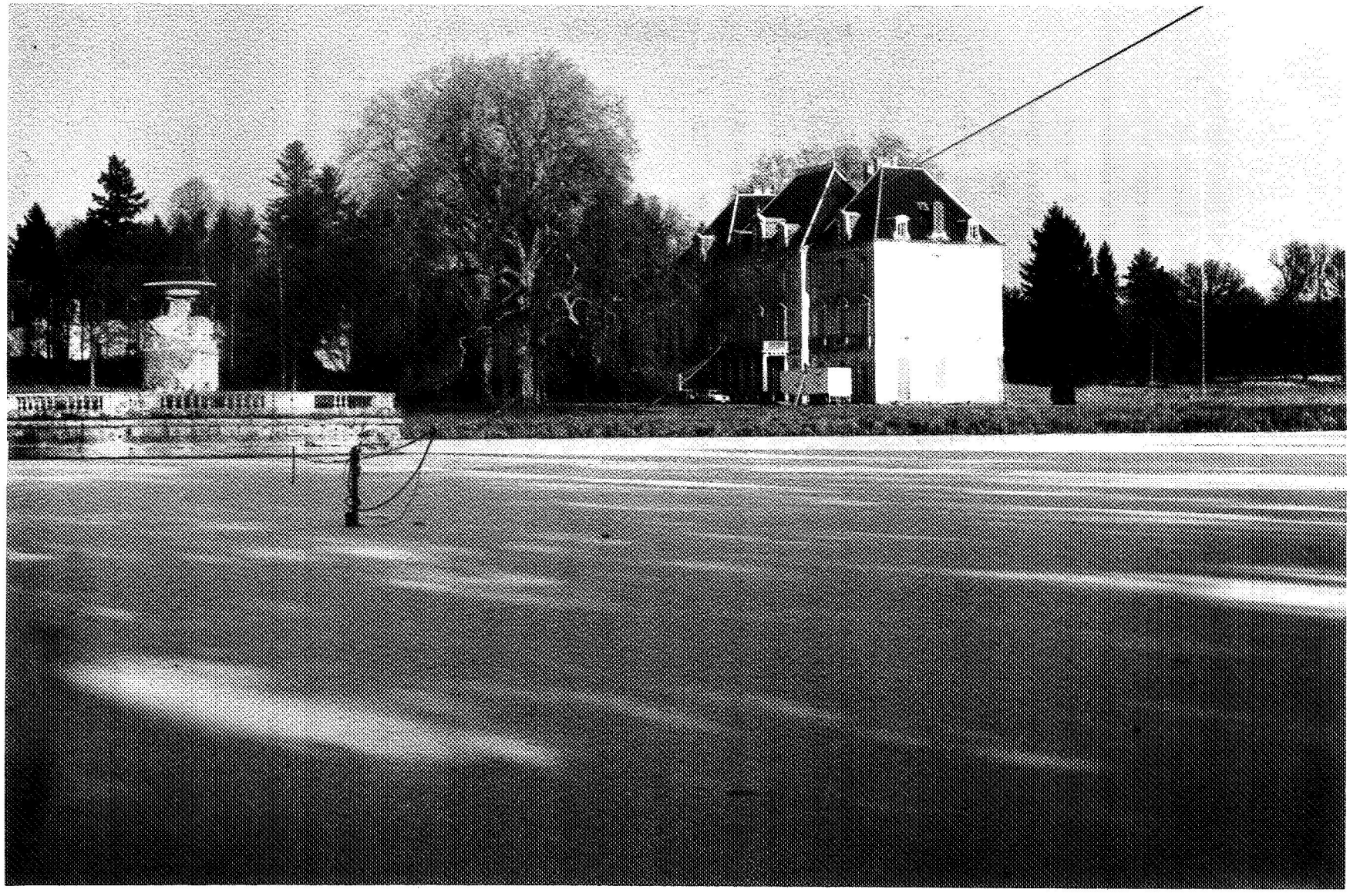

Fig. 10. View of Chateau Bierre-les-Semur Site. View from lake, with south receiving dipole antenna suspended over ice, left foreground. Laboratory trailer stationed near chateau. 150' antenna tower with Vertex-down Log Periodic Antenna behind chateau to right. Electric power to chateau supplied underground, fortunately eliminating parasitic structures.

The tractor and trailer were stationed at the front of the chateau where we could take advantage of the 3 - phase 220/117 V. electrical system of the chateau; switches at the diesel generator permitted the chateau power to be used for all purposes (heat, light, troubleshooting) except during actual data collection.

Bids for erection of the transmitting antenna tower were requested of two firms in Paris and two others in Dijon. The latter two were the highest and lowest, respectively (at $250 and $2,000, respectively), with the Paris bids falling neatly into binary positions of $500 and $1,000. In the end, the lowest bidder actually billed us at about half his estimate, since we were able to help him complete the work in less than one day.

The transmitting antenna itself was suspended between the chateau, the 45^{m} tower, and a large (28^{m}) spruce tree, thus reducing the need for excessively long ropes from the ends of the higher (longer) antenna elements to the ground. The completed structure (fig. 5) proved very satisfactory, particularly considering the deliberately long (130 ^{m}) transmission line which was intended to minimize the parasitic coupling among the receiving antennas via the transmitting antenna.

Unfortunately, a severe windstorm brought down our 45^{m} tower in mid-February, and after unsuccessful attempts to make repairs, we constructed a broad-banded (kite-shaped) dipole, 160 meters long, between another tree and the chateau. Although probably some 15 db inferior to the LPA, this antenna permitted successful data collection throughout the remainder of the experiments at Bierre-lés-Semur.

Data Campaigns: The schedule of the Meteor Radar program, to which the Kinesonde adhered during this period, provides for one 10-day campaign each month. The Kinesonde was not operational for the December 1969 campaign, 10 - 19 December (our first test recordings were made 21 December), but successful measurements were made during the campaigns of 26 January - 6 February, 18 - 27 March, and

Fig. 11. Detail of North Receiving Antenna Construction. Two 15-meter lengths of 3-cm open-wire transmission line form the dipole antenna, connected directly to 200:50 Ω balun transformer, thence directly to broadband RF preamplifier (gain 9db). RF transmission line (heavy cable) of RG9/U 50 Ω coax is 204.8 meters in length for each of 4 receiving antennas, regardless of position. DC power for amplifier (20 V, 40 mA) is supplied over variable length of RG58/U cable.

21 - 30 April. Figure 12 provides a detailed key to the data coverage during all campaigns. Very little data were obtained at night, since except for sporadic E (rare in winter nighttime) no nighttime E-region radio reflections are possible even at the lowest Kinesonde frequency (1.025 MHz). We did, however, obtain a few recordings at night when sporadic E layers were found.

A schedule of priorities has been established for the analysis of the data from these campaigns, based upon selecting the potentially most informative sequences for first attention. The principal factor in the quality of the meteor data is the background noise level, most of which is attributable to F-region backscatter; this, of course, varies with time and from day to day. From the standpoint of the Kinesonde data, the ionospheric conditions (as shown by the ionograms) vary considerably in complexity from day to day, and much of this complexity must be attributed to the very motions under observation. Thus it seems better to progress from sequences of simple, smooth E-region variation to those in which layers of sporadic E frequently occur. A few very early results from the first priority days are given at the end of this report.

Table 1

Antenna / Parameter	N	E	S	W	LPA
X meters	0	91.924	0	-91.924	135.0
Y meters	91.924	0	-91.924	0	147.5
Z meters	2	0	0	0	+2
Orientation, E of $N_{mag.}$		132^{o}	132^{o}	132^{o}	42^{o}
Cable length, m	204.8	204.8	204.8	204.8	

Origin at 47^{o} 25' 18" North
4^{o} 18' 47" East, 350 meters > MSL.

Azimuth, origin to LPA Tower, 37.8^{o} E of $N_{mag.}$

Magnetic Declination -4.284^{o} E of $N_{geog.}$

Magnetic Dip 63^{o}; Electron Gyrofrequency at 200 km 1.84 MHz.

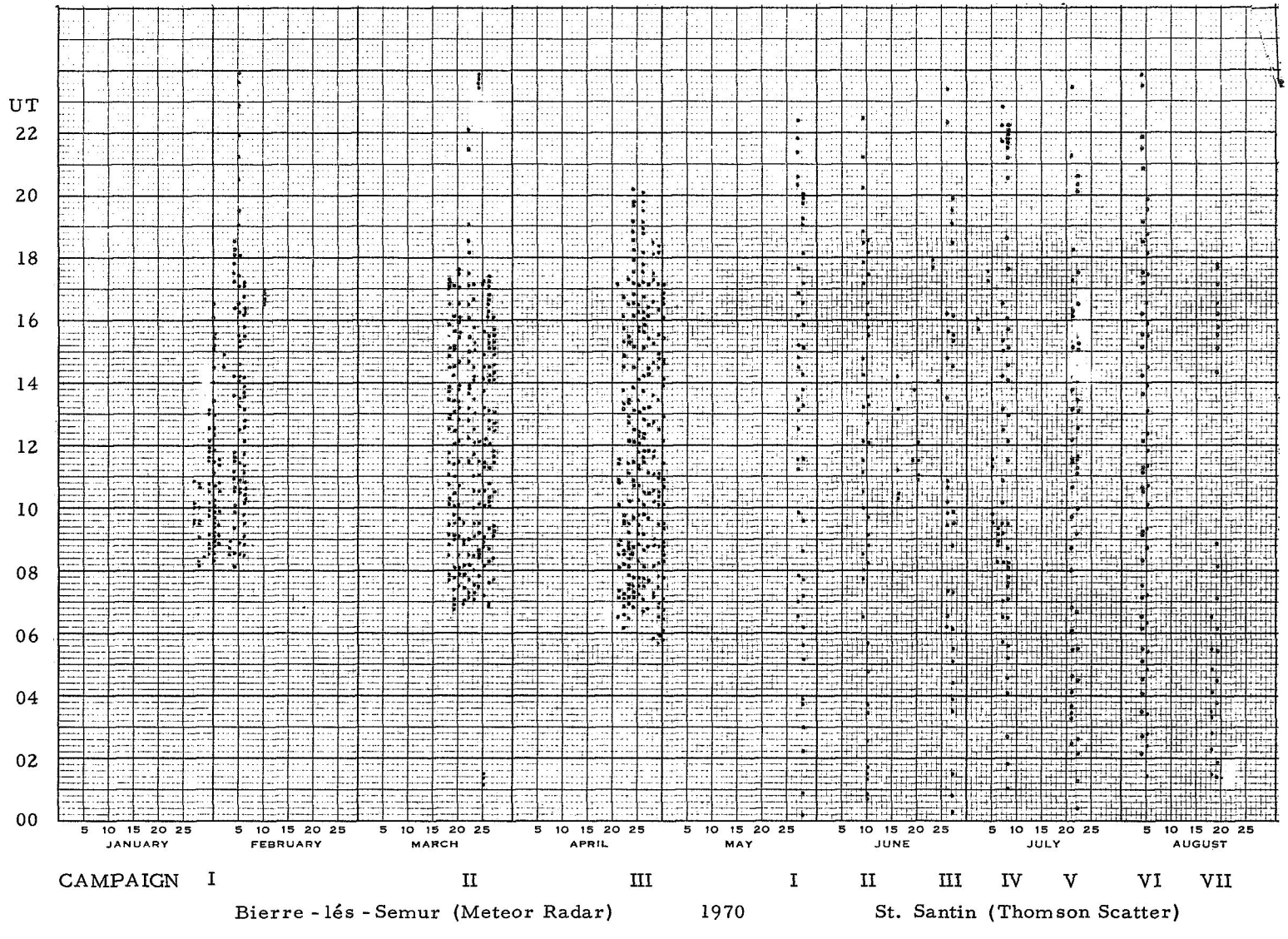

Fig. 12. Graphic Timetable of Kinesonde Recordings. Three campaigns at Bierre-les-Semur of 10-days' duration, and 7 2-day campaigns at St. Santin. Few nighttime observations are possible in the E-region, due to normally low ionization densities, but a few nighttime sporadic E recordings were obtained.

The Kinesonde in France: Thomson Scatter Comparisons

Site Selection and Installation: Immediately following the last recording at Bierre-lés-Semur, we began dismounting that installation and packing for transport to the Thomson Scatter site at St. Santin de Maurs (Cantal). A planning visit to St. Santin had convinced us that we could not do better than to locate the Kinesonde at the Thomson Scatter transmitter site itself: The only serious disadvantage was the possibility of severe interference to the Kinesonde from their strong RF field, but the obvious economy and convenience of a prepared site, and simplified communications, were compelling. The hilltop terrain, while not ideal for the spaced-antenna type of measurement, was felt to be better than the valleys nearby where reflections from the hillsides might affect our measurements.

The geometry of the Kinesonde-Thomson Scatter experiment is shown by fig. 13. The beam of the scatter transmitter is vertical and it defines the volume within which the Thomson scatter measurements occur. The receiver 300 km to the North scans this volume in altitude. The common volume of the two antennas is about 5 km wide by 13 km thick, at 300 km altitude, and of course diminishes with decreasing altitude. This horizontal extent is remarkably similar to the width of the first fresnel zone for the frequencies and altitudes of measurement by the Kinesonde.

The limited flat area of the hilltop was much too small for the 122-meter square receiving array. Since only a precise knowledge of the relative antenna positions is important in analysis of the data, while the regularity of the square is not, we undertook an approximate layout with compass and measurement chain following the contours of the land. We then engaged a professional surveyor to measure the actual positions of the antennas, including their relative altitudes. The latter are important since height differences among the antennas will introduce phase differences $2\pi\Delta z/\lambda$ in the data. Table 2 gives the measured locations of the Kinesonde antennas at St. Santin.

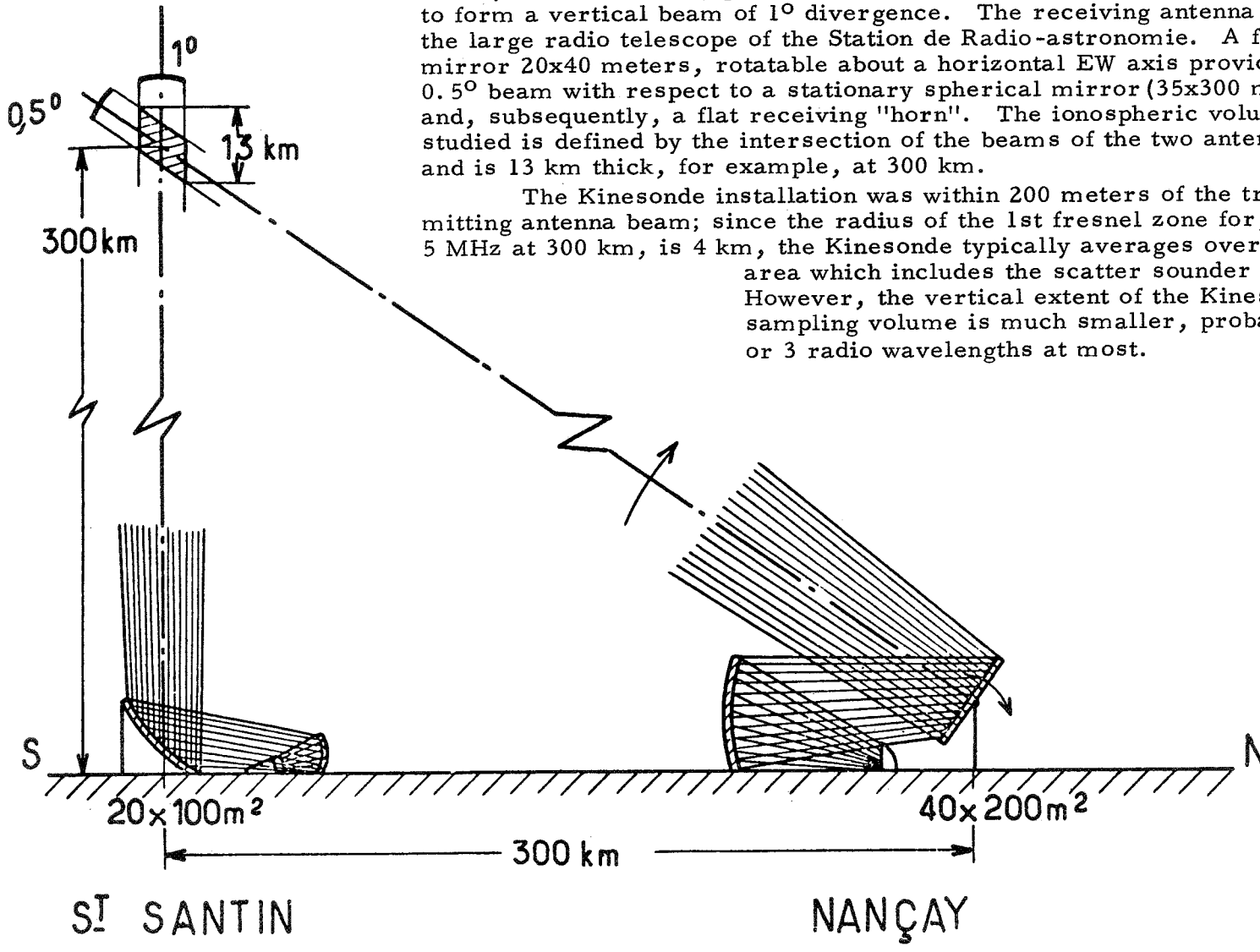

Fig. 13. The scatter sounder of the CNET comprises a transmitter at St. Santin-de-Maurs (Cantal) and receiver at Nançay (Cher). The transmitting antenna consists of a horn at the ground to illuminate an elliptic reflector which in turn directs the beam to the parabolic reflector. The latter, inclined at 45°, presents a projected horizontal area 20x100 meters to form a vertical beam of 1° divergence. The receiving antenna is that of the large radio telescope of the Station de Radio-astronomie. A flat mirror 20x40 meters, rotatable about a horizontal EW axis provides a 0.5° beam with respect to a stationary spherical mirror (35x300 meters) and, subsequently, a flat receiving "horn". The ionospheric volume studied is defined by the intersection of the beams of the two antennas, and is 13 km thick, for example, at 300 km.

The Kinesonde installation was within 200 meters of the transmitting antenna beam; since the radius of the 1st fresnel zone for, say, 5 MHz at 300 km, is 4 km, the Kinesonde typically averages over a larger area which includes the scatter sounder beam. However, the vertical extent of the Kinesonde sampling volume is much smaller, probably 2 or 3 radio wavelengths at most.

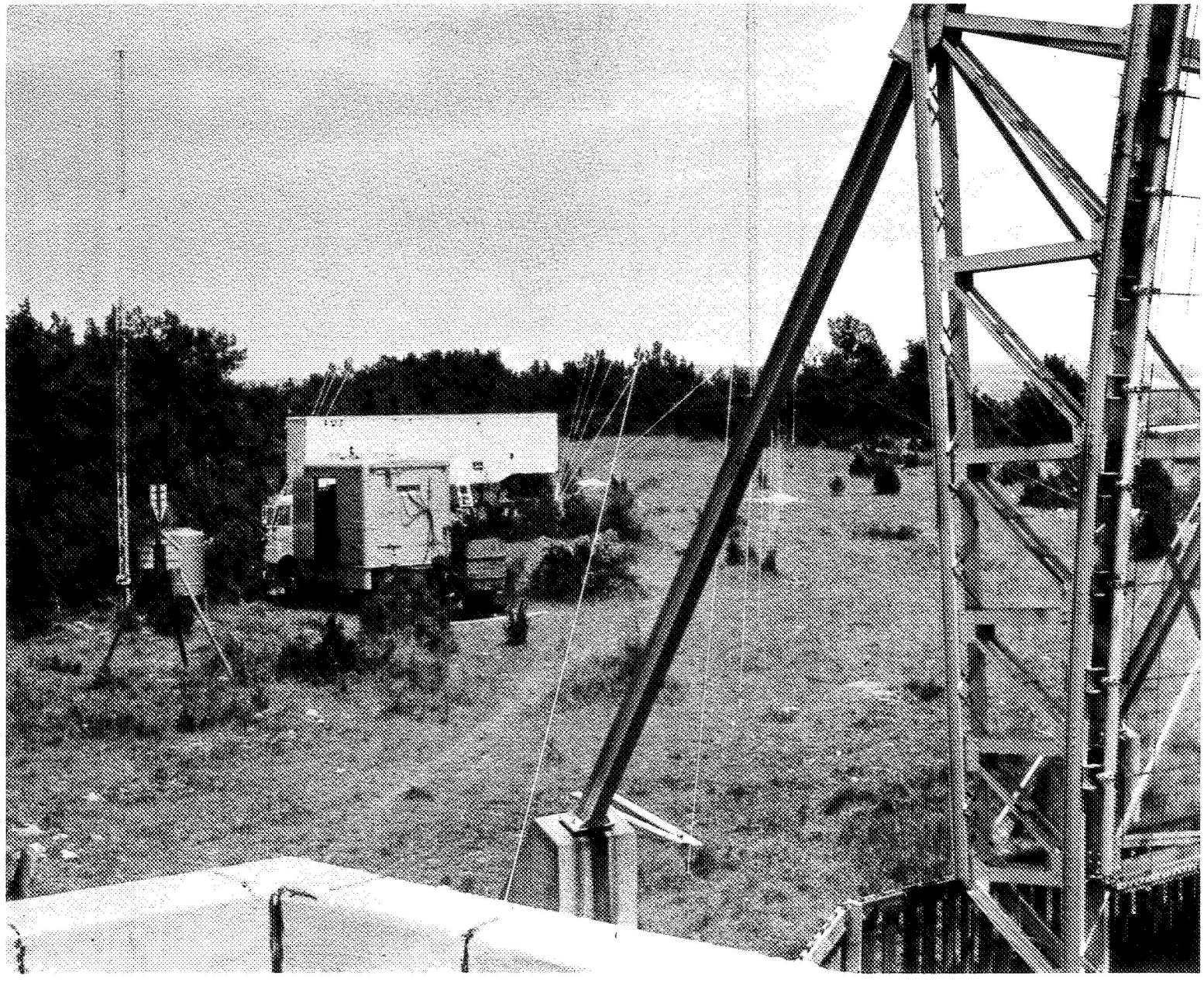

Fig. 14. View of Kinesonde Installation at St. Santin. The Vertex-down Log Periodic Antenna is suspended from the 150 ft. tower (right). Thomson Scatter transmitting antennas are behind and to the right. Receiving array is ahead, behind low trees and extends downhill to right.

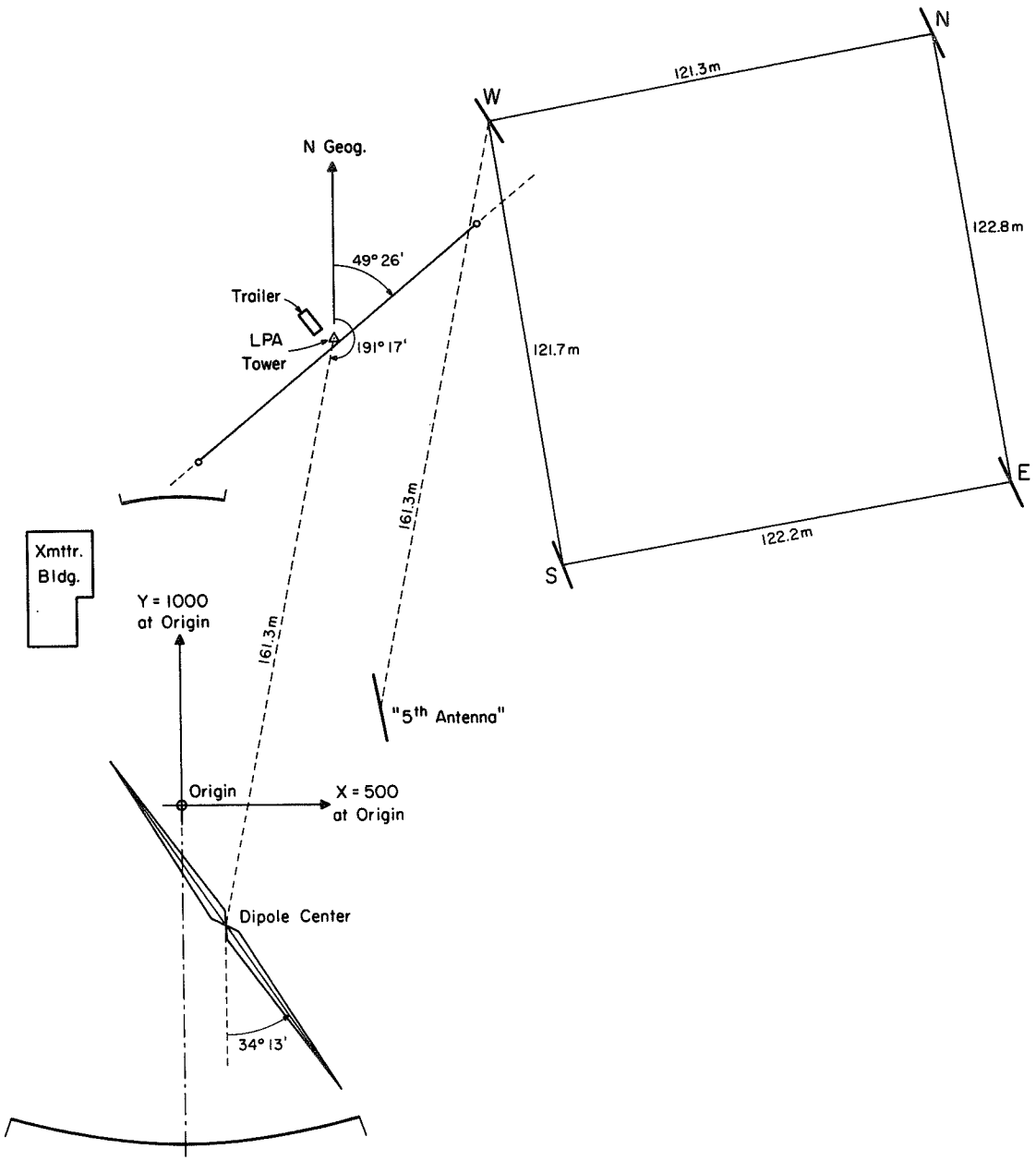

Fig. 15. Surveyed Layout of Kinesonde Installation at St. Santin de Maurs (Cantal). The two curved reflectors and Transmitter Building represent the permanent Thomson Scatter installation of the Centre National D'Etudes Des Telecommunications. The "Dipole" and "5th" antennas were only temporarily installed for a short, secondary Kinesonde experiment. The Kinesonde LPA transmitting antenna, laboratory trailer and receiving array were in place May-Aug. 1970. The receiving antenna locations are projected on a horizontal plane; actually, the E, S, and W antennas were at altitudes of -10.1, -4.7, and +5.1 meters relative to the N. antenna.

Table 2

Parameter \ Antenna	N	E	S	W	LPA	Dipole	"5th"
X (meters)	203.63	223.20	102.93	84.47	42.2	111.5	54.5
Y "	206.79	85.58	63.84	184.17	126.0	-32.0	26.5
Z "	65.88	55.71	61.41	70.97	61.5	71	61
Orientation E. of N. Geog.	156° 12'	156° 52'	156° 38'	157° 10'	49° 26'	325° 47'	157° 47'
Cable length, meters	204.64	204.80	204.72	204.72	10	150	204.72

Origin at 44° 38.87' N, 2° 11.38' E;
relative altitude at origin 62 meters (362 meters > MSL).
Bearing, LPA to dipole, 191.17 deg. (= bearing West to 5th Antenna)
Distance LPA to dipole (centers) 161.3 meters (=West to "5th" distance)

In planning our installation at St. Santin it was anticipated that the LPA antenna, on its 45_m tower, would be left in place after our departure for use with the French ionosonde maintained at the station. This placed several additional constraints on our installation: a more secure construction was necessary for a 'permanent' antenna, and all risk of either mechanical or radiation interference to the large reflectors of the Thomson Scatter system was to be avoided. The hill at St. Santin is composed of limestone, which outcrops through thin topsoil. We spent several days with airhammers to prepare for the concrete tower and guy anchor footings. Six new tower sections, to replace those damaged at Bierre-lés-Semur by the February storm, had been flown to Wiesbaden, Germany through the kind cooperation of the Wyoming Air National Guard. The installation was complete and operable (figs. 14, 15) after just 11 days of effort including layout, airhammer and cement work, tower erection, antenna assembly, system and

Table 3

Date (1970)	Day	Night
27 May	Transition Level	Complete Profiles
28 May	----- Complete Profiles -----	
9 June	E-region	E + F
10 June	E + F	
26 June	Transition Level	Complete Profiles
27 June	----- Complete Profiles -----	
7 July	F-region	Gradient, High Alt.
8 July	----- Gradient, High Alt. -----	
21 July	E-region	Complete Profiles
22 July	----- Complete Profiles -----	
4 Aug.	E + F	F-region
5 Aug.	----- F-region -----	
18 Aug.	Transition Level	Complete Profiles
19 Aug.	----- Complete Profiles -----	

Table 4

Types of Observation Program
St. Santin - Nançay Thomson Scatter

Type	Approx. Cycle Time	Altitudes (Km)
1) F-region	20-30 minutes	200, 225, 250, 275, 300, (325), 350, 400, (450).
2) Gradients	50 - minutes	200 to max. accessible; Region F+ 500, 550, 600, 700.
3) E + F	40 - minutes	100, 120 + F-region.
4) Complete Profiles	60 - minutes	100, 120, 135, 150, 165, 180, 200, 225, 250, 275, 300, (325), 350, 400, 450.
5) Transition	40 - minutes	100, 120, 135, 150, 165, 180, 200, 225, 250.
6) E-region	40 - minutes	95, 100, 105, 110, 120.

Note: Observations are impossible if the electron density is $\leq 5 \times 10^4$ (F region) or $\leq 2 \times 10^4$ (E region). Therefore, programs 5) and 6) are impossible at night, and programs 1), 2), 3), 4) terminate in general near 275 km.

diesel-generator checkout. This was much shorter than the time required at Bierre-lés Semur, and illustrates the advantages of a prepared site and appreciable prefabrication.

The times and durations of the seven Thomson Scatter data campaigns conducted jointly with the Kinesonde are described in Tables 3 and 4, and the final observing program is shown in fig. 12. Coordination of the two systems to assure measurements near the same height and time posed a problem. The height of measurement was dependent in a variable manner on the integration time required by the Thomson Scatter system to attain a prescribed ratio of signal to noise. The system scans downward in altitude (typically from 500 km to 90 km in 25 km steps), requiring 40 - 70 minutes for each height profile. The preceding and present heights of measurement can be read out directly, but the dwell-time at a given height can only be estimated in real time. On the other hand, no useful estimate of the real height of measurement (in the F-region) can be made in real time at the Kinesonde, as this information can only be recovered later from the electron density-height profile. The time-height coordination of the two kinds of measurement was simplified by the ability of the Kinesonde to observe 3 - 6 heights simultaneously (depending upon the use of the frequency pattern to obtain vertical components of motion), but we still felt it desirable to choose Kinesonde frequencies for reflection at nearly the same altitude as the Thomson Scatter measurements whenever possible. An account of the degree of correspondence actually achieved awaits completion of the electron density profile calculations.

Other Experiments

A number of other Kinesonde experiments were conducted between the Thomson Scatter campaigns at St. Santin.

a) Antenna coupling: A study underway by L. S. Fedor in this laboratory suggests the probable importance of coupling among spaced receiving channels in leading to erroneous velocity values. Some radiation coupling will exist among antennas in the same RF field, dependent upon the level of isolation between the antennas; other coupling might be introduced, in a carelessly designed system, within the signal-processing portions of the equipment. We undertook, therefore, to measure the internal and external isolation of the Kinesonde receiving channels. The internal isolation (i.e., with antennas disconnected, and the antenna inputs properly terminated) was in excess of 70 db between channel pairs, independent of frequency. The external isolation, between the antennas themselves, was smaller but still negligible: it varies with frequency (and antenna pair) in the range 50 - 70 db. The measured values have been found to be in good agreement with an antenna-theory calculation, and we feel confident in concluding that coupling cannot be a significant factor in the analysis of the Kinesonde data.

b) A point-source test: Our earliest attempts (Wright and Fedor, 1969; Wright, 1968) to compare spaced-antenna measurements against ionospheric motions obtained by more direct methods suggested that the factor of 0.5 commonly applied to the measured velocities from the radio experiment, to correct for the 'point source' nature of the transmitter, might be invalid. A direct experimental test of this principle is to switch rapidly between two spaced transmitting antennas. The echo pattern should be oppositely displaced (in direction and distance) to the displacement of the transmitting antennas if the point source effect is valid, but should not change if the ionosphere responds as if illuminated by a plane wave.

We erected a provisional transmitting antenna (dipole, fig. 15) at a distance of 161.3 meters bearing 195.50° from the LPA, and constructed a vacuum switch driven in such a manner that the even-numbered full cycles of the 6 frequency x 4 receiving antenna commutation pattern would employ the LPA, while the odd-numbered cycles would employ the second antenna. This in effect provides 48 receiving channels in the Kinesonde, at the sacrifice of half its normal time resolution; except for the most rapidly fading cases, this causes no difficulty. By analyzing either the odd or even cycles alone, for a single frequency (or frequency pair), the usual correloid description of the drifting diffraction pattern will be obtained. The odd and even cycles should give the same result, at least within their statistical confidence limits. The 'point source' test is then performed by mixing odd and even cycle channels in a single correloid analysis, and assigning antenna coordinate locations appropriate to either the "point-source" or "no-point-source" expectations. Since the dipole⟶LPA direction is not repeated among the pairs of receiving antennas (see fig. 15), the foregoing experiment does not easily facilitate direct demonstration of the pattern shift expected of the point source effect, but it does accomplish what is much more important for our present purposes: it tests whether the pattern shift expected from a transmitter displacement enters the time-averaging correloid analysis process in a manner consistent with the correlation properties of the unshifted pattern. Nevertheless, a more direct demonstration is also desirable, and for this reasons, in a second series of trials, a "5th" receiving antenna location was established on a vector from the West antenna. Ionospheric recordings were made comparing these two antennas alone as the transmitter was switched as before. Depending upon the order in which the antennas are switched and, again, on the channel pairs compared by cross correlation, the experiment will provide several decisive demonstrations of the pattern shift (or of its absence).

Early Results:

There are two principal phases to the study of the reduced data from this program and they apply with only differences of detail to the Meteor and Thomson Scatter campaigns: First, it is essential to establish a basis for interpreting the velocity and structure parameters obtained from Kinesonde measurements. This was, of course, one of the principal motivations of the program at the outset. Next, it is desirable to combine the results in time-dependent height profiles of atmospheric motions, permitting consideration of the scales of motion in 3 spatial dimensions. Because the periods of observation were coordinated among workers over the entire European continent (see Introduction and Appendix V) these campaigns can hopefully lead to descriptions of motions at high altitudes of unprecedented extent.

At present the three groups closely collaborating on the Kinesonde experiments in France are heavily engaged in reducing their data from the campaigns of 1970, and comparisons among them are only just now becoming possible. Since experience with a new data sample invariably leads to new ideas, changes of strategy, and shifts of emphasis as the analysis proceeds, the first results must always be considered with caution. Thus, in the first analysis of the Kinesonde data we solve for two-dimensional (horizontal) components of motion only. When V_Z is small compared to V_N and V_E (usually the case in the E-region), the resulting error on the horizontal components is also small; aside from a considerable saving in computer time, the analysis is simplified since electron density profiles are not required for two dimensional analyses.

Appendix III provides examples in figs. III-1 through III-5 of some of the steps involved in analyzing Kinesonde observations, using as examples the observations made in France. These culminate (fig. III-6 a three-dimensional example) in a summary of the motion and structure parameters for each recording and each choice of frequency or frequency pair.

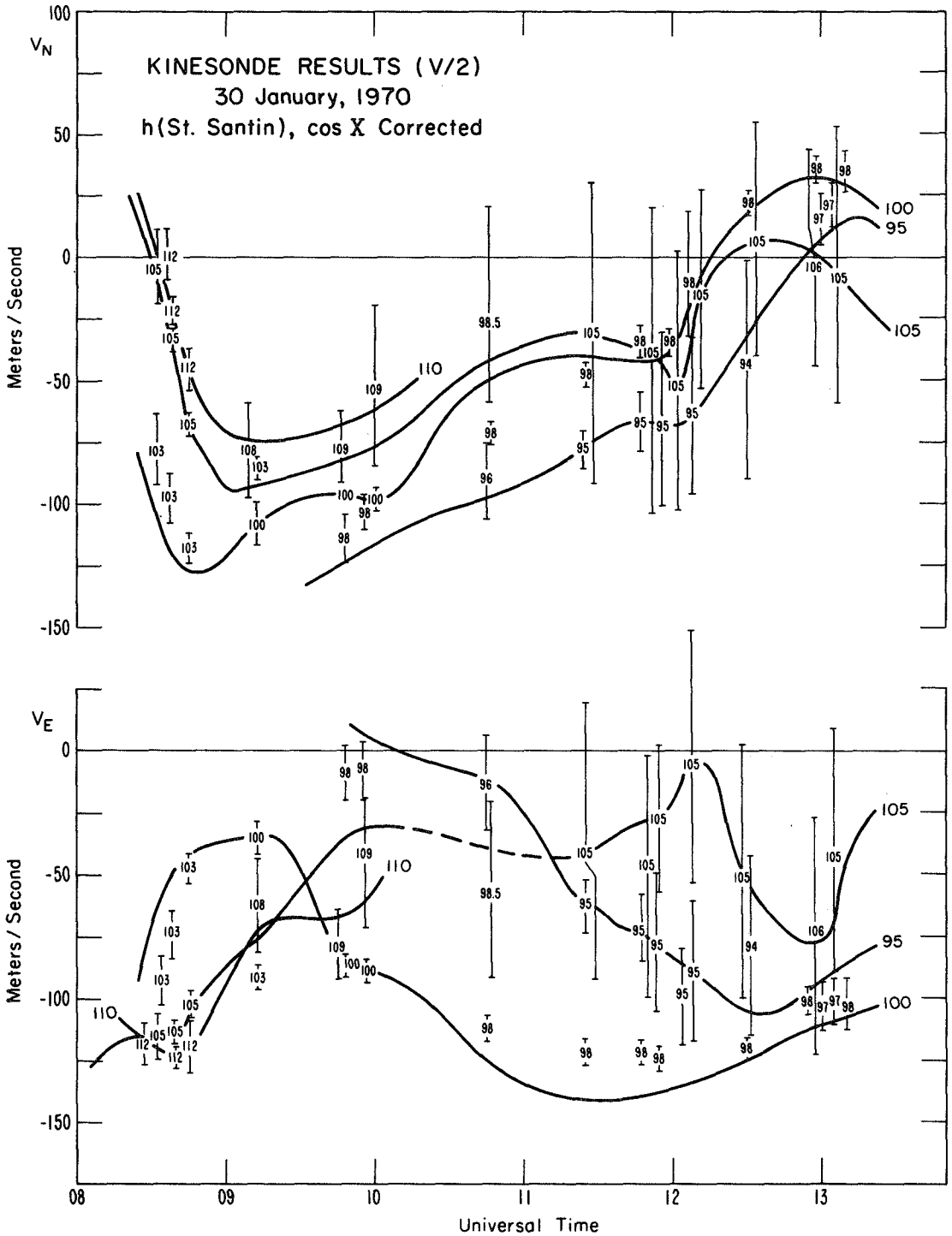

Fig. 16. Time variations of the North (top) and East (bottom) components of half the mean drift velocities observed at three heights simultaneously by the Kinesonde, 30 January 1970. Heights of reflection of the Kinesonde frequencies, deduced from electron density profiles, are noted for each plotted value. Interpolated variations for 95, 100, 105, and 110 km are shown by continuous lines.

A sequence of Kinesonde results from 30 January 1970 is shown in figure 16 in a form which brings out the time variations which may be identified at fixed altitudes when spaced antenna measurements are made at more than one frequency simultaneously. At each time (horizontal scale) 3 pairs of Kinesonde frequencies give values of the North (top) and East (bottom) components; the usually small vertical component is also available, but this analysis step has not yet been performed. Generally three heights are observed simultaneously, but these vary with the chosen frequencies and with the heights of the corresponding electron densities, which themselves vary with the time of day; interpolation may therefore be performed to recover the variation at fixed heights. This illustrates a point made at the beginning to explain the motivation for the Kinesonde: a fixed-frequency spaced antenna experiment cannot provide motion measurements at even one known height, in a changing ionosphere.

Even when our attention is restricted to the study of a single wind component (U_E, as in the meteor wind comparison case) the needs for interpolation in height and time pose problems of comparison. Perhaps the most simple way to examine the agreement between our early results is given in the height profiles of fig. 17. These show smoothed profiles (continuous curves) of U_E from the meteor data (Spizzichino, private communication), together with values of V_E derived from the Kinesonde observations. Results spanning 1 or $1\frac{1}{2}$ hours are grouped together; these include all of the Kinesonde observations from the initial "priority day", January 31, 1970.

Confidence limits shown on each Kinesonde value of V_E are estimated in the Correloid Analysis process. This estimation is rather involved (Fedor, 1967), but an indication that the confidence limit magnitudes are plausible has been obtained by a simulation study as an incidental to a validation of the parameter estimations by Correloid Analysis (Pitteway, et al. 1971). It is found that the confidence limits on V grow approximately linearly with the estimated random

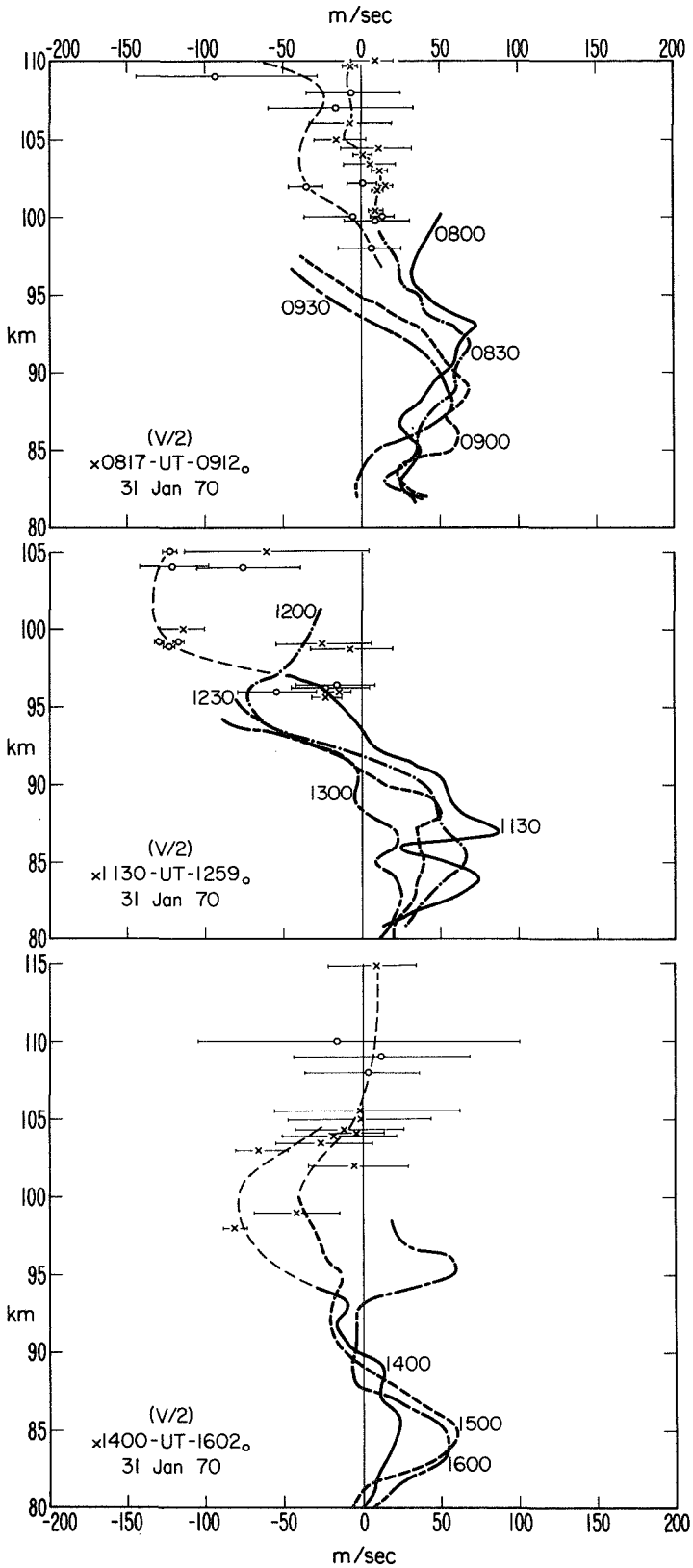

Fig. 17. Height profiles of half the East Component of horizontal drift observed by the Kinesonde, grouped in three periods of 31 January 1970, together with meteor wind profiles for the same time periods.

velocity component, V_c; thus the confidence limits in fig. 17 should be interpreted as an indicator, not simply of the estimated error on V, but of the variability about the mean velocity in each case.

Each value of V_E (and its associated confidence limits) plotted in these figures represent half of the value obtained by correlation analysis. This is the conventional correction applied on the assumption that the ionospheric scattering process sees the transmitter as a "point source", and we have applied the correction here despite earlier results (Wright, 1968) suggesting that it might not be applicable. Our first results from the present series shed new light on the question (see below), and in either case it has seemed better to use a standard interpretation rather than prejudice an eventual discussion of the problem using data from the entire program.

The principal difficulty apparent in fig. 16 is that the two types of measurement do not often overlap in altitude. Meteor results through 105 km (and occasionally to 110 km) will be available later, but they are not analyzed in the first computer examination of the meteor data, as their short duration hinders their discrimination from noise.

In the three examples of fig. 17, there is generally good agreement in both the height and time variations of the Kinesonde and meteor wind profiles. Where the data do overlap, the agreement at corresponding heights and times is quite good -- generally to within half the confidence interval on the Kinesonde result. This in itself is an indication that the confidence interval is mainly controlled by the variability of the measured motions, and that even the variabilities sampled by the two experiments may be correlated.

In a last example, fig. 18 shows the data of fig. 16 compared with the currently available meteor data. Again, the velocities observed by the Kinesonde have been divided by two to accommodate the point source effect, and this figure presents perhaps the most convincing evidence yet available that the Kinesonde experiment observes the E-region neutral wind directly.

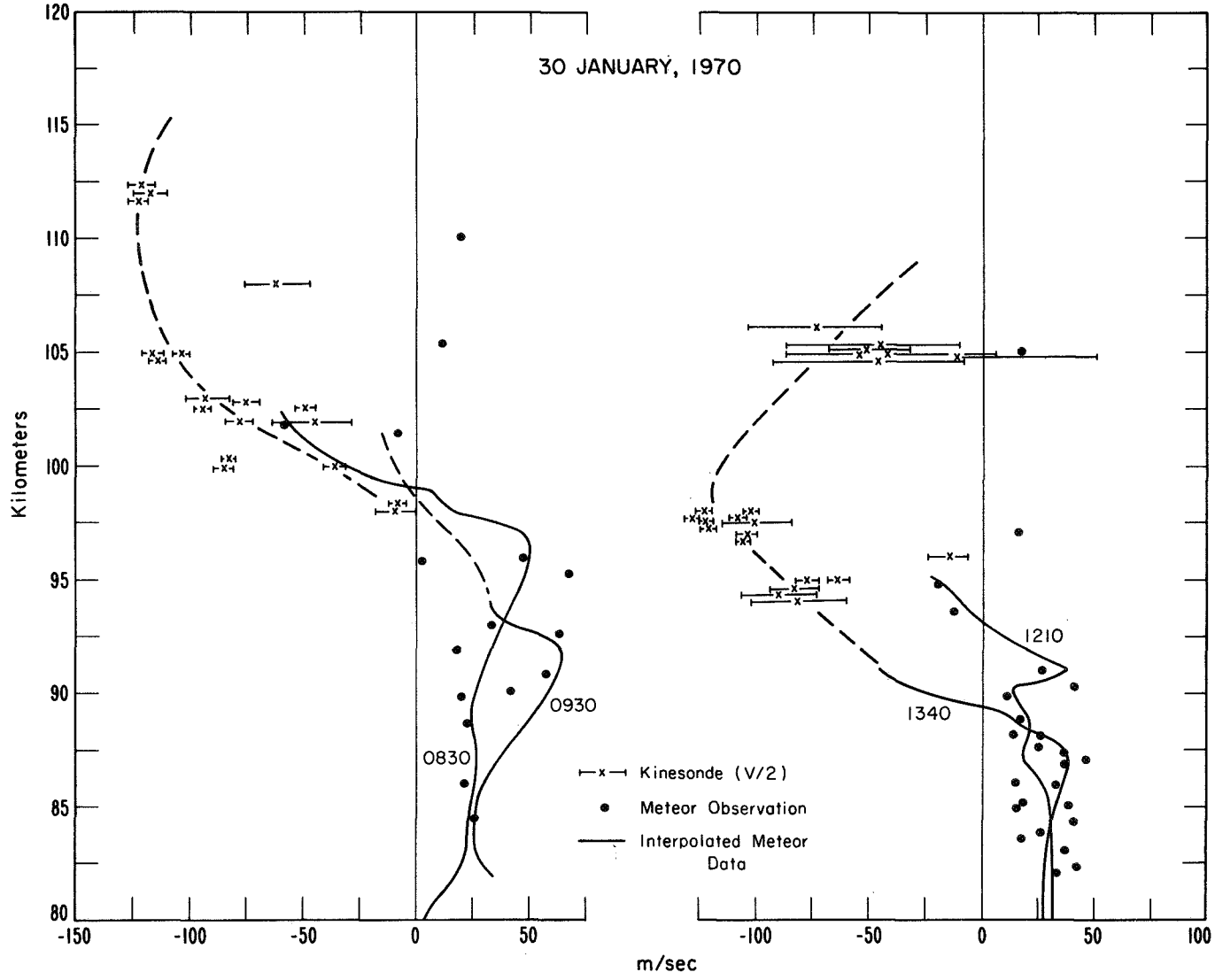

Fig. 18. Height profiles of half the East Component of horizontal drift observed by the Kinesonde, grouped for comparison with meteor wind profiles at same times.

Acknowledgments

Our deeply felt appreciation to the National Aeronautics and Space Administration, the Scientific Affairs Division of the North Atlantic Treaty Organization, and to our own laboratory, the sponsors of this experiment, is perhaps best expressed by continuing enthusiasm and perseverance -- and success -- in the analysis of our data. We appreciate as well the cooperation of many staff members of the Centre National D'Etudes des Télécommunications, in particular M. Duval, M. Provost, and M. Leduigou, for their aid in site selection, surveying, and instrumentation transport. The office of the Science Attaché, U. S. Embassy, Paris, provided frequent assistance in regard to communications and supplies. To our versatile and imaginative friend A. Lavigne of Semur-en-Auxois, go special thanks not only for securing us an ideal experimental site at Bierre-lés-Semur, but for his consideration of our families' well-being. In Bierre, the guardian of the chateau, M. Lefebvre and his family, became ours as well, and to the venerable M. Sodoyer of Bierre go our thanks for his hospitality and for the front cover illustration of this report.

In the second part of our program, M. Subsol, M. Demessance, and M. Regis at the Station du CNET, St. Santin, aided our work of installation at St. Santin, and coordinated each observing campaign with the Thomson Scatter receiving site at Nançay.

First and last, of course, we express our gratitude to our French colleagues, Drs. A. Spizzichino, I. Revah, G. Lejeune, and G. Vasseur for their initial encouragement and continuing cooperation, and to our NOAA colleagues Dr. A. K. Paul, A. R. Laird, and M. R. Clore for their advice, and participation in this work.

References

Awe, O. (1964) Effects of errors in correlation on the analysis of the fading of radio waves, J. Atmosph. Terrest. Phys. 26, 1257-1271.

Banerji, R. B. (1960) Radio-measurement of ionospheric drift as a problem in parameter estimation, in Statistical Methods in Radio Wave Propagation, Proc. Symp. at U.C.L.A., June 18-20, 1958, edited by W. C. Hoffman, pp. 40-48, Pergamon Press.

Booker, H. G., J. A. Ratcliffe, D. H. Shinn (1950) Diffraction from an irregular screen with applications to ionospheric problems, Phil. Trans. Roy. Soc. A 242, pp. 579-609.

Briggs, B. H., G. J. Phillips, and D. H. Shinn (1950) The analysis of observations on spaced receivers of the fading of radio signals, Proc. Phys. Soc. London, B63, pp. 106-121.

Dougherty, J. P. (1960) A statistical theory of ionospheric drifts, Phil. Mag. 5, pp. 553-570.

Fedor, L. S. (1967) A statistical approach to the determination of three-dimensional ionospheric drifts, J. Geophys. Res. 72, pp. 5401-5415.

Gusev, V. D., and S. F. Mirkotan (1960) Korreliatsionnyi analiz v primenenii k sredam s ob emnymi kharakteristiki, Issled. neodrorodnostei v ionosfere, Moscow, Isdatel'stvo Akad. Naukk SSSR, 4, pp. 7-19.

Herlofson, N. (1951) Plasma resonance in ionospheric irregularities, Ark. Fysik 3, p. 247.

Hines, C. O. (1964) Ionospheric Movements and Irregularities, in Research in Geophysics, Vol. 1, Ed. by H. Odishaw, MIT Press, p. 307.

Howe, H. H., and D. E. McKinnis (1967) Ionospheric electron-density profiles with continuous gradients and underlying ionization corrections. II. Formulation for a digital computer. Radio Science, Vol. 2 (new series), No. 10, pp. 1135-1158.

Kato, S., C. A. Reddy, and S. Matsushita (1970) Possible hydromagnetic coupling between the perturbations of the neutral and ionized atmosphere, J. Geophys. Res. 75, 2540-2550.

Lindzen, R. S. (1969) Data necessary for the detection and description of tides and gravity waves in the upper atmosphere, J. Atmos. Terr. Phys., 31, p. 449.

Mercier, R. P. (1962) Diffraction by a screen causing large random phase fluctuations, Proc. Camb. Phil. Soc. 58, pp. 382- .

Orhaug, T. Å. (1965) Scintillation of discrete radio sources. Trans. Chalmers Univ., Gothenburg, No. 299.

Paul, A. K. (1967) Ionospheric electron-density profiles with continuous gradients and underlying ionization corrections. I. The mathematical-physical problem of real-height determination from ionograms, Radio Science Vol. 2 (new series), No. 10, pp. 1127-1133.

Phillips, G. J., and M. Spencer (1955) The effects of anisometric amplitude patterns in the measurement of ionospheric drifts, Proc. Phys. Soc. London, B68, 481-492.

Pitteway, M. L. V. (1960) The reflexion of radio waves from a stratified ionosphere modified by weak irregularities II., Proc. of Roy. Soc., A, 254, pp. 86-100.

Pitteway, M. L. V., J. W. Wright, and L. S. Fedor (1971) The interpretation of ionospheric radio drift measurements - III. Validation of correlation analysis by computer simulation. J. Atmos. Terr. Phys. (in press).

Salpeter, E. E. (1967) Scintillation of discrete radio sources. Trans. Chalmers Univ., Gothenburg No. 299.

Spizzichino, A., J. Delcourt, A. Giraud, I. Revah (1965) A new type of continuous wave radar for the observation of meteor trails, Proc. IEEE, 53, p. 1084.

Spizzichino, A. (1967) Mesure de vents ionosphériques au moyen d'un radar météorique, Space Res. VII, p. 73.

Suchy, K. (1967) Correlation analysis of an irregular pattern, in Handbuch der Physik, Ed. S. Flügge, Vol. 49/2 pp. 422-433, Springer Verlag, Berlin.

Vasseur, G. (1969) Dynamics of the F-region observed with Thomson-scatter - I. Atmospheric circulation and neutral winds. J. Atmos. Terr. Phys. 31, pp. 397-420.

Wright, J. W. (1967) Ionospheric electron-density profiles with continuous gradients and underlying ionization corrections. III. Practical procedures and some instructive examples. Radio Science Vol. 2 (new series) No. 10, pp. 1159-1168.

Wright, J. W. (1968) The interpretation of ionospheric radio drift measurements - I. Some results of experimental comparisons with neutral wind profiles. J. Atmos. Terr. Phys. 30, pp. 919-930.

Wright, J. W. and L. S. Fedor (1969) The interpretation of ionospheric radio drift measurements - II. Kinesonde observations of micro-structure and vertical motion in sporadic E. J. Atmosph. Terr. Phys., 31, pp. 925-942.

Appendix I. Kinesonde Technical Description

The Kinesonde is a specialized ionospheric sounding system derived by modification from a Granger Associates Model 1904 step-frequency oblique-incidence "Skip-Finder" sounder. The original modifications were undertaken by the Lowell Technological Institute Research Foundation in accord with our specifications for an advanced digitized version of the spaced antenna experiment. The basic digital control, frequency conversion (down by a factor of 1/4 from the Granger 4 - 64 MHz system), frequency resolution, and data format design features were developed by LTIRF in 1967. A number of necessary improvements and developments have been undertaken by us since then.

A functional diagram for the Kinesonde appears in figure 6, which also contains some of the principal performance specifications. In the following paragraphs the main inter-unit relationships and operational features are explained with reference to figure 6 (Part 1).

Description of Principal Functions

Frequency synthesis: The required continuous sine-wave frequencies are coherently synthesized in the Fixed Frequency Synthesizer (FFS) and in the Variable Frequency Synthesizer (VFS) units from a 1.0 MHz Master Oscillator (MO). Overall frequency stability is that of the MO and is better than $\pm$ 1 part in 10^9 over a 24-hour period.

The FFS supplies (a) the receiver with several fixed Local Oscillator (LO) functions, (b) the Frequency Translator with the A-band Intermediate Frequency (IF_A) of the receiver, (c) the Timing unit with 100 kHz, and (d) the VFS with 1.0, 0.1, and 0.01 MHz.

The VFS produces any one of 1600 frequencies required for the 1st LO receiver function in four octave-related bands. This octave relationship provides the required band-to-band coherence. The LO_C is the directly-synthesized octave, while the LO_D is derived from it by multiplying LO_C by two; LO_B and LO_A are derived by successive division by two.

The four octaves of the operating frequency (RF), LO, discreet (unit) frequency steps (Δf), and the 1st IF's of the receiver are shown in the table below.

Table I-1

Band	RF MHz	L.O. MHz	Δf kHz	1st Receiver IF, MHz
A	1.0125 - 1.9875 $(\frac{1}{4})$ RF_C	3.75 - 4.725 $\frac{1}{4}$ LO_C	2.5	2.7375 $\frac{1}{4}$ IF_C
B	2.025 - 3.945 $(\frac{1}{2})$ RF_C	7.5 - 9.45 $\frac{1}{2}$ LO_C	5	5.475 $\frac{1}{2}$ IF_C
C	4.05 - 7.95 RF_C	15.0 - 18.9 LO_C	10	10.95 1 IF_C
D	8.1 - 15.9 2 RF_C	30.0 - 37.8 2 LO_C	20	21.9 2 IF_C

The frequency step and band commands present in the Frequency Step Counter at any given PRF period uniquely determine the operating frequency of the transmit/receive channels.

The octave-bands of the LO are provided as continuous wave signals to the Frequency Translator where the four respective IF's are subtracted, producing four parallel channels of RF. One of these channels is then enabled by the Band Command to enter the RF Power Amplifiers where it is then pulse-modulated. The Granger 10 W and 500 W amplifiers feed a transmitter power amplifier of our own design.

Transmitter: The transmitter is a class AB, push-pull broad-band RF pulse amplifier using two 4PR-60 vacuum tubes. The amplifier provides a nominal 18 db gain between 1.5 and 12 MHz. Balun transformers at the input and output result in input and output impedances of 50 Ω and 300 Ω, respectively. Maximum continuous power output is about 100 W into a matched load. With the usual 50 μs pulse at 100 Hz repetition maximum peak power is corona-limited at about 20 kW. A schematic diagram of the transmitter power amplier is found in fig. I-8.

Output pulse parameters:

PRF = 100 Hz (50, 20, 10, 5, and 2 Hz also available)

P.W. = 50 μsec (100, 200, 500, and 1000 μsec also available)

Max. $P_{out\ peak}$ = 20 kW at 5×10^{-3} duty factor ($\frac{50\mu s}{10\ ms}$)

Rectangular Pulse Shape (Rise time 1.0 μ sec; fall time 0.1 μ sec.)

The amplified RF from the transmitter is then applied to the transmitting antenna over an inexpensive shielded 300 Ω balanced transmission line.

Observing modes: The Mode Logic unit determines how the Frequency Step Counter is set to a frequency state. In the Kinesonde mode the flip-flops of this counter are set directly to the BCD frequency step demanded at the given PRF period by one of six manual digitally-coded frequency selectors. In the Kinesonde mode, the initiation of a tape record causes the antenna commutator to step. At the pulse

repetition rate of 100 pps, the system switches from one of the six selected frequencies to the next, and in turn to the four spaced receiving antennas. (See diagram, page 13.) Thus twenty-four receiving channels are established, and a data rate of $\frac{100}{24}$ echoes per second is available in each channel. Any six of the 1600 frequencies may be selected by the six dial assemblies.

Echo selection: For each of the six frequencies an independent range gate may be positioned in coherent 10 -μs steps to select the desired ionospheric echo pulse for digitization.

Echo parameter digitization: The echo peak amplitude and RF phase within the range gate are digitized for each echo and converted to BCD notation. The RF phase is obtained by counting cycles of a 4-MHz reference between the leading edge of the range gate and the first negative zero crossing of the 50 - kHz undetected receiver output (fig. I-6). Echo amplitude is obtained by counting a group of 1-MHz pulses during the decay-time of a capacitor charged by the full-wave detected 50 kHz echo signal within the gate (fig. I-7).

Amplitude and phase, dynamic range and resolution: Receiver output is closely logarithmic over 60 db, with 80-db total dynamic range; amplitude is digitized in 0.5 - db steps. RF phase resolution is 4.5^{o}, or about 0.08 rad

Recording length: Tape records of any duration from 0.5 min. to 4.0 min. (in 0.5 min. steps) are initiated manually. Tape transport speed is 2.5 in/s.

Recording format: Three amplitude and two phase digits are recorded for each echo pulse while the tape moves uniformly. Longitudinal and transverse parity checks are provided. The system records in low density, 7-track, IBM tape format, 200 bits/inch. About 50 four-minute records may be accumulated on 2400 ft. $\frac{1}{2}$" tape.

Ionosonde mode: In the ionosonde mode the direct-set inputs are disabled and the Frequency Counter advances to the next step when the timing unit determines that the required number of frequency repetitions occurred. This can be set to 1, 2, 4, or 8 pulses/frequency step. The counter may also be manually incremented.

From the receiver, the video echo pulses are combined with frequency markers (every 100th step) and range markers (at 1.5, 15.0, and/or 150 km of virtual height). This mixed video range data is then recorded by a 35mm camera with a date/time capability. The linear film motion provides the frequency axis. The sample ionogram shown in figure 3 was obtained using one of the standard Kinesonde receiving dipoles, which are about 18 db inferior to the LPA.

An auxiliary output of the video mixing unit, together with a frequency-analog (staircase) voltage is used to provide a real-time ionogram display on the face of a storage oscilloscope. This display can be retained up to several hours and is used by the operator in setting the frequencies and gates for Kinesonde recordings.

Minimum detectable radar cross section: A standard analysis, assuming 10 kw peak radiated power, +6 db antenna gain, -12 db D-region loss, leads to 380 meters as the minimum-detectable diameter of a totally-reflecting sphere at 100 km altitude. This is equivalent to a square target 0.34 x 0.34 km.

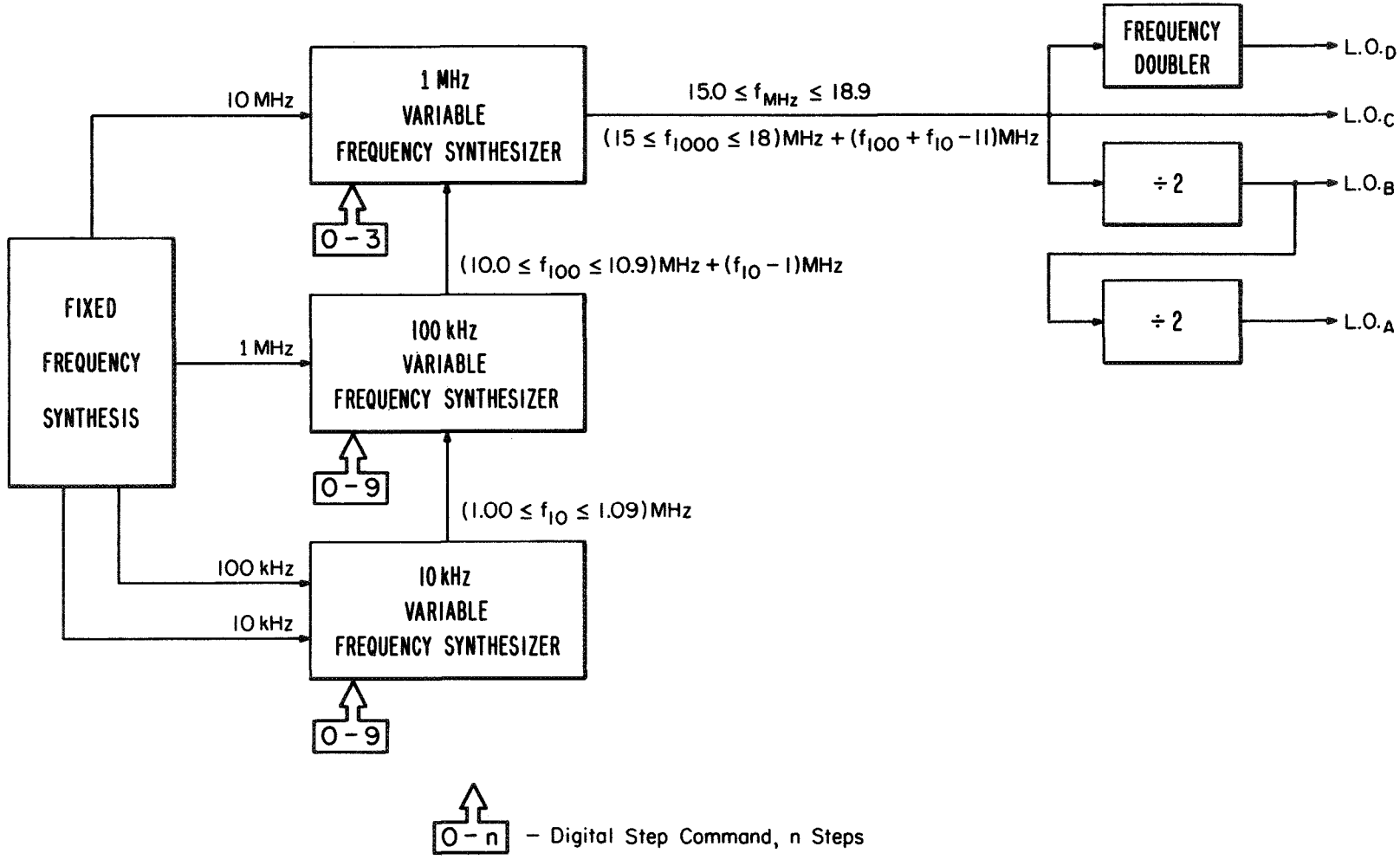

Fig. I-1. The Variable Frequency Synthesizer.

Technical Details, Principal Kinesonde Sub-units

Variable frequency synthesizer: The Variable Frequency Synthesizer of the Kinesonde (fig. I-1) contains three decade-related sub-units which coherently synthesize the required 1000, 100, and 10 kHz steps. The three VFS' are basically identical units using the so-called triple-mix frequency synthesis method. The first two units were parts of the original Granger "Path Sounder"; the original 10 kHz unit was constructed by LTIRF. The three units differ in principle only by the circuit constants to make them perform at different frequencies. The triple-mix method uses an incoherent steering oscillator to align the desired n-th step harmonic of a coherent frequency input with a narrow-band filter. This steering oscillator in the Granger 1 MHz VFS and 100 kHz VFS changes its frequency in steps by adding trimmer capacitors to its L-C resonance circuit. The capacitance adding is done by switching diodes.

The 1 MHz Variable Frequency Synthesizer provides three 1 MHz (f_{1000}) steps while the remaining two units provide 9 steps each of 100 kHz (f_{100}) and 10 kHz (f_{10}), respectively. Thus the complete synthesizer provides 399 10 kHz steps from 15 to 18.9 MHz; this frequency range is that of the Local Oscillator in Band C (LO_C) i.e., the RF ($4.05 \leq f_{MHz} \leq 7.95$) plus the IF = 10.95 MHz. Thus, $f_{LOC} = f_{IF} + if_{1000} + jf_{100} + kf_{10}$ where $i = 1, 2, 3$ and $j, k = 1, 2, \ldots 9$. This LO_C frequency is multiplied by two to obtain LO_D, and divided by two and by four for LO_B and LO_A, respectively. As f_{10} appears at all frequency steps, it is obvious that any inaccuracies in it will be reflected in the system's accuracy and/or noisiness. Furthermore, inaccuracies between adjacent 10 kHz steps can directly affect many of the important measurement capabilities of the Kinesonde which depend directly upon an accurate, small, Δf.

The LTIRF 10 kHz VFS was found to have undesirable characteristics, and it was therefore modified during the past year. This modification is described next in some detail.

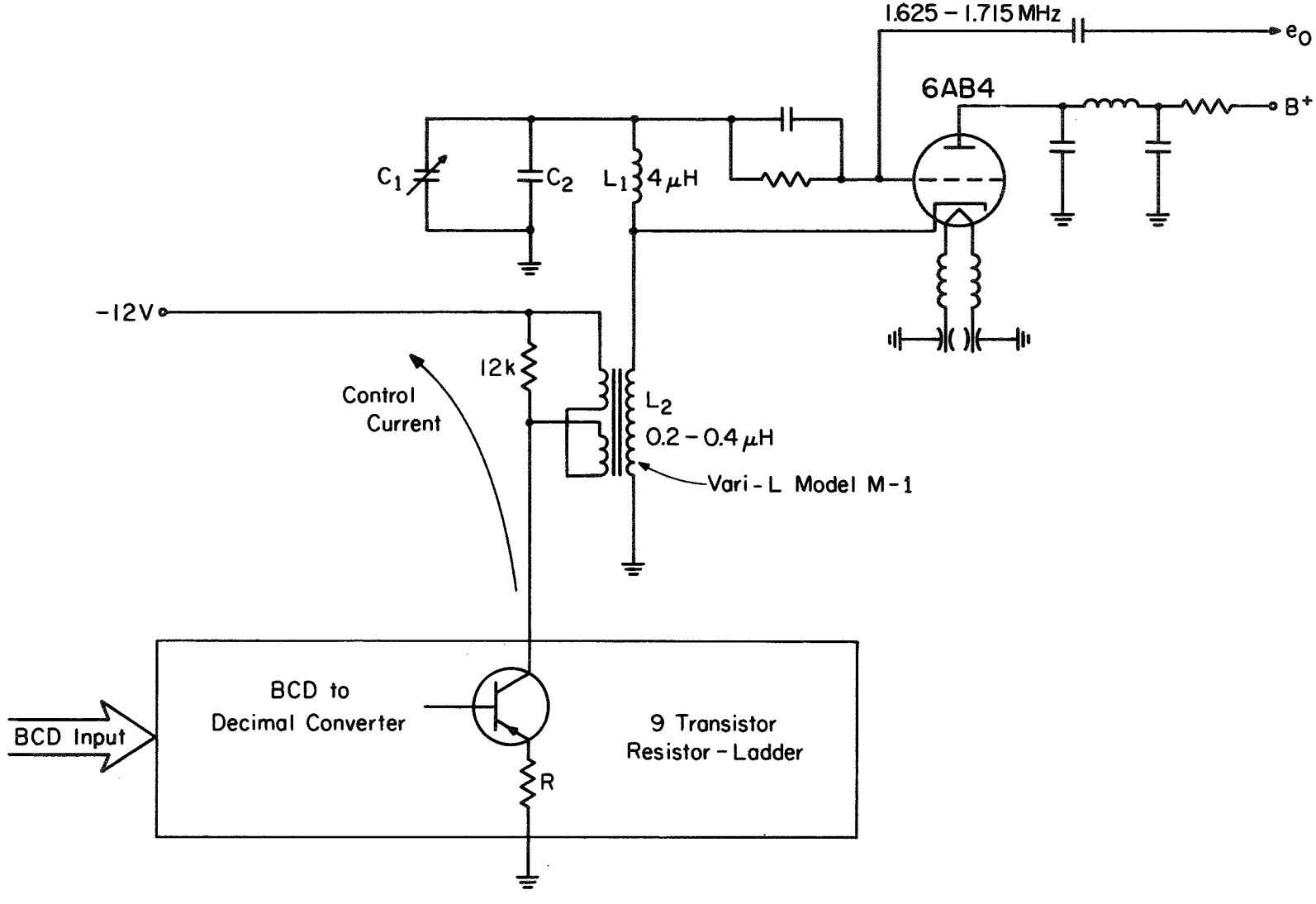

Fig. I-2. The original Kinesonde steering oscillator for the 10 kHz Variable Frequency synthesis.

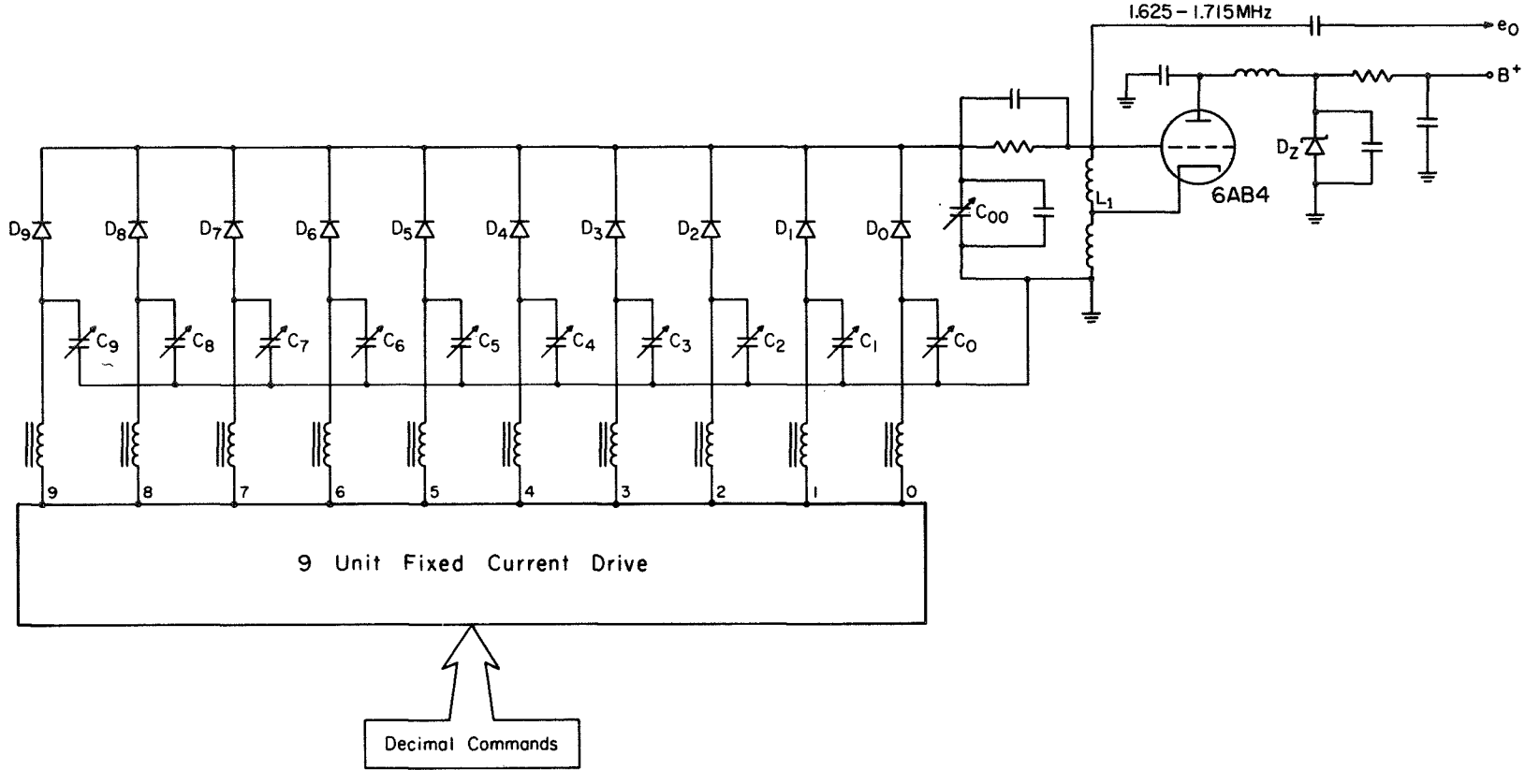

Fig. I-3. New Kinesonde Steering Oscillator for 10 kHz VFS (replaces unit of Fig. I-2).

10 - kHz unit modification: The original 10 kHz VFS unit (fig. I-2) differed from Granger VFS designs by employing a current variable inductor to change the steering oscillator frequency. The resulting circuit had neither the minimum required long-term stability nor the necessary frequency step accuracy of 2.5 kHz for the following reasons:

- The variable inductor L_z had a fairly high temperature coefficient.
- The overall control current circuit had a high temperature coefficient.
- The control current varied with the -12V power supply (i.e., not a constant current drive).
- The inductor was reset to zero current rather than to reverse magnetic saturation to take care of the hysteresis of the core.

As a result:

- Some 10 kHz steps could be correctly selected only when all six frequencies were the same (hysteresis effect).
- Some 10 kHz steps, even when correct, would produce very noisy system behavior due to borderline alignment of the required 10 kHz harmonic with the bandpass filter (hysteresis and temperature drift).
- The whole range of steps could shift down or up by one increment (power supply and/or temperature drifts).

Since the original measurement goals of the Kinesonde, and particularly the plans for experiments in France, depended upon observations at precisely-known small frequency differences, design of a new 10 kHz subcomponent was undertaken.

The new unit is a frequency-modified Granger steering oscillator design and is shown in fig. I-3. All components were chosen to give sufficient temperature stability; for example, C_{00} - C_9 are quartz piston trimmer capacitors. To maximize Q of the circuit, L_1 is an air-core inductor with a very low stray capacitance temperature coefficient.

C_{00} adjusts the gross oscillator frequency when all other C's are OFF while their diodes are back-biased. The 9th step of frequency occurs with the turning-on of D_9, the 8th with the turn-on of D_9 and D_8, etc., until all diodes are turned on for the zeroth frequency step.

This unit has shown itself to be rugged, dependable, stable, and accurate. Its use has all but eliminated the internal coherent interference previously observed on many frequency steps.

Receiver: The present LTIRF receiver is a transistorized, frequency-scaled copy of the Granger receiver. It consists of four dual-IF receivers (one for each band) with a common 500 kHz output to another dual-IF, single conversion unit. The final IF is 50 kHz. The amplitude output is logarithmically compressed over the 80-db operating dynamic range by a forward-biased two-diode network. The resulting output is log-linear ($\pm$ 2 db) over a minimum of 60 db. The sense of 'phase' from band to band alternates because of the choices of the fixed frequency conversions to arrive at the 50 kHz final IF. The reason for this is clear from the following table of IF and Local Oscillator frequency choices:

Table I-2

Frequencies in MHz

Band	A	B	C	D
RF range	1.0125-1.9875	2.025-3.975	4.05-795	8.1 - 15.9
1st LO	3.75-4.725	7.5-9.45	15.0-18.9	20.0 - 37.8
1st IF	2.7375	5.475	10.95	21.9
2nd LO	2.5	4.0	10.0	20.0
2nd IF	0.2375	1.475	0.95	1.9
3rd LO	0.7375	0.975	1.45	1.4
3rd IF	0.50			
4th LO	0.55			
4th IF	0.05			
Phase	+	−	+	−

It can be seen that in Band B the 2nd LO was chosen to be 4.0 MHz instead of 5.0 MHz (for a consistent octave progression). This produced a 2nd IF of 1.475 instead of 0.475 MHz; in turn this forces the production of the 3rd IF by $(f_{IF2} - f_{LO3})$ instead of $(f_{LO3} - f_{IF2})$ as in Band A. A similar change occurs in Band D because LO3 is 1.4 MHz instead of 2.4 MHz. A better choice of the LO3 frequencies would be $f_{LO3\ n} = n(0.2375) + 0.5$ MHz $n=1,2,4,8$. This would retain a consistent phase sense. However, the present plan operates satisfactorily, once the alternation of phase sense is included in analysis of the data.

The receiver transient response is as follows:

pulse delay	$\approx$	20 μs
total rise time	$\approx$	30 μs (with 20% overshoot)
total decay	$\approx$	60 μs .

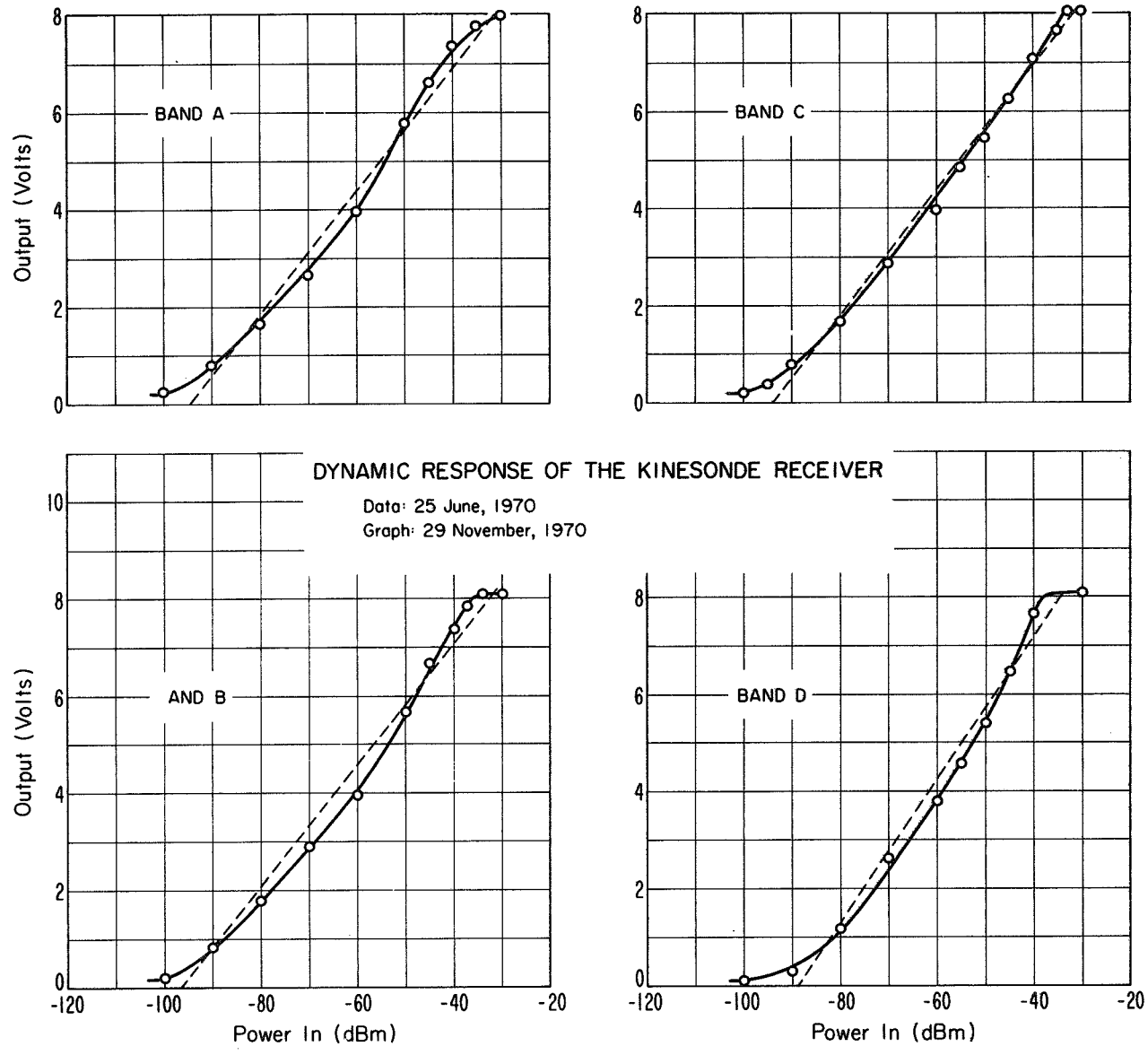
DYNAMIC RESPONSE OF THE KINESONDE RECEIVER
Data: 25 June, 1970
Graph: 29 November, 1970
BAND A
BAND C
AND B
BAND D
Output (Volts)
Power In (dBm)
0
2
4
6
8
10
-120
-100
-80
-60
-40
-20

Fig. I-4.

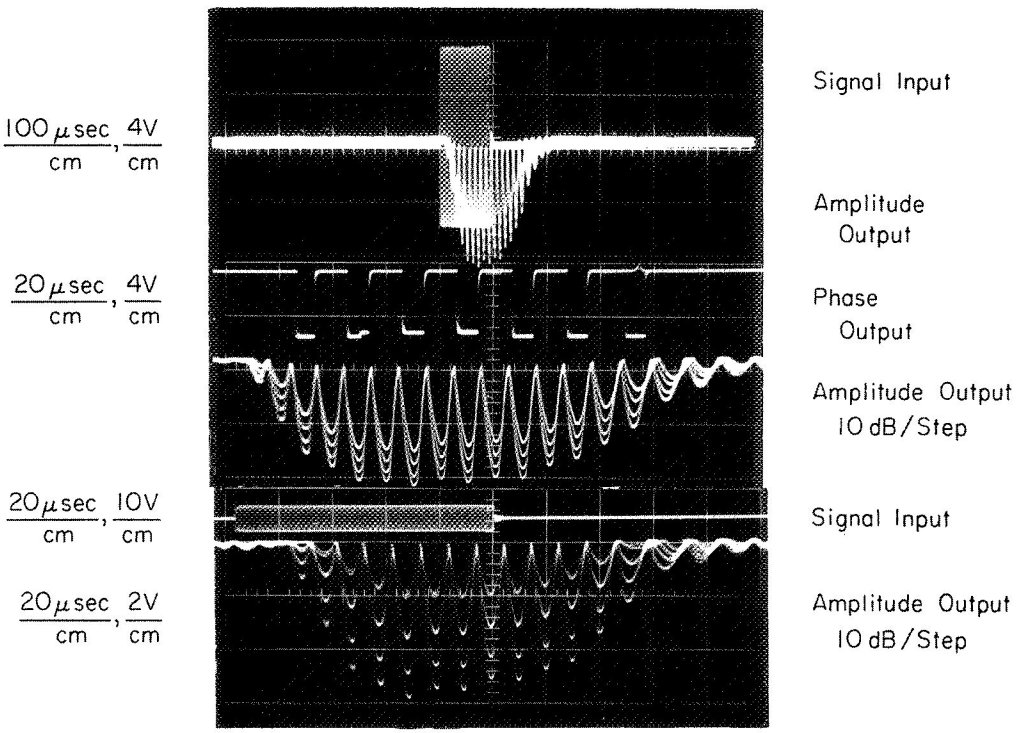

Fig. I-5. An Illustration of the Receiver Transient and Dynamic Response

The dynamic response shown in fig. I-4 is produced by logarithmic compression of the 50 kHz IF output. The result is satisfactorily log-linear over the normal operating dynamic range. The response varies somewhat with frequency, within limits of + 3 db about the best-fitting straight lines. The receiver has a measured steady state 3 db bandwidth of 12 kHz; the response is approximately Gaussian.

The logarithmically compressed receiver output voltage illustrated in fig. I-5, ranges from 0 - 8 VDC. After digitization to one of 200 levels (or 'counts') the effective amplitude calibration of the system is as shown in the following table:

Table I-3

Band	Freq. Range (MHz)	db/Volt out	db/Count
A	1 - 2	7.8	0.28
B	2 - 4	8.0	0.29
C	4 - 8	7.8	0.28
D	8 - 16	7.0	0.25

Six manual sensitivity positions are available independently for each band; they provide approximately 10 db gain per step. The data of the preceding table apply approximately to all steps, although the effective dynamic range decreases about 10 db per step.

Echo phase digitization: The Phase Detector (fig. I- 6) of our design replaced an LTIRF detector in 1968 and consists of two NAND gates (a and b) and two flip-flops (F_1 and F_2). The clipped 50 kHz receiver output (φ_R) appears at NAND-b input only during the Height Gate (HG). The output of NAND-b then runs F_1 and F_2 which are set to the TRUE state by the differentiated leading edge of the HG. The coincidence of HG and F_2 at NAND-c allows 4 MHz pulses to appear at the Phase Counter. The down-going condition of F_2 occurs at the 1st negative-going portion of φ_R. This determines the count of

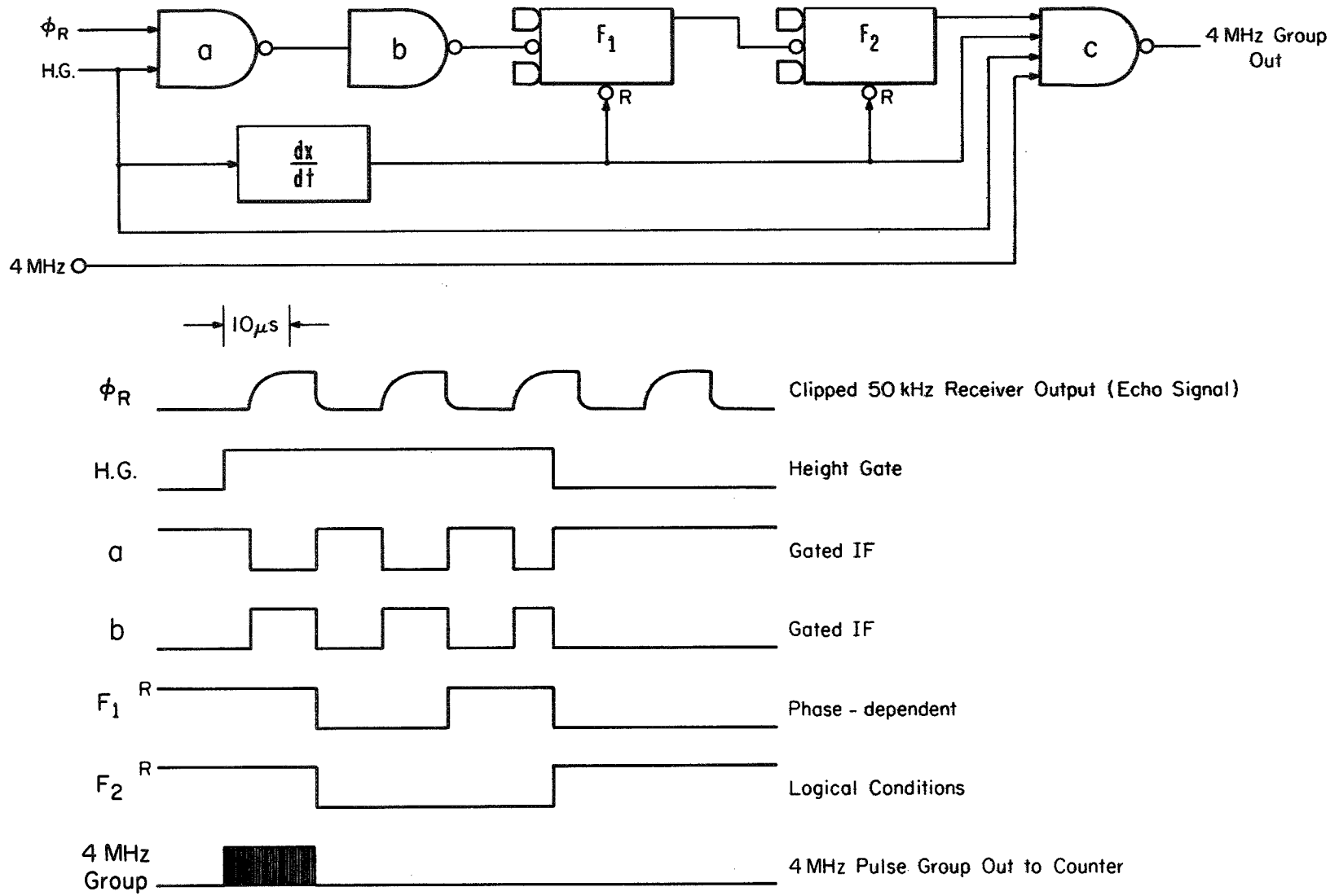

Fig. I-6. The Phase Detector and Digitizer.

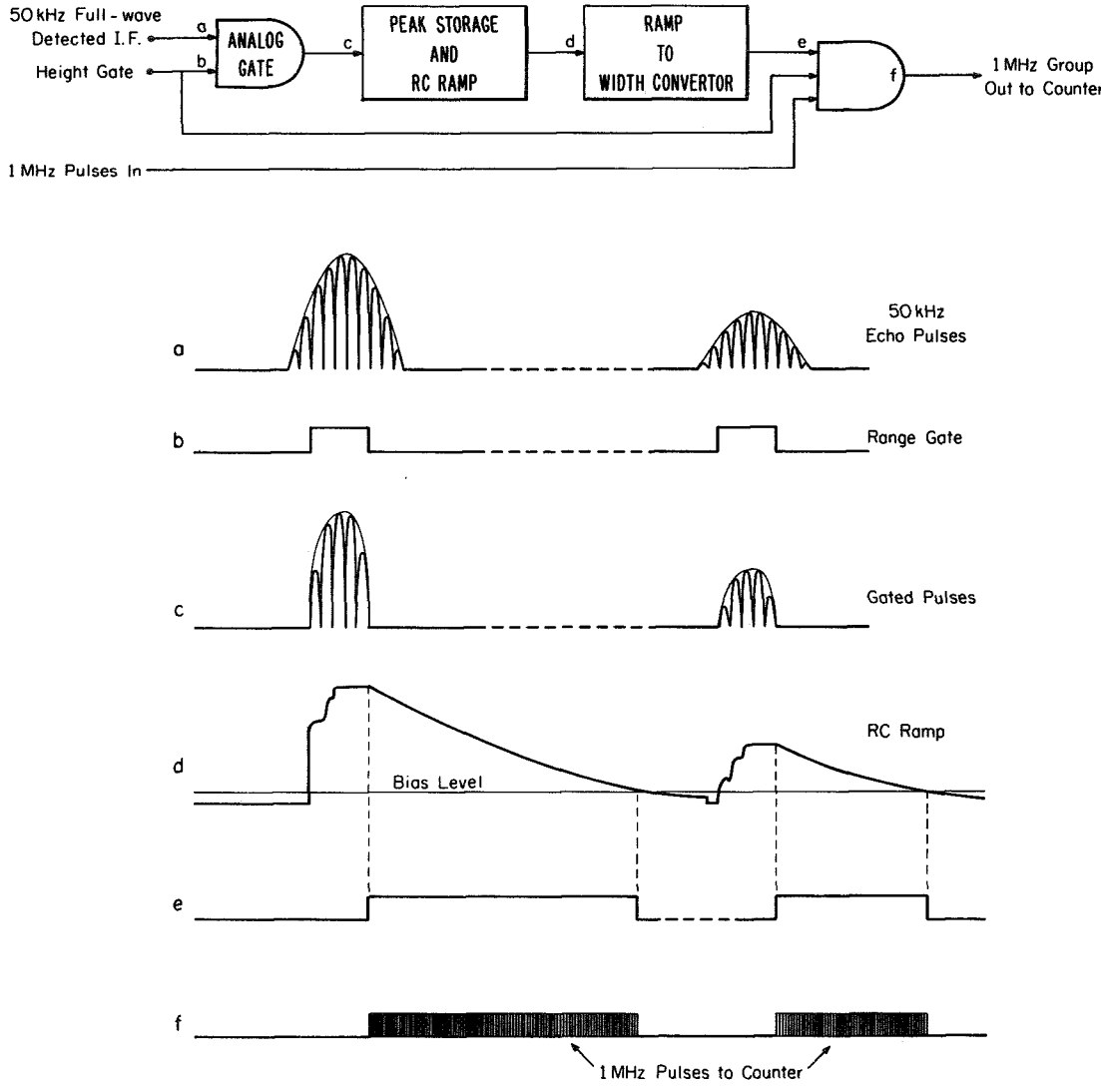

Fig. I-7. The Analog-to-Digital Converter for the Echo Amplitude.

the 4 MHz pulse group passed by NAND-c. The maximum duration of the interval between HG and F_2 is $\frac{1}{50\ \text{kHz}}$ for one full period of the phase. The phase resolution achieved is $\frac{50\ \text{kHz}}{4\ \text{MHz}} = \frac{1}{80}$ rotation, or 4.5° per phase count.

The amplitude-limited, 50 kHz IF phase output of the receiver is first operational at a receiver output of 0.075 volts, well below the receiver noise level at the lowest sensitivity setting. The phase measurement is, however, amplitude dependent up to an output of about 1 volt, i.e., at about -90 dbm.

Echo amplitude digitization: The A/D conversion (fig. I-7) of the echo peak amplitude within the range gate is accomplished by a capacitor which attains a charge proportional to the peak amplitude during the range gate. The long time-constant discharge crosses a fixed bias level at a time proportional to the total stored charge and thus proportional to the echo amplitude. This time window controls the number of 1 MHz pulses fed to a 0-199 counter. The counter's value is therefore proportional to the 50 kHz IF level.

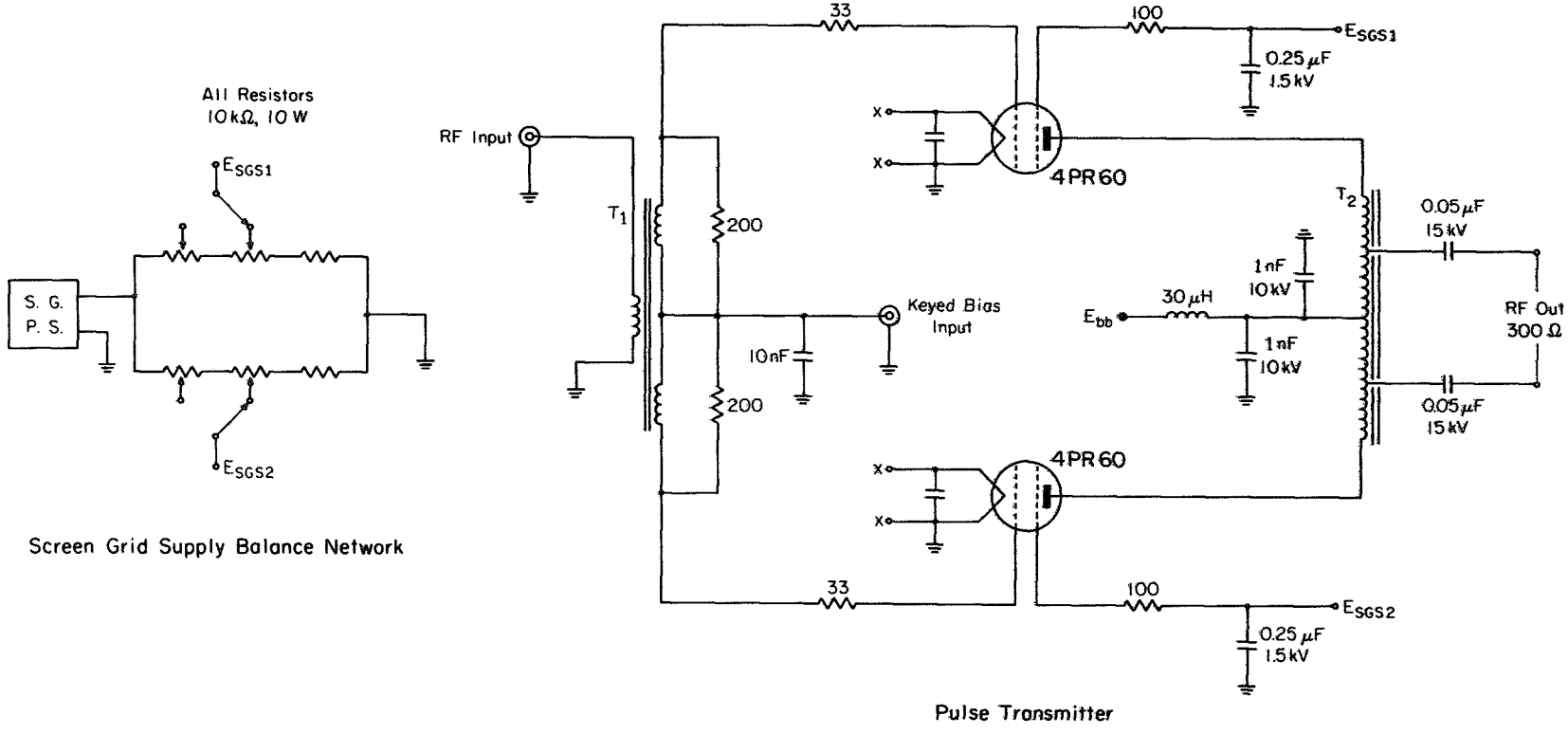

Fig. I-8. Diagram, Transmitter Pulse Amplifier.

Appendix II. Antenna System

Transmitting Antenna

A Vertex-Down Log-Periodic Antenna (VDLPA) was designed for use with the Kinesonde. Experience with various other antennas had shown that it was desirable to increase the efficiency and improve the multilobing behavior of the transmitting antenna, as the Kinesonde measurements require a higher signal-to-noise ratio than a simple ionosonde. The resulting design offers significant advantages over previously available antennas for vertical soundings, particularly comparing cost vs. performance.

In some previous experiments of this type we have used a two-plane LPA with its Vertex Up (VULPA). The VULPA was itself a significant improvement over the "standard" delta-antenna often used in vertical soundings.

The VDLPA and the VULPA were compared using a computer program developed by our colleague, Dr. M. T. Ma. Some results of the computer program appear in fig. II-1. The power gain of the VULPA reaches that of the VDLPA (and its own mean value) at 2.8 MHz, although both designs have their longest elements self-resonant at 1.63 MHz. The low-frequency performance degradation, observed also in the full-scale structures, occurs because of the close proximity of the longest elements to the ground.

The height of the entire vertex-up structure must be increased to about 93.5m (from 53.5m) to obtain equal power gain with the VDLPA at 1.63 MHz. This would increase the required tower height by a ratio of 1.75 and the cost by about a factor of 3.

Another defect of the VULPA is the inevitable occurrence of multiple lobes above 4.6 MHz (or above 3.5 MHz with the higher mast).

Figures II-2 and II-3 show the comparison between the power gain patterns of these two LPA's in the E- and H-planes, respectively.

The design of the VDLPA shown in figs. 4 and 5 (Pt. 1) was itself a compromise to allow erection on a single mast; the dipole arms, which ideally should be horizontal, were declined at an angle (β) of 30°.

Modeling studies of a 1/50 scale model (fig. 4 (Pt. 1)) with our colleague P. Arnold, showed no significant lobe-splitting for $\beta = 14.25^{\circ}$; the $\beta = 30^{\circ}$ model revealed a 9 db lobe-split at 9 MHz. Thus some 63% of the antenna's design range is well-behaved.

The VDLPA at St. Santin (and another in Colorado) show a slow progressive performance decrease at about 6 f_{LO} (9.6 MHz) which appears to be caused by a deterioriating VSWR. The theoretical computer model does not predict this effect and its cause is not yet known.

Receiving Antenna System

Each of the four receiving dipoles (fig. II-4) is made of two parallel-connected #18 wires for an effective diameter of $\frac{1}{2}$ inch. They are self-resonant at about 5 MHz. The low height of the dipoles above the ground plane reduces phase variations with frequency due to ground reflections, as well as the dipole-dipole coupling but at the price of reduced signal power. Each dipole feeds a +9 db solid-state 0.5 MHz amplifier through a 4:1 impedance ratio balun. This configuration tends to lower the VSWR on the long (204-meter) coaxial transmission line and to reduce the effect of signals stray-coupled into the line.

The significance of antenna coupling to the spaced antenna experiment, only recently recognized, has received intensive study by our colleague L. S. Fedor in the past year. For experimental comparison, a method of measuring the lower-bound of the total antenna-system isolation was devised. These measurements show (see fig. II-5)

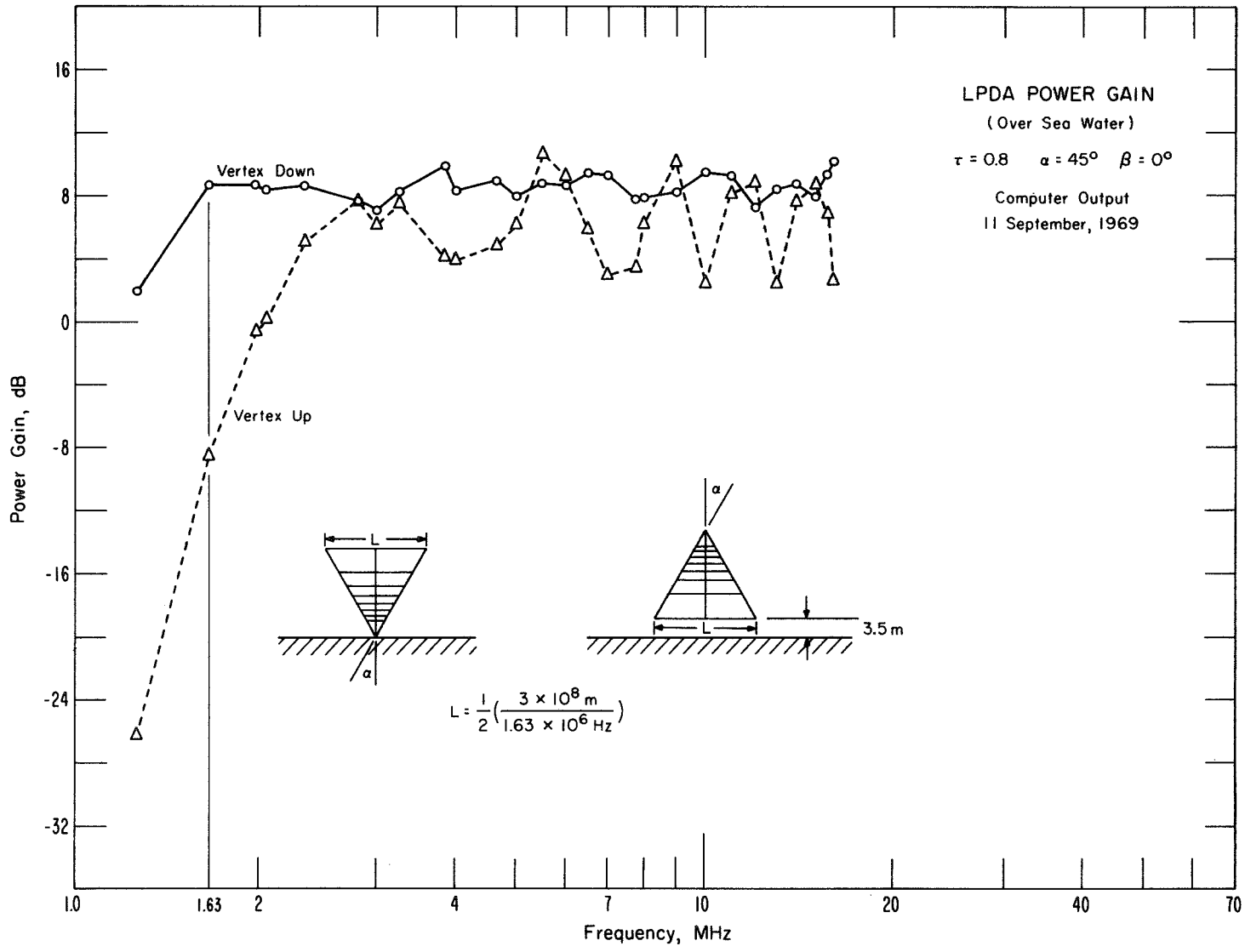

Fig. II-1. Comparison of the Power Gains for Vertex-Down vs. Vertex-Up LPA's.

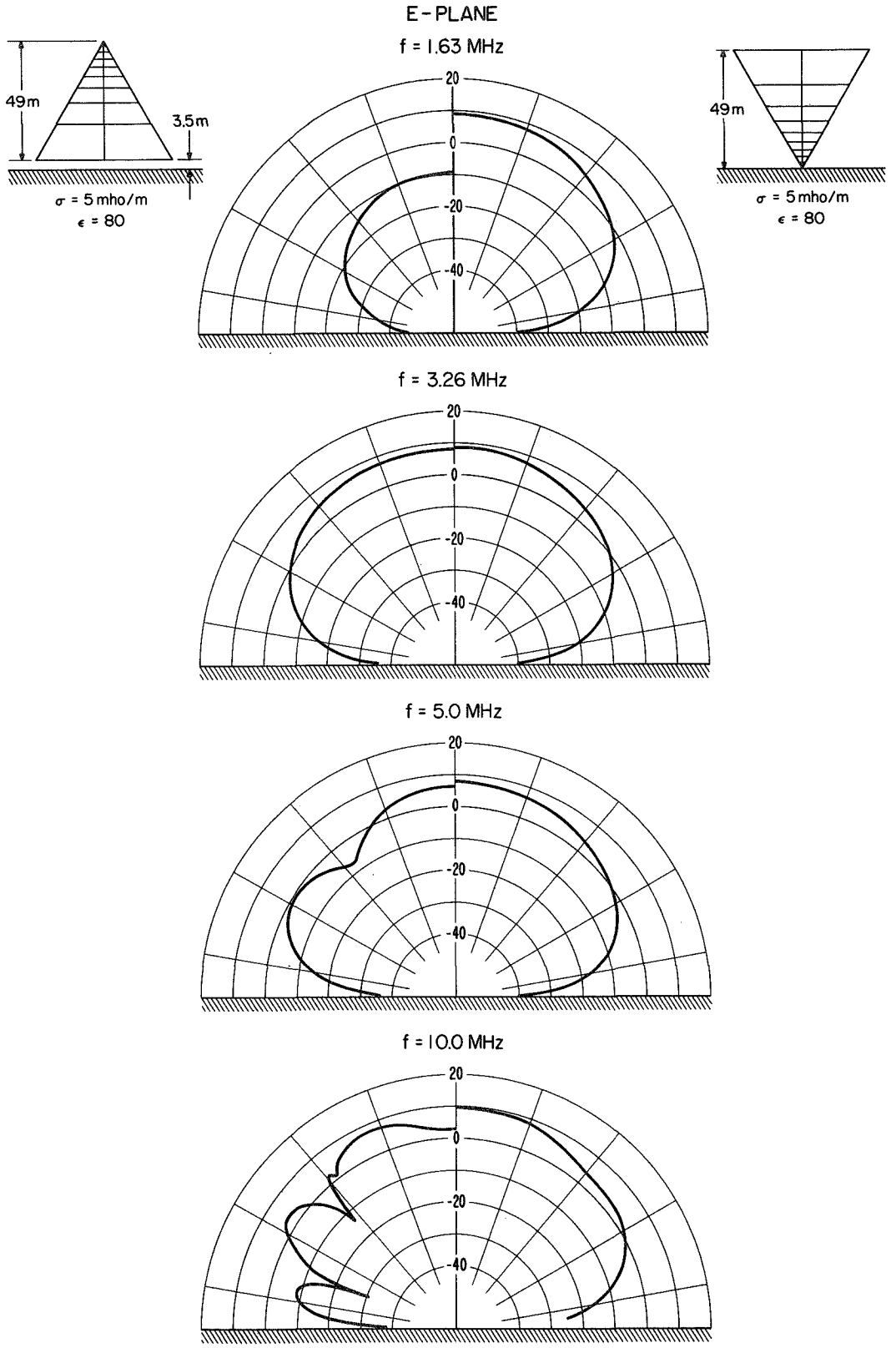

Figs. II-2 and II-3. E- and H-plane calculated power gain patterns of the vertex up (left half of each diagram) and vertex down (right half) Log Periodic Antennas.

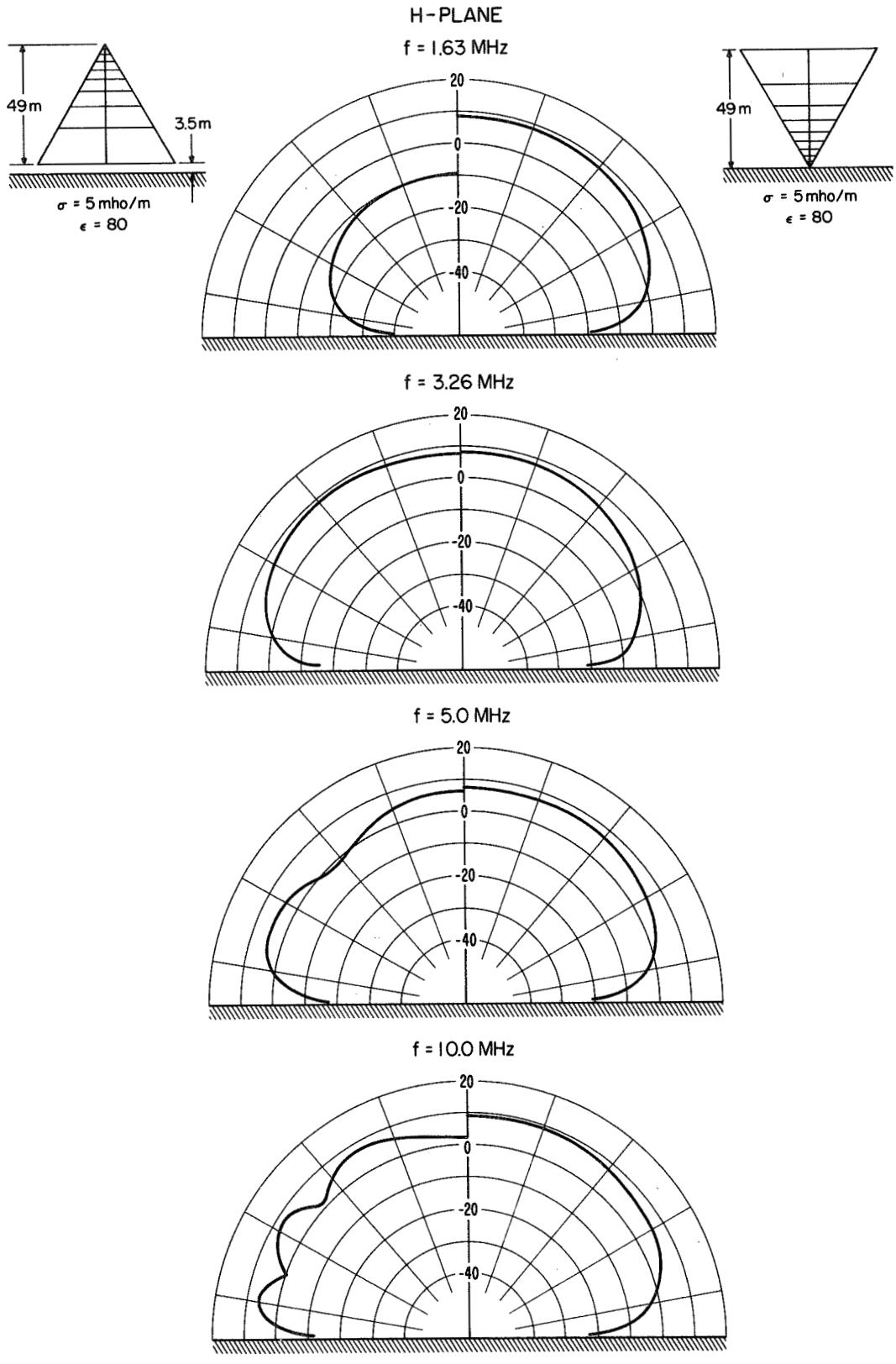

Fig. II-3. (See fig. II-2.)

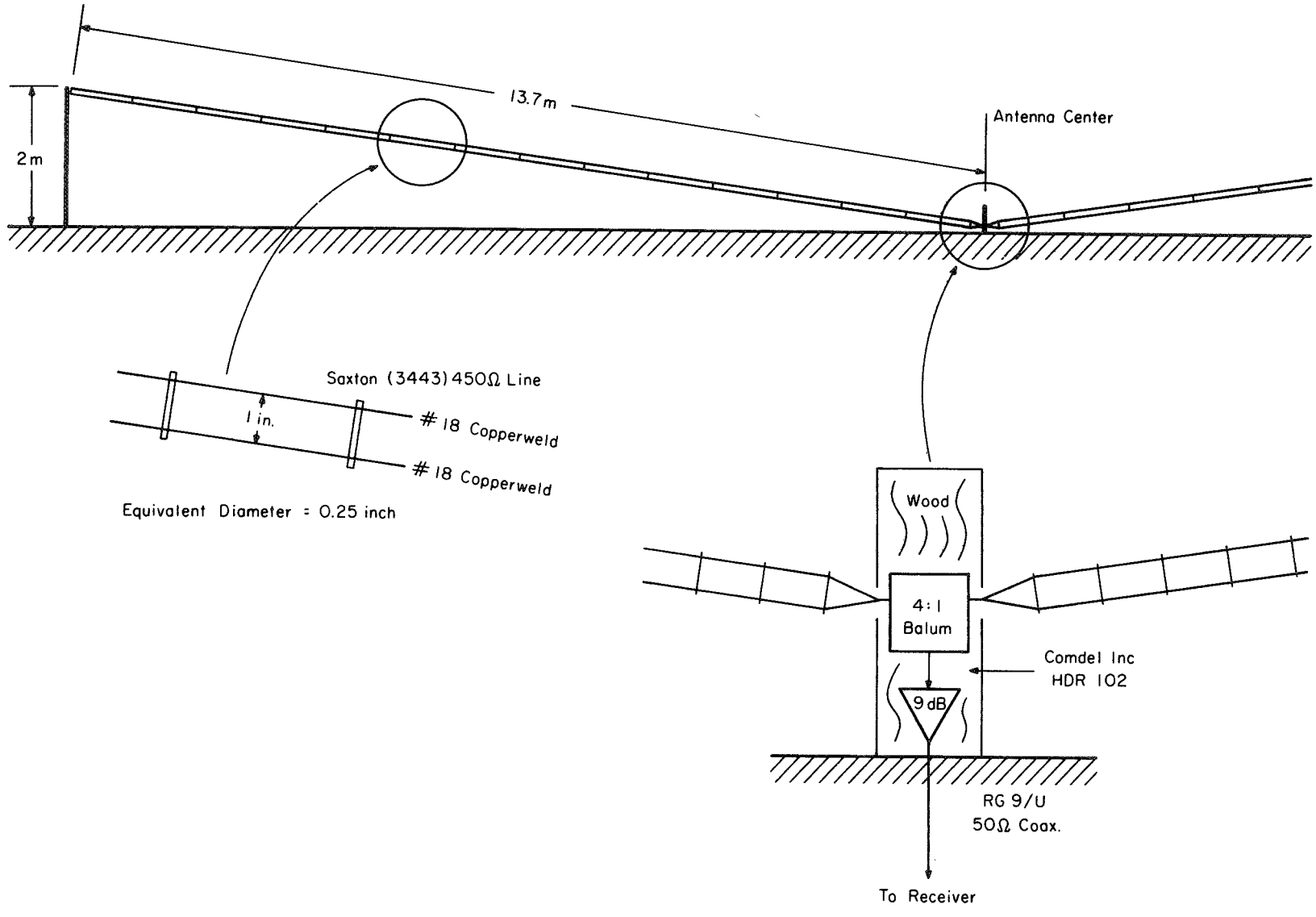

Fig. II-4. Receiving Antenna Dipoles.

that the total antenna-system isolation is greater than about -60 db at all frequencies of operation. The measurements also suggest that it is the cable-cable coupling that limits the total isolation at low frequencies as the values found there are all much lower than those predicted by a computer program (up to about 6 MHz). Beyond that, the influence of the upturned dipole arms, and actual ground inhomogeities, may influence the coupling behavior more strongly.

As expected, a higher isolation appears between antennas on the main diagonals of the array.

Receiving Antenna Commutation

The spaced antenna inputs to the receiver arrive at a digitally-controlled four-position Antenna Commutator Switch. This switch can also contribute antenna channel coupling, analogous to that discussed in the preceding paragraphs. A channel isolation of 45 db appears to be an acceptable minimum to assure velocity errors of less than 5%.

The present Kinesonde Antenna Switch is an improved re-design of the original unit. Figure II-6 compares the measured channel isolation of three antenna commutators. The modified version uses the same SPST reed relays as those of the original; but an isolation improvement exceeding 24 db was obtained by isolating the output signal bus from the four inputs by a copper plane connected to the chassis common.

Another design using SPDT reeds offer a further improvement of about 10 db for a total of 75 db channel isolation. Of equal importance, it assures that all the incoming transmission lines are terminated by their correct impedances, whether switched to the receiver or not; this reduces variations with frequency of the line-to-line and antenna-to-antenna coupling by preventing the periodic occurrence of very low impedances at the output port of the antenna-amplifier units.

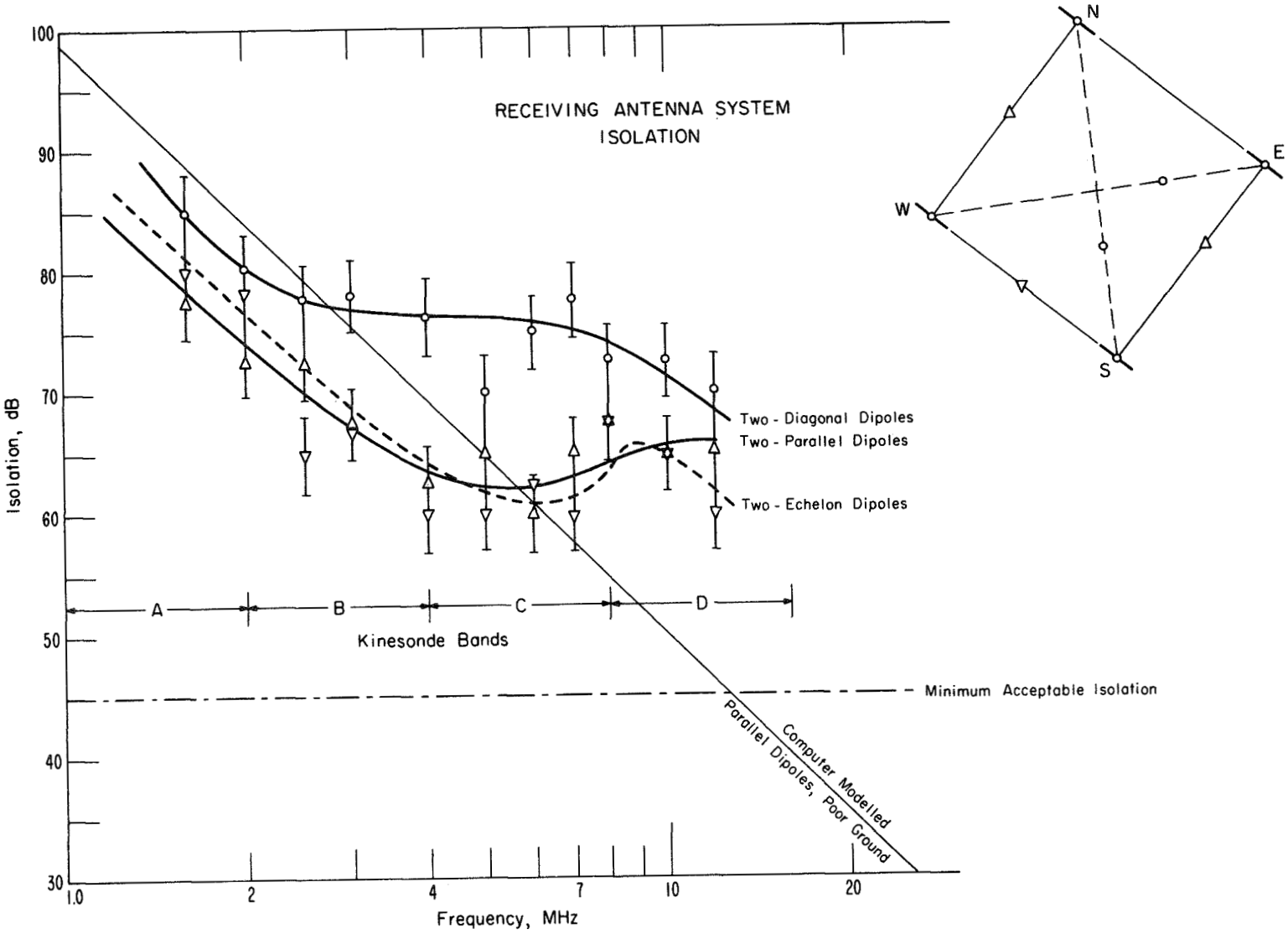

Fig. II-5. Receiving Antenna Isolation. Field measurements vs. frequency for various antenna relative orientations, compared with theoretical behavior. The minimum acceptable isolation is chosen (Fedor, private communication) to maintain drift velocity errors attributable to antenna coupling below 5%.

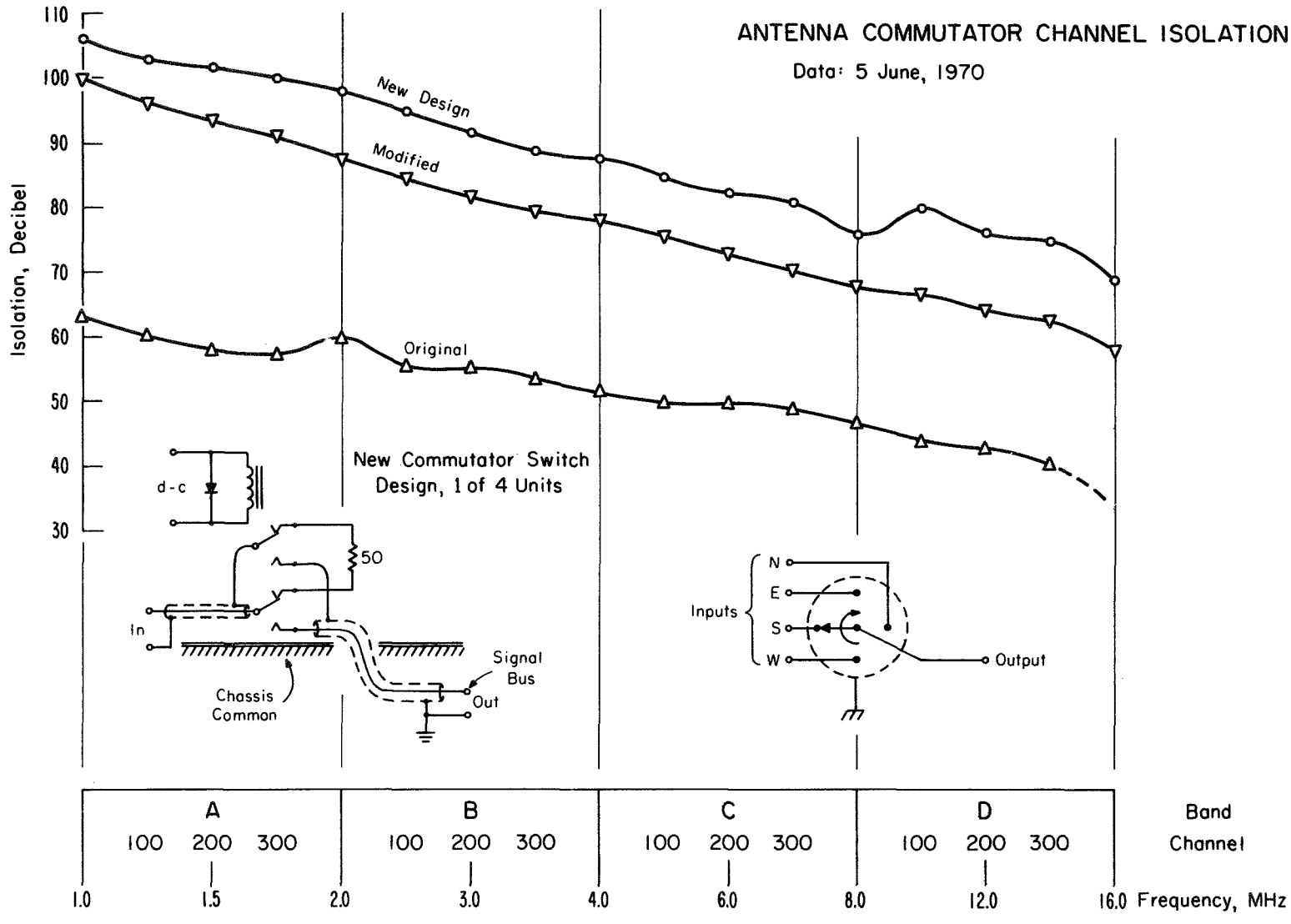

Fig. II-6. Antenna commutator channel isolation. Measured for three switch grounding and shielding designs. An isolation of 45 db is considered minimal.

Appendix III. Data Processing

Kinesonde recordings have been designed from the outset to be fully compatible with a general-purpose large computer for speed and economy in data reduction. Here we provide a description and illustrations of each significant step.

Editing: This program reads the (BCD) field tape, examines each record for parity, illegal characters, and other format errors, if any, adds time, date, frequency channel, etc., information, and writes each record in binary form at high density on a permanent tape. An example of the editing notes produced for each record is shown in fig. III-1. It contains a small sample of the numerical data from the beginning and end of the record, sorted by antenna and frequency, to permit checks on the plausibility of later results. This example has been chosen to show some of the (relatively infrequent) defects recognizable by the computer; the analysis of data from two channels of this particular example (four antennas, for frequencies 1 and 2) are illustrated throughout this discussion.

The amplitude and phase in any of the 24 channels of each record may be plotted by the computer on microfilm. Two such plots are compared in fig. III-2 to illustrate the similarities existing in the amplitude and phase measured at spaced antennas and spaced frequencies.

The Fast Fourier Transform: Several of the subsequent analysis steps employ the crosscorrelations among the 24 antenna/frequency channels taken in pairs. The amplitude (A) and phase (φ) define the complex amplitude $R(t) = A(t)e^{i\varphi(t)}$, and it is this quantity (not A alone, as available from earlier experiments) which the theory of diffraction relates to the scattered wave field in the ionosphere.

One of the significant advances of practical mathematics in recent years is the development of the Fast Fourier Transform algorithm (FFT), with which processes of Fourier transformation and convolution

Fig. III-1. Editing notes produced in the first step of the sequence of computer operations on Kinesonde digital tape recordings. Information on record number, date, time, station location, radio frequency, receiver gain, and range gate are merged with the appropriate channels of complex amplitude. The Editing Notes repeat this information and give a sample (the first and last 5 data words) of each of the 24 frequency-antenna channels. The first 3 digits of each word represent $\log_{10} A$; the last two digits represent ϕ, in units of $\frac{2\pi}{80}$ radians of the complex amplitude $A \exp(\phi)$. Various record format faults (illegal BCD characters, parity errors, record-length pecularities, etc.) found in editing, are noted. Unless very numerous these faults do not seriously affect statistical treatment of the data.

```
30 JAN 1970  09-12-00 GMT  SEMUR, FRANCE   TAPE K-V      LOG SEQ. NO. 21


CHANNEL-A BIT PATTERN (11111) IN     SET    1   ANTENNA N   FREQUENCY 6
/ / / INCOMPLETE / / /      SET    1
(ILLEGAL CHARACTERS)   SET  53   ANTENNA W   FREQUENCY 4        :    8   (0)   1    9
(ILLEGAL CHARACTERS)   SET 133   ANTENNA N   FREQUENCY 2        :    6   (0)   6    5
(ILLEGAL CHARACTERS)   SET 183   ANTENNA E   FREQUENCY 3        :    5   (0)   5    8
(ILLEGAL CHARACTERS)   SET 515   ANTENNA S   FREQUENCY 2        :    7   (=)   3    4
(ILLEGAL CHARACTERS)   SET 561   ANTENNA W   FREQUENCY 5        :    6   (0)   8    1
(ILLEGAL CHARACTERS)   SET 711   ANTENNA S   FREQUENCY 2        :    4   (=)   9    1
(ILLEGAL CHARACTERS)   SET 757   ANTENNA W   FREQUENCY 6        :    2    6    6   (0)
(ILLEGAL CHARACTERS)   SET 765   ANTENNA W   FREQUENCY 4        :    5   (0)   6    4
(ILLEGAL CHARACTERS)   SET 963   ANTENNA W   FREQUENCY 6        1    :   (0)   4    8
ARRAY  MAPLPHAS  CANNOT HOLD ALL THE INFORMATION TRANSMITTED.   THE FIRST 24,000 VALUES WILL BE USED.
 1000 SETS WERE EXPECTED IN RECORD   18 WHEREAS  1001 SETS WERE ACTUALLY FOUND BY SUBROUTINE TAPEDIT.   THERE ARE   1 SHORT SETS.
FIELD TAPE RECORD 18 CONTAINS 4.0 MINUTES OF RECORDING.    24000 AMPLITUDE AND PHASE VALUES COUNTED.

30 JAN 1970  09-12-00 GMT  SEMUR, FRANCE                                  TAPE RECORD  18                4.0 MINUTES
 CHANNEL     1 = 1.6113 MHZ (GAIN,1A),  115.5 KM       2 = 1.6163 MHZ (GAIN,1A),  115.5 KM       3 = 1.9438 MHZ (GAIN,1A),  118.5 KM

  SET  ANTENNA  N        E        S        W          N        E        S        W          N        E        S        W

    1        64 43    999 99   999 99   999 99      51 71   999 99   999 99   999 99      91 19   999 99   999 99   999 99
    2         5  3      6  3     6  3    33 37       5  3    66 19    73  3    41 66      87 20    86 12    53  9    95 18
    3        46  4     72 74    63 63    33 16      59 33    62 22    58  8    40 43      80 15    95  9    79 11    90 16
    4        61  2     68 77    52 69    44  0      72 34    74 27    35 16    49 34      89 10   102  8    97 10    89 11
    5        71  5     72 84    55 74    63  4      77 35    79 30    53 27    61 33      84  6    96  7   106  9    97  6
  996        74 52     95 51    70 49    51 51      83  2   102 79    82  3    73  2      72 52    81 63    52 56    83 45
  997        67 50     95 50    81 51    61 52      83 80   103 78    92 80    73 80      63 46    79 66    76 66    73 47
  998        65 44     37 46    88 49    52 48      74 76    99 77    95 78    69 77      67 26    50 76    85 71    58 43
  999        60 38     80 42    83 46    50 42      64 69    92 74    96 75    58 74      81 20    65 11    78 74    57 27
 1000        62 33     73 38    76 44    53 36      60 63    79 72    87 74    48 66      87 16    77 11    64  7    77 19

30 JAN 1970  09-12-00 GMT  SEMUR, FRANCE                                  TAPE RECORD  18                4.0 MINUTES
 CHANNEL     4 = 1.9488 MHZ (GAIN,1A),  118.5 KM       5 = 2.4025 MHZ (GAIN,1B),  126.0 KM       6 = 2.4075 MHZ (GAIN,1B),  126.0 KM

  SET  ANTENNA  N        E        S        W          N        E        S        W          N        E        S        W

    1       100 37    999 99   999 99   999 99      80 27   999 99   999 99   999 99     999 99   999 99   999 99   63 32
    2        97 43     82 43    89 45   106 39      84 13    78 83    47 50    70 22      89 26    74 22    43 70   78 28
    3        72 43     78 31    84 42    99 39      80 15    79 82    65 71    83 20      85 20    74 22    52 88   91 28
    4        40  8     73 14    57 35    63 37      50 21    69 67    67 71    81 19      84 27    60 90    56 89   85 29
    5        60  5     77 10    65 22    48  4      50 34    77 59    69 66    56 26      46 38    61 70    55 88   65 30
  996        57 67     68 75    61  2    75 68      86 31    93 40    88 33    88 31      86 44    87 52    89 44   90 44
  997        41 57     55 64    75  3    63 66      84 34    87 44    88 36    85 34      83 43    77 53    88 48   85 47
  998        70 47     76 43    64  5    55 59      64 36    75 43    82 40    73 38      69 43    69 53    76 50   75 48
  999        83 43     96 40    32 20    71 46      43 29    65 35    66 41    33 30      46 41    67 47    63 48   51 44
 1000        87 41     97 38    80 38    85 41      63 13    75 28    49 32    62 89      57 24    77 38    56 38   54 28

FIELD TAPE RECORD 18 WITH ID [30 JAN 1970  09-12-00 GMT  SEMUR, FRANCE   TAPE K-V      LOG SEQ. NO. 21] WAS WRITTEN ON L.U. 7.
     E-O-F BEFORE REC.  19
     E-O-F BEFORE REC.  19
```

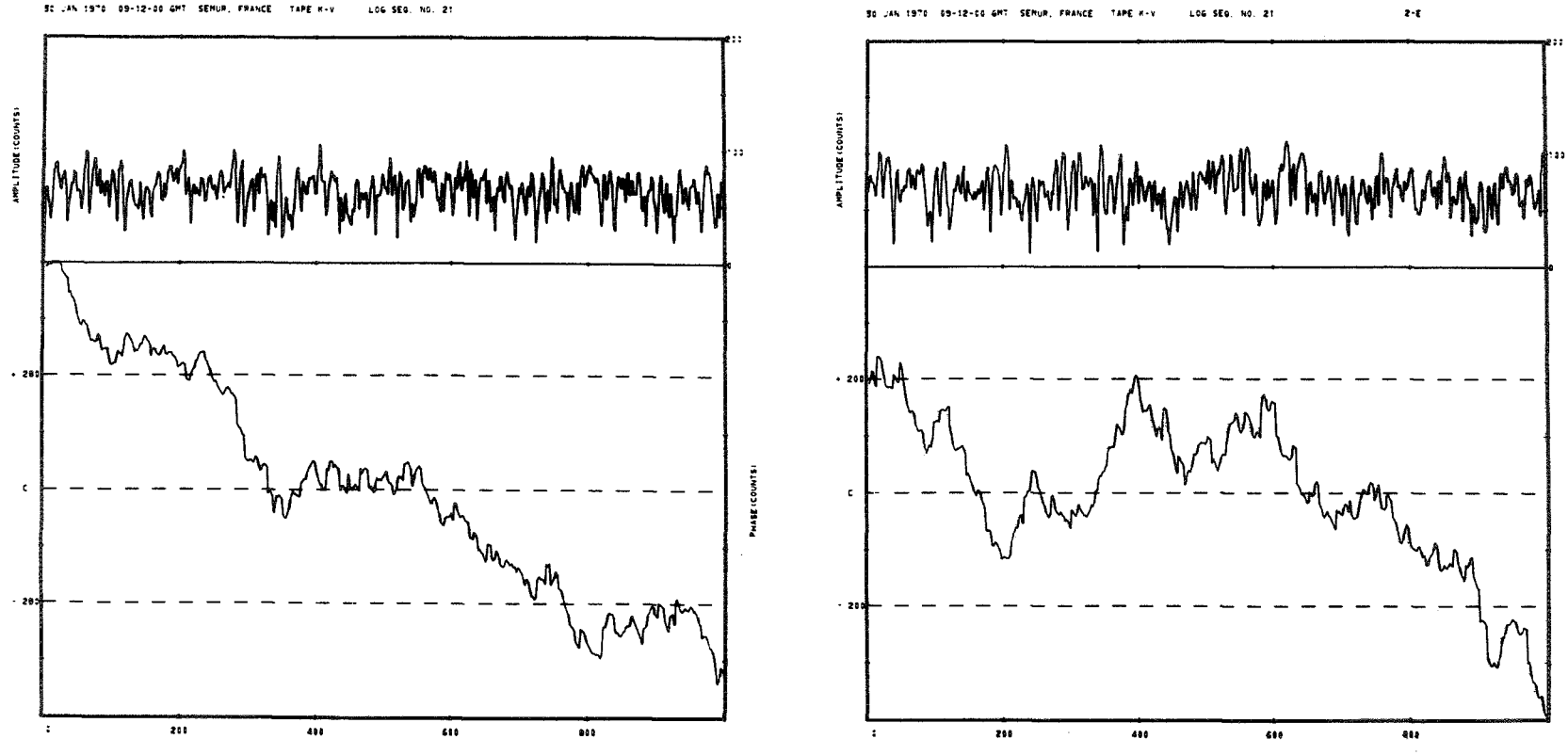

Fig. III-2. Two of 24 simultaneous complex amplitude time-series, recorded at Bierre-lés-Semur 0912 UT, 30 January 1970. These two figures represent a part of the data input to the FFT and "correloid" calculations illustrated in the following figures. The sample at left represents the amplitude (top) and phase (bottom) each 0.24 sec. during 4 minutes, at 1.6113 MHz observed at the North antenna. The sample at right shows the amplitude and phase at the East antenna and at a frequency 50 kHz higher. An N(h) profile calculation locates the reflection heights of these two frequencies at 105.6 km, separated by a 'vertical space lag' of 39 meters. The horizontal space-lag, of course, is given by the antenna separation, 130 meters. The amplitude of the complex cross correlation between these channels is shown by the Λ-symbols in figure III-5c; it has a maximum value of about 0.8 at a time lag of about -0.3 seconds.

of discrete series may be performed with great efficiency by digital computers. Prior to the invention of the FFT it was usual practice to calculate the power spectrum of a discrete series from the Fourier transform of the "lagged product" expression for the crosscorrelation,

$$\rho(\tau) = \left\langle R_1(t)\, R_2^*(t+\tau) \right\rangle .$$

(Here, for simplicity, a dependence upon time t only is shown, although in our problem ρ is 4-dimensional, depending upon the three spatial lags, x, y, z.)

Although we are mainly interested in the function ρ, with the FFT is is actually now more expedient to obtain the Fourier amplitude spectrum of the original time series by direct application of the FFT, and then to obtain ρ by a second application of the FFT.

A typical 4-minute Kinesonde record includes 24,000 samples of amplitude and phase distributed over three pairs of closely-spaced frequencies and four antennas. Usually the analysis seeks to obtain 3-dimensional drifts at 3 heights, necessitating the calculation of 36 correlation curves for each frequency pair (108 in all), each consisting of the correlation for, say, 50 time-lags. (Fewer are used in the subsequent 'correloid' analysis, but it is not known in advance what the characteristic time-scale of the correlation will be.) If, as usual, the analysis employs the complex amplitude, this in effect doubles each of the figures above. In any case, the FFT brings this sizable computational task into reasonable balance using a fast computer, as the table makes clear by comparing calculation times by the FFT with the lagged-product calculation times:

Correlation Computation Times (CDC 3800), 4-min. Kinesonde Recording

	By Lagged Product	By FFT
Amplitude only	4 1/2 min.	3/4 min.
Complex	9 min.	3/4 min.

Complex Spectra and Correlations: The results of the FFT operations are obtainable for inspection on graphs generated directly from the digital tape data by a computer-driven optical plotter.

Figure III-3 represents the result of the first application of the FFT to the complex amplitudes observed at 4 antennas and at two closely-spaced frequencies. The four resulting positive (right) and negative (left) spectra for each frequency are superimposed in the graphs; the near identity of the spectra is a first indication of statistical similarity among the antenna/frequency channels. This is more evident from the four complex auto-correlations, which are obtained in the next step.

The bell-shaped curves of fig. III-4 represent the amplitude of the complex crosscorrelations of complex amplitude observed at spaced frequencies and spaced antennas. There are $n(n+1)/2$ correlations among n antenna-frequency channels, or 36 in the typical case described here. Each cross-correlation is a time-lag cross-section in a particular spatial direction; the various directions may be visualized from the "box" of the adjacent figure. The top and bottom faces represent the 4-antenna array for the lower and higher members of a frequency pair. Only the diagonals eminating from the west antenna are drawn for clarity, but all possible combinations are employed in the analysis.

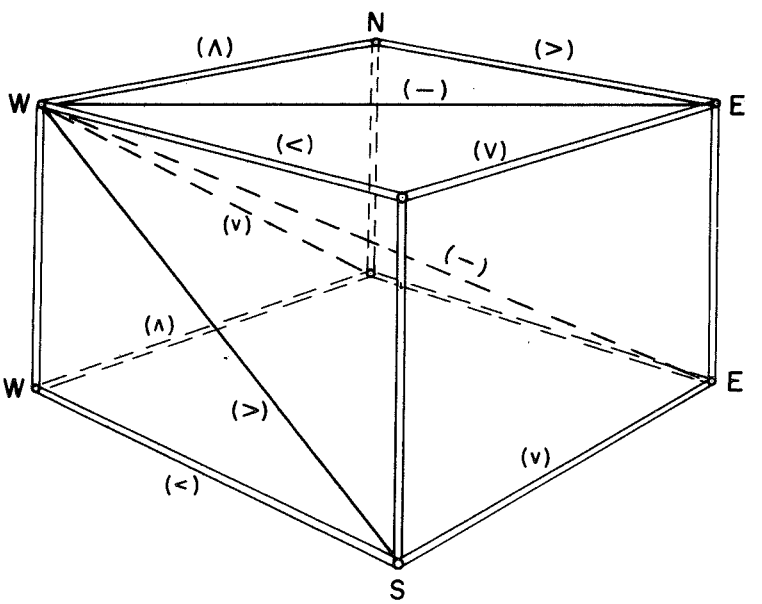

Fig. III-3. Amplitude Spectra $F(\omega)$ for negative and positive fading frequencies (left and right, respectively), for the complex amplitudes of echoes at two closely-spaced radio frequencies (top and bottom). The spectra extend from $|\omega| = 0.026$ to 13 radians/second, corresponding to limits imposed by the record length (4 minutes) and the sampling frequency (0.24 seconds). Spectra for 4 antennas are superimposed in each figure providing an indication of their statistical similarity.

The spectra are obtained by application of the Fast Fourier Transform to the echo complex amplitude -- in this case, to the two time series illustrated in fig. III-2.

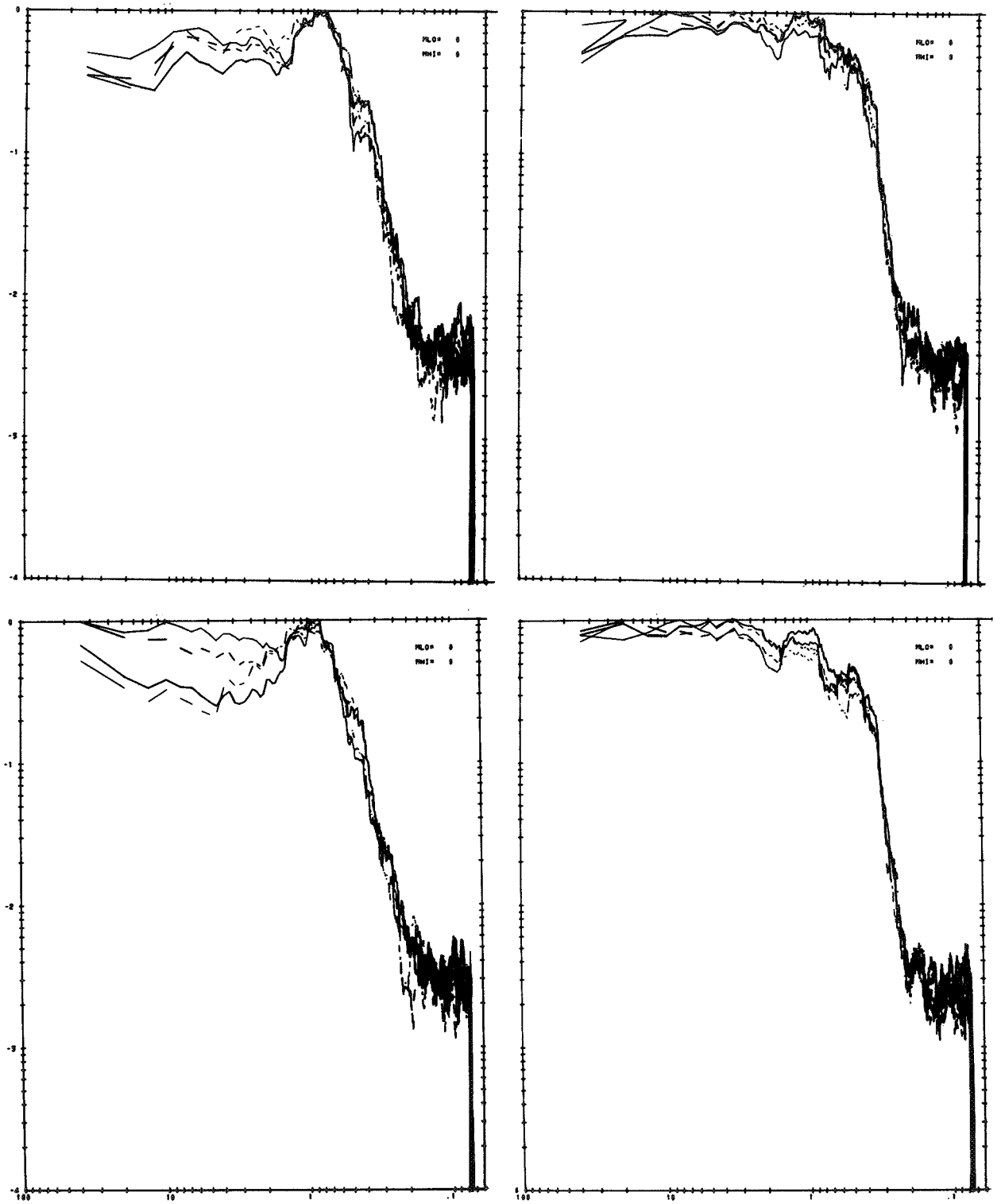

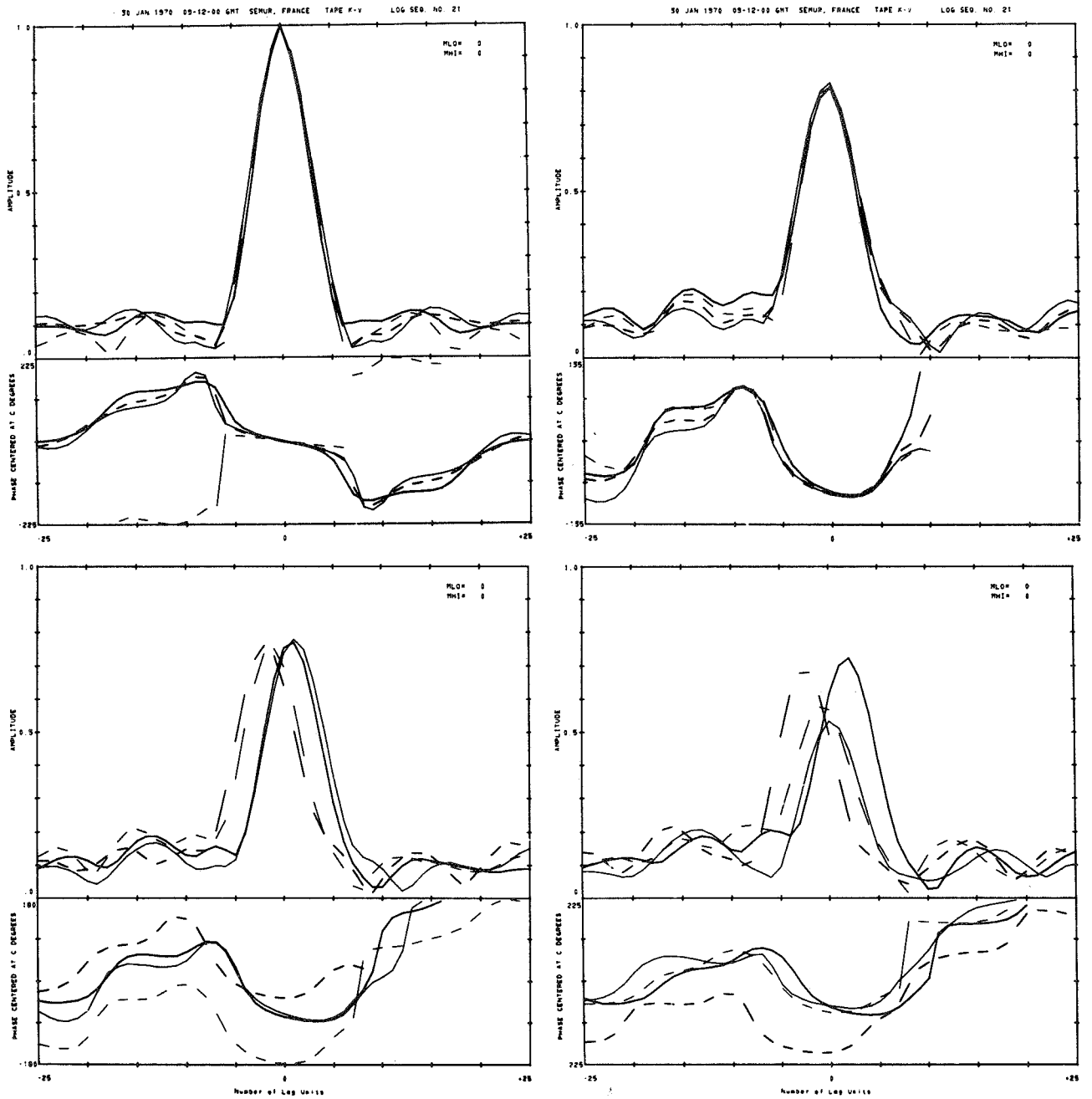

Fig. III-4. Complex correlations obtained by applying the FFT to various antenna-frequency combinations of the amplitude spectra shown in the preceding figure. A total of 36 correlation curves are obtained from the time series at two frequencies and 4 antennas, of which only 16 are shown here. In the upper left figure the amplitude and phase angle of the autocorrelations of the complex amplitude at four antennas, for one frequency, are superimposed. Four very similar autocorrelations for the second frequency are also available, but are not shown. The upper right figure represents the "Common-Antenna, Frequency-Crosscorrelations"; the four curves are of course nearly identical, but maximize at a slightly non-zero time lag. The two bottom figures include a total of eight of the frequency-antenna 'diagonal' crosscorrelations; pairs of parallel "face" diagonals give closely similar curves (left figure), while the "interior" diagonals of the antenna-frequency "box" give distinctly different cross-correlations (bottom right figure).

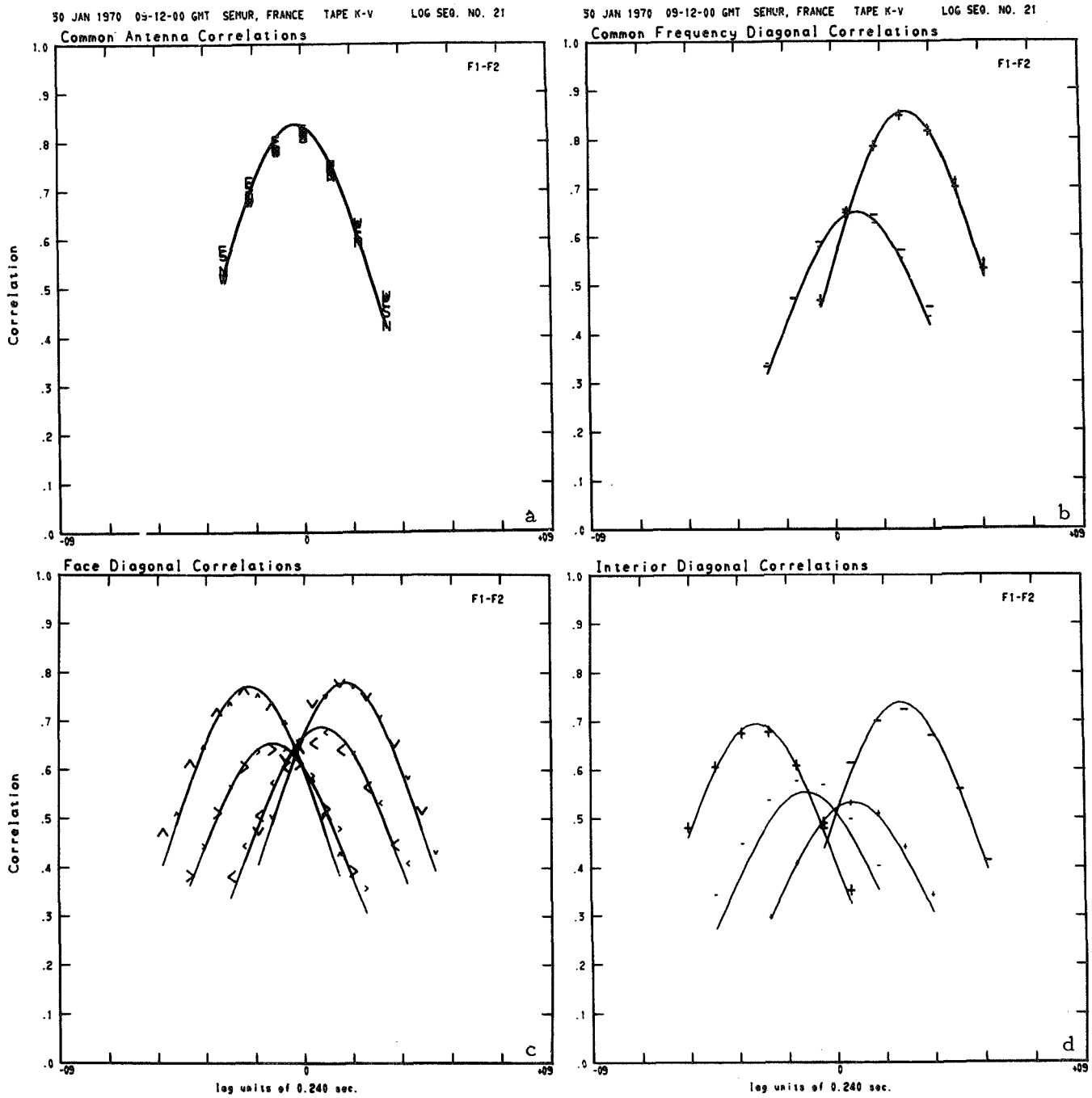

Fig. III-5. Correloid cross sections (continuous lines) compared with the observed correlation values from which the correloid is determined, to illustrate the degree of fit achieved. Part a, for example, compares the frequency cross correlations observed at 4 antennas (NESW) (first illustrated in fig. III-4 upper right) with the curve calculated from the best-fit function. The "common frequency diagonals" lie in the horizontal plane, and so the higher and lower frequencies (large and small) symbols, respectively) each provide data fitting the two orthogonal diagonals of the "box" (page 79). A similar degree of observational redundancy can be seen in the "Face diagonal correlations" (lower left), while the four interior diagonals of the box are of course "observed" by one antenna-frequency pair each.

Correloid Analysis: The first statistically rigorous treatment of the now classical "correlation analysis" problem was developed during the first year of the present program. It employs the basic definitions first laid down by Briggs, Phillips and Shinn (1950) and Phillips and Spencer (1955) that identify the drift velocity of the radio echo pattern across the ground as the velocity of an observer who adjusts his rectilinear motion so as to observe, on the average, a minimum of echo fading. Other quantities, such as a superimposed random velocity, scale size, anisotropy, orientation, and lifetime of the irregularities, all in the moving echo pattern, are also defined.

Although these concepts are inherently statistical, and have long been applied to more-or-less statistically-valid data samples, previous methods of analysis have fallen far short of a full statistical treatment of the problem. In their original papers Briggs et al., Phillips and Spencer showed that the desired quantities could be obtained by 'exact' calculation from the various correlations among 3 spaced antennas. It was implicitly assumed that the experimentally-obtained correlations were exact, and by using only 3 antennas no decisive test of this assumption was possible.

Gusev and Mirkotan (1960) suggested that the entire matter might usefully be escalated to three spatial dimensions, using closely-spaced probing frequencies to provide information regarding the vertical components of motion and structure; once again, the analysis method was conceived as an exactly-determined problem. Only a very few results, of uncertain meaning, have been published from the Soviet work in this field.

The statistical nature of the problem was discussed very thoroughly by Banerji (1960), who showed how the errors of determining the various wanted parameters could be related to the covariances among the correlations. Awe (1964) illustrated the matter with some actual data, emphasizing the estimation of the degree of independence among the

correlation values. All of the foregoing developments were combined in the statistically-rigorous least-squares treatment of the problem by Fedor (1967), which is employed in the analysis of our data. The correlation curves are taken as the cross sections of a generalized four-dimensional correlation ellipsoid (or "correloid") of the following form:

$$\rho(\xi_1, \xi_2, \xi_3, \tau) = \exp\left\{-\tfrac{1}{2}\left[\frac{(\xi_1 - V_1\tau)^2}{d_1^2} \frac{(\xi_2 - V_2\tau)^2}{d_2^2}\right.\right.$$

$$\left.\left. + \frac{(\xi_3 - V_3\tau)^2}{d_3^2} + \frac{\tau^2}{b^2}\right]\right\}$$

V_1, V_2, V_3 are three orthogonal components of motion of the correloid along its three principal axes (directions ξ_1, ξ_2, ξ_3) of length d_1, d_2, d_3. The parameter b represents the correlation lifetime of the structure. Coordinate transformations relate these quantities to the North, East, and vertical orientations of interest, resulting in ten unknown coefficients to be determined by least squares in such a manner that the resulting figure best-fits the observed correlations. Fedor's process applies statistical weights to the correlation values determined by their variance and independence. From this are estimated the variances of the ten coefficients and in turn the confidence limits for the parameters of interest are found. The "fit" of the final correloid to the correlation values from which it was determined is illustrated in a series of graphs such as the examples shown in fig. III-5.

The physically meaningful parameters of the correloid, together with its 10 coefficients, are summarized on a single page of computer output as in the example of fig. III-6. A key to the content of this tabulation is given in fig. III-7.

CORRELOID ANALYSIS

RECORD NO 18 30 JAN 1970 09-12-00 GMT SEMUR, FRANCE TAPE K-V LOG SEQ. NO. 21 COMPUTED 02/18/71

WITH DEL TAU = 0.24

N(H) 12 0 /0./40 10 FH = 1.18398

FREQ	MHZ	LOG FN	N/CC	WL	GATE	HEIGHT
***1	1.6113	0.2072	0.3220	186.1	115.5	105.612
***2	1.6163	0.2085	0.3240	185.5	115.5	105.651
3	1.9438	0.2886	0.4686	154.2	118.5	108.438
4	1.9488	0.2898	0.4710	153.8	118.5	108.485
5	2.4025	0.3807	0.7159	124.8	126.0	114.563
6	2.4075	0.3816	0.7189	124.5	126.0	114.682

COMMENTS

DRIFT VELOCITY

V = 232.12 + 10.79 M/S
THETAH(M) = 203.09 + 3.08 DEG
THETAV(M) = 0.15 + 1.15 DEG

VH = 232.11 + 10.79 M/S

VX = -91.03 + 12.35 M/S
VY = -213.52 + 10.91 M/S
VZ = 0.59 + 4.67 M/S

THETAH(G) = 198.81 DEG
VE = -74.82 M/S
VN = -219.72 M/S

VL = -97.46 M/S
VT = 210.66 M/S
RHO = 295.60 DEG

CORRELOID PARAMETERS

PHI(M) = 87.54 DEG
PSI = 89.70 DEG
OMEGA = 85.05 DEG

DV = 173.71 + 14.09 M

DI = 185.79 M
DJ = 174.73 M
DK = 64.93M

PHIC(M) = 87.37 DEG
CI = 185.79 M
CJ = 174.17 M

AREA = 101.66+003 M2
VOLUME = 662.18+004 M3
(I/J)(J/K)(I/K) = (1.063)(2.691)(2.861)

PARAMETERS OF RANDOM MOTION

VC PRIME = 252.23 + 13.21 M/S
V PRIME = 274.09 + 14.42 M/S
VC = 98.71 + 14.95 M/S

TAUV = 0.69 SEC

B = 1.76 + 1.72 SEC
VC/V = 0.43 + 0.05

SCINTILLATION PARAMETERS

S4	0.606	0.707
S2	0.293	0.322
RMSP	0.93	0.87
MSP	0.87	0.76

ESTIMATE OF FIT

MEAN SQ RESIDUAL = 0.005
NO OF POINTS USED = 220
EQ DEG OF FREEDOM = 7

SIGMA UPPER(90%) = 0.009

SIGMA LOWER(90%) = 0.004
STD DEV(R=0.593) = 0.046

	A11	A22	A33	A44	A12	A13	A14	A23	A24	A34
1	2.8309-005	3.2718-005	2.2724-004	1.9095+000	-3.6156-006	-8.9147-006	4.9022-003	3.3112-005	1.3161-002	6.2062-003
4	2.8994-005	3.4258-005	2.3567-004	2.1084+000	-6.3909-007	-3.7054-006	5.1439-003	3.5017-005	1.4551-002	6.8605-003
5	2.8994-005	3.4258-005	2.3568-004	2.1084+000	-6.4116-007	-3.7041-006	5.1437-003	3.5016-005	1.4551-002	6.8603-003
6	2.8994-005	3.4258-005	2.3568-004	2.1084+000	-6.4109-007	-3.7040-006	5.1437-003	3.5016-005	1.4551-002	6.8603-003

COMPLEX CORRELATIONS. LO PASS X-Y FILTER = 0 HI PASS X-Y FILTER = 0
LO PASS AP FILTER = 0 HI PASS AP FILTER = 0

0 -1 0 -2 -2 0 -1 -1 1 0 0 1 2 1 0 0 0 2 1 -1 0 -2 -1 0 -1 -2 -2 0 -1 0 1 0 -1 0 1 0

Fig. III-6. Sample computer output, Correloid Analysis.

CORRELOID ANALYSIS

KINESONDE RECORD NO. DATE TIME OBSERVING LOCATION

DATE COMPUTED

WITH DEL TAU = Time lag (seconds) among points used in the analysis.

Electron density profile information for the six Kinesonde frequencies used. Adjacent stars show the frequencies used in the correloid analysis; o, x, or z indications of echo type.

COMMENTS

Space reserved for notations on the result of the analysis.

DRIFT VELOCITY

V = Total speed; standard error, m/s
THETAH(M) = Magnetic azimuth (E of N) of V
THETAV(M) = Angle to horizontal of V
VH = Horizontal component of V
VX, VY, VZ = East, North vertical components of V
THETAH(G) = Geographic azimuth of V
VE, VN = Geographic components of V
VL = Component of V along geomag. field
VT = Component transverse to field
RHO = Angle of V_T from mag. meridian (cw)

SPATIAL CORRELOID (at $R=e^{-\frac{1}{2}}$)

PHI(M) = Magnetic az. of maj. axis
PSI = Zenith angle of maj. axis
OMEGA = Zenith angle of median axis
DV = Spatial scale in direction of V (meters).
DI, DJ, DK = Major, median, and minor semi-axes of ellipsoid.
PHIC(M) = Mag. az. of enveloping cylinder
CI, CJ = Major, minor axes of enveloping cylinder.
AREA of ellipsoid in sq. meters
VOLUME of ellipsoid in cubic meters
Axial Ratios of ellipsoid

PARAMETERS OF RANDOM MOTION

VC PRIME = RMS of mean and random drift
V PRIME = Apparent velocity } in direction of V
VC = Random velocity }
TAUV = Mean 'duration' of irregularity for stationary observer
B = Irregularity lifetime
V_C/V

SCINTILLATION PARAMETERS

	(freq. 1)	(freq. 2)
S4 = RMS power fluctuation		
S2 = RMS amplitude fluctuation		
RMSP = Root mean Sq. phase variation		
MSP = Mean Sq. phase variation		

(all averaged over 4 antennas).

ESTIMATE OF FIT

MEAN SQ. RESID.: RMS correlation residuals divided by Deg. of Freedom
NO. OF POINTS USED: Total no. of correlation values used in Least Squares fit.
EQ. DEG. OF FREEDOM: No. of degrees of freedom if the residuals were distributed as χ^2.
SIGMA UPPER, SIGMA LOWER } 90% probability that the true value of MEAN SQ. RES lies between these limits.
STD. DEV(R=0.xxx) Estimate of standard error of autocorrelation at 0.xxx level.

The ten coefficients, A_{11} -- A_{34}, defining the correloid are listed here on the last line. The first (unweighted) and last three of a variable number of iterations performed to determine best statistical weights for the input data are listed to show the convergence achieved.

COMPLEX or AMPLITUDE (only) correlation indicator. LO or HI PASS Complex (XY) or Amplitude (A), Phase (P) filter specifications.

Fig. III-7. Key to tabulation (fig. III-6).

The spatial correloid itself is visualized with the aid of fig. III-8. If the Kinesonde were a direct, rather than remote probe of the ionosphere, this figure could readily be taken to represent the size, shape, and orientation of an average irregularity; the application of the analysis to in situ probes of other fluids would be an interesting and informative investigation. In the present application the correloid must be interpreted with the aid of scattering and diffraction theory to deduce the corresponding ionospheric properties.

Noise Filtering: The Kinesonde has been designed to assure adequate signal-to-noise performance under most conditions; more than 70 db dynamic range is available for amplitude measurements, with a resolution of 200 steps or 0.5%. However, noise of substantial magnitude is often present within the Kinesonde frequency channels; even if the noise level is low, because we use the time variations (fading) of echo amplitude as the 'signal' employed in crosscorrelation, the 'signal' to noise ratio may become poor if the fading is shallow. Thus the system digitization error of $\pm$ 1 count in amplitude has a far more serious effect upon shallow fading of $\pm$ 10 counts variation than upon deep fading of $\pm$ 100 counts variation. Fortunately, however, shallow fading is almost always slow fading (the converse is not necessarily so), and the noise may be effectively removed by filtering. The filter is most easily applied to the original data (time series), but the effect is best judged from its power spectrum in the frequency domain. Perhaps the (conceptually) simplest filter is the running average, in which all values within a specified "window" are given equal weight. It, and several other simple choices, are undesirable in careful work because they pass "side lobes" in addition to the desired frequency band. We employ a digital "RC" filter, so-termed by analogy with electrical circuits. The observed time series $X(t_n)$ (which may be complex) may be filtered to obtain the time series $Y(t_i)$, by the relation

$Y(t_i) = \alpha \sum_{n=1}^{i} (1-\alpha)^{i-n} X(t_n)$, where α is a parameter which determines

the band pass of the filter, and is obtained from $\frac{\alpha^2}{4(1-\alpha}$ = $\mathrm{Sin}^2(2\pi f_c/f_N)$. Here, f_N is the sampling frequency (4.167/sec. for the Kinesonde) and f_c is the desired cut-off frequency. The frequency response of this filter is proportional to $(1+Q^2)^{-r}$ where r is the number of passes of the data "through" the filter, and $Q = \frac{\mathrm{Sin}(2\pi f/f_N)}{\mathrm{Sin}(2\pi f_c/f_N)}$. Figure III-9 shows the frequency response of this filter for $\alpha = \frac{1}{2}$ and for r = 1, 2, 4. Also shown is the frequency response of a simple moving average. Evident advantages of the RC filter are the absence of side lobes, sharp roll-off, and the ability to control the "attenuation" of the filter by multiple applications.

Validation of Correloid Analysis by Computer Simulation: One consequence of the prevailing uncertainty of interpretation to which spaced-antenna measurements are subject, is an equal measure of doubt concerning the methods used in analyzing the measurements. Doubts of this kind in fact led from näive "similar fades" analyses of the observations to the rigorous definitions of correlation analysis (Briggs, Phillips and Shinn, 1950), and it might be argued that a correctly-applied correlation analysis is not subject to such doubts because of the rigor of the definitions. However, because the problem is inherently statistical, there remains the possibility that the analysis seeks to extract too much information from the data; the parameters wanted might not be distinguishable in a limited data sample. Furthermore, it does not seem mathematically practical to implement the definitions without an assumed "model" for the form of the correlation function employed to summarize the data. Immediately, therefore, there arises the possibility that the wanted parameters (e.g., the mean drift velocity) depend upon the choice of model. Clearly they might, with an ill-advised choice. Finally, we may repeat that until a statistically rigorous form of correlation analysis became available (Fedor, 1967) it was not practical to deal objectively with doubts about the applicability of the principles.

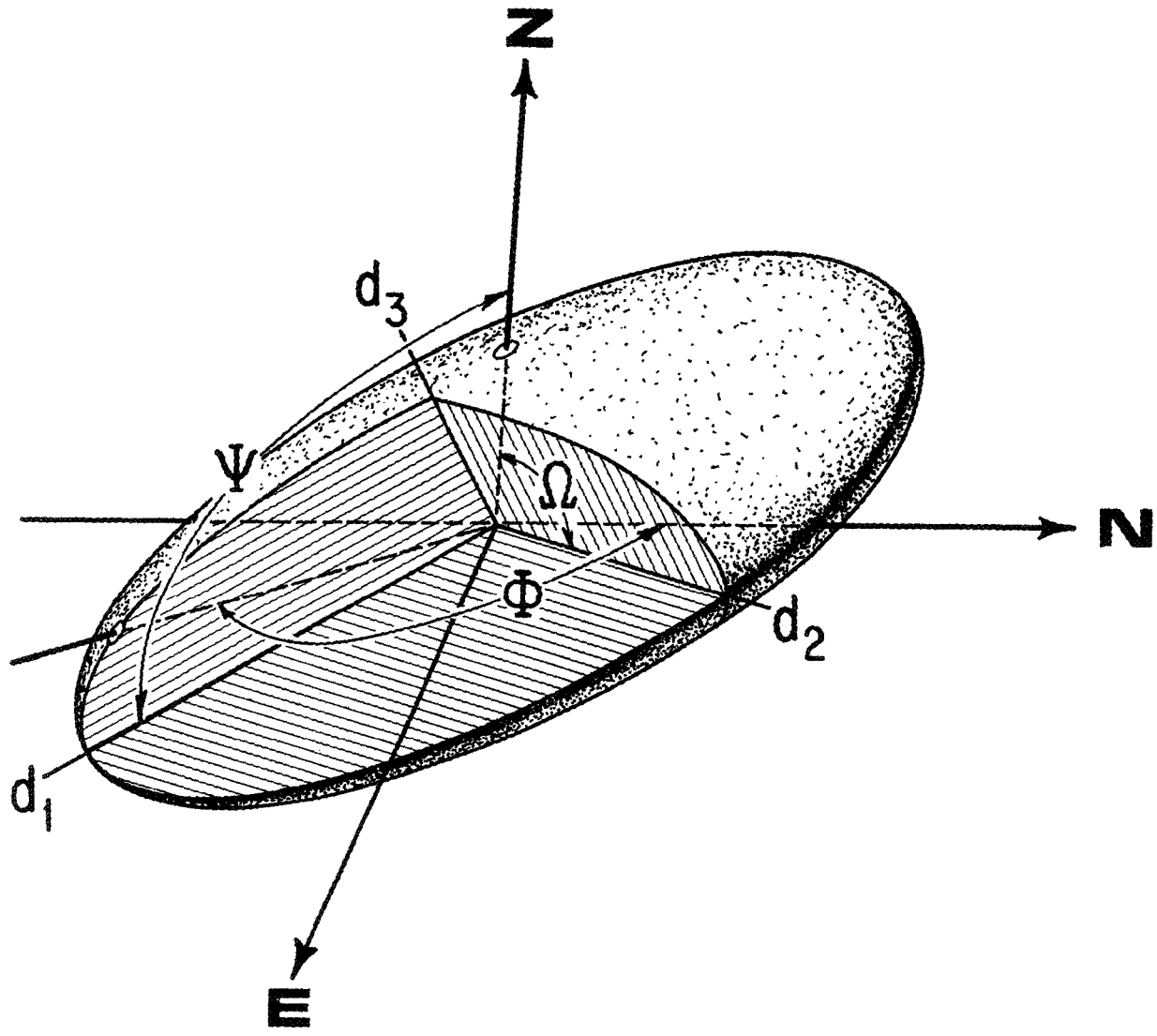

Fig. III-8. The spatial "correloid", illustrating its shape and orientation parameters. Correlation is assumed to vary radially from the center in a gaussian manner, and the size of the present figure is determined from the condition that the correlation be $\rho = e^{-\frac{1}{2}} = 0.61$ over its surface. The anisotropy of the irregularities is indicated by three independent axes (DI, DJ, DK in fig. III-6), and their mean spatial orientation is defined by the angles Φ, Ψ, Ω. The spatial correloid moves with mean velocity components VX, VY, VZ, and has a correlation lifetime (again where $\rho(\tau) = e^{-\frac{1}{2}}$ of B seconds.

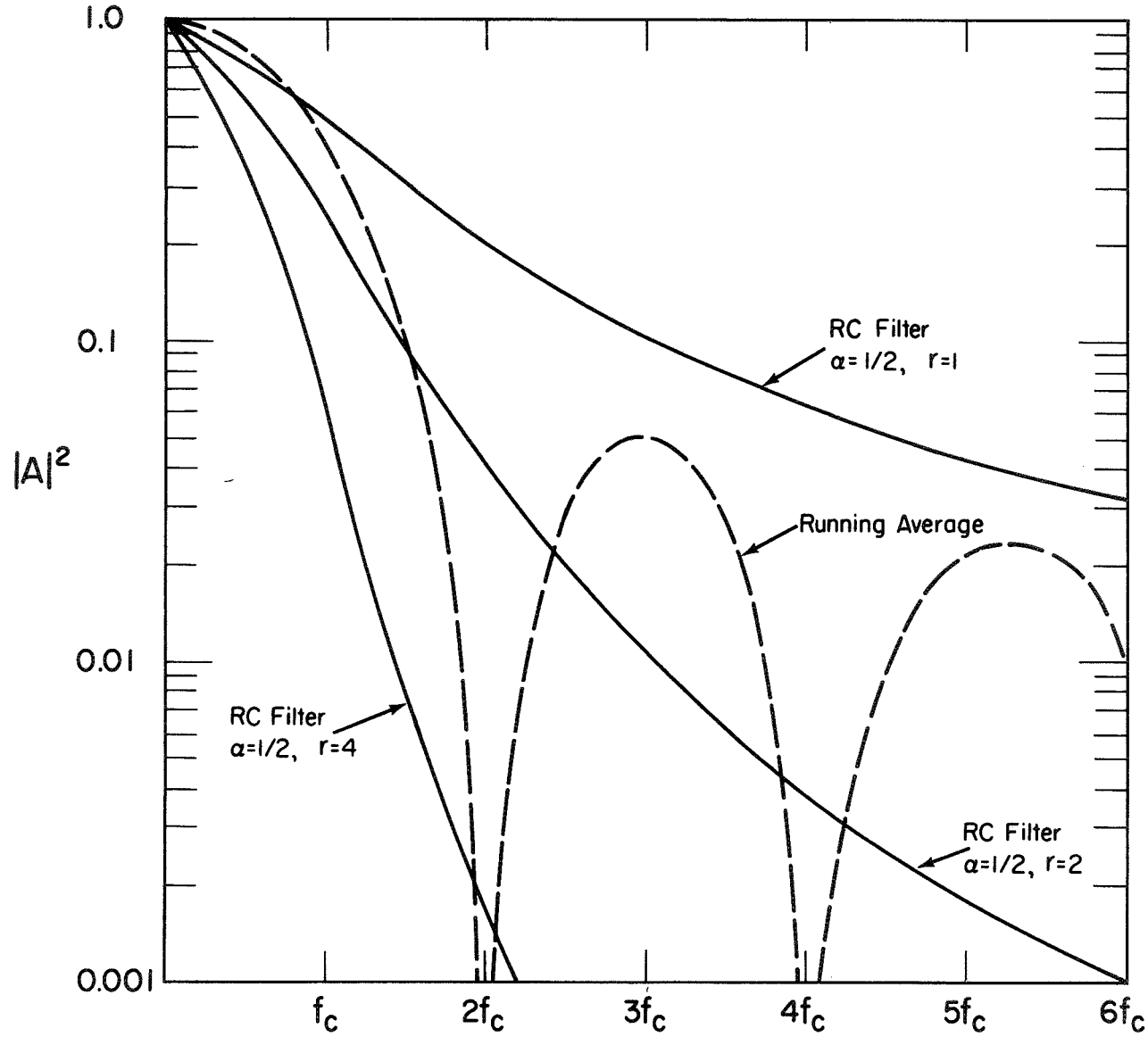

FILTER RESPONSE CURVES

Fig. III.9

We have therefore undertaken a study (Pitteway, Wright and Fedor, 1971) to test these questions. We constructed model records of complex amplitude at four spaced antennas by summing the scattering from a statistically large number of randomly-located irregularities moving at the same "height". In most cases, the scatterers were illuminated by a 'point source' transmitter located near the receiving array. Various kinds of random and steady motion were tested. For example, in some cases, the velocity of the scatterers varied randomly (and independently of one another) around a mean value during the sequence; in other cases, each irregularity maintained a constant velocity which bore a random relationship (again around a mean value) to the others. In still other cases, the random variations were introduced with respect to a 'mean' which changed linearly during the sequence. Such parameters as the ratio of mean to specular signal could could be varied.

The fading records synthesized in this manner were then subjected to the correloid analysis procedure described in the preceding section. Our principal conclusions are:

1) The expected 'point-source' effect is recovered in all cases by correlation analysis of the fading; the effect is not "lost" somehow, in the random motions or in the statistical errors of the analysis.

2) The mean velocity is found, in all cases, with good fidelity, even when it requires a rather special definition. Thus, for example, when the "mean" velocity increases from 50 - 90 m/s in one series of tests, correlation analysis deduced a value of 71 ± 20 m/s. This result is particularly applicable to interpreting real data, where it must be recognized that what is averaged in the mean depends entirely upon what is allowed to come into it: true stationarity does not exist in nature.

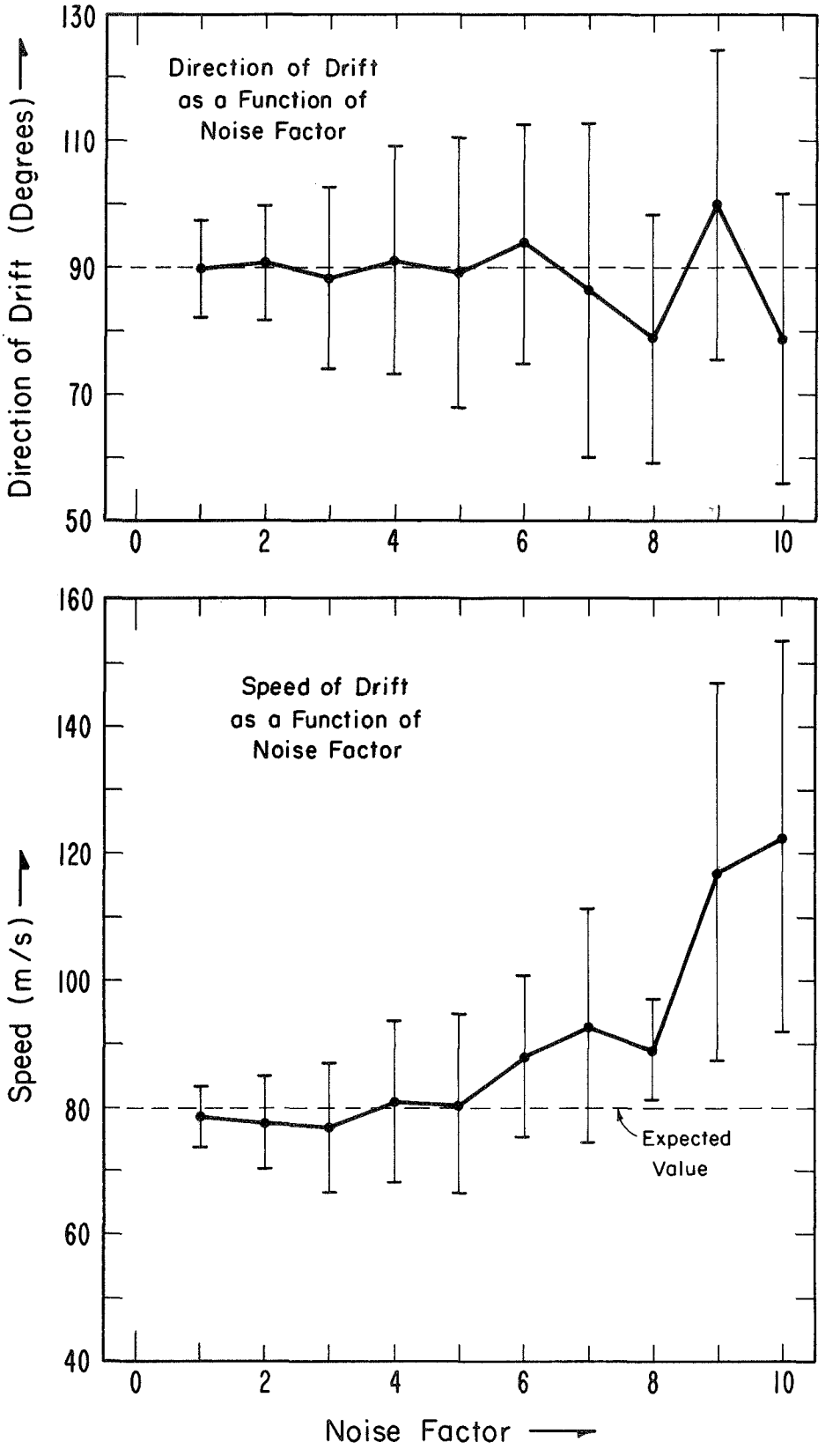

Fig. III-10.

B-84052

3) Realistic estimates of the confidence limits on the parameters found by Correloid Analysis, are obtained. There is a tendency, in some models, for the estimated velocity to increase above the true mean as the random component increases, but the confidence limits increase still more rapidly to include the true value (fig. III-10).

4) The estimated random velocity increased systematically with the "amount" of randomness introduced, but the relationship was different for different kinds of randomness. Thus, the analysis method is not likely by itself to define the nature of the randomness in the ionosphere, but it does provide a quantitative measure of it.

Appendix IV. Some Considerations Regarding Applicable Theory.

Although theoretical foundations exist for most aspects of this subject, no continuous treatment has yet been attempted for the entire problem. Several very unsatisfactory gaps persist, due in part to mathematical difficulties or to limited physical models. Nevertheless, the initiative lies, at present, with experiment to reveal agreement or disagreement with the available body of theory. The following table references the relevant theoretical work, in one plausible sequential order, and notes significant deficiencies, some of which are discussed more fully below.

Topic	Relevance	Major Difficulties	References
Radio Scattering	Makes density fluctuations detectable.	a) singularities near total reflection. b) anisotropies of irregularities and due to propagation	Pitteway (1958) (1960) Herlofson (1947) Booker, et al (1950)
Diffraction	Modifies and conveys fluctuation information to the observer.	a) results exist mainly for limiting cases of induced phase fluctuations and irregularity scales. b) continuous waves (not pulses) usually treated.	Ratcliffe (1956) Salpeter (1966) Orhaug (1965) Mercier (1962)
Analysis of Observations	Provides quantitative parameters.	a) appropriateness of parameter definition. b) allowance for effects of antenna coupling. c) 3-dimensional analysis of complex amplitude.	Briggs, et al (1950) Fedor (1967)
Ionospheric Irregularity Motions	Guides interpretation of results.	a) identification of irregularities as waves or other density fluctuations. b) identification of motions as winds, waves, or combination. c) identification of the medium measured: plasma alone, neutral atmosphere alone, or combination. d) description of plasma and ionized-irregularity flow in medium with electric, magnetic, wind, and turbulent fields.	Dougherty (1960) Kato et al (1970) Hines (1964)

Radio Scattering: The principal problem is to describe adequately the way in which the illuminating radio wave interacts with spatial fluctuations of electron density to produce fluctuations in the echo. Since in these experiments the ionosphere is always examined remotely (typically at a distance of 1000 radio wavelengths), diffraction effects are always important; many authors ignore the scattering problem altogether, suggesting that the scattered field may be simply described near the ionosphere, for example by its angular power spectrum or by its Fourier transform, the spatial autocorrelation function. In fact, many authors suggest that the spatial autocorrelation of phase within the field near the ionosphere should be identical to the spatial autocorrelation of the electron density fluctuations. The subsequent diffraction calculation can operate upon this description of the field at the ionosphere to describe the result at the ground, and it is true that the scattering process need not be considered in detail simply to set up instructive diffraction problems. However, what one obtains from a diffraction calculation depends upon what is put into it. Despite the fact that all conceivable scattering mechanisms might lead to a smaller number of field descriptions near the ionosphere, the problem remains to perceive the features essential to the actual scattering process.

Some insight concerning the unsatisfactory state of the theory is perhaps given by the following simple ray-theory argument.

The scattered power is considered to be proportional to the mean-square fluctuation of dielectric constant,

$$P_S \approx \overline{\left(\frac{\Delta \epsilon}{\epsilon}\right)^2}$$

In the ionosphere, neglecting the geomagnetic field and collisions,

$$\epsilon = \mu^2 = 1 - \frac{\omega_o^2}{\omega^2}$$

where ω is the radio frequency and $\omega_o = \sqrt{\frac{Ne^2}{m\epsilon_o}}$ is the plasma frequency dependent upon electron density N. Thus,

$$\overline{\left(\frac{\Delta\epsilon}{\epsilon}\right)^2} = \overline{\left(\frac{\Delta N}{N}\right)^2} \left(\frac{\omega\omega_o^2}{\omega_o^2 - \omega^2}\right)^2$$

This suggests that electron density fluctuations located near the total reflection level, where $\omega_o \rightarrow \omega$, are much more heavily "weighted", more effective in scattering the incident wave, than those located elsewhere. While it must be acknowledged that this argument fails at and near the 'singularity' $\omega_o \rightarrow \omega$, it probably indicates in more than a simply qualitative way, how the scattering varies with proximity to the total reflection level.

We may go further, and relate the scattered power to the angle of incidence on the layer, for simple reasoning shows that the wave does not reach the singularity except at normal incidence. By Snell's law, a wave incident at an angle θ to the vertical (assuming a plane parallel-stratified ionosphere) becomes horizontal (i.e., is 'reflected' at) a plasma frequency level where $\omega_0 = \omega \cos\theta$, as illustrated in the adjacent sketch. Combining this relationship between ω_0, ω, and θ, with the result above, we obtain an expression for the dependence of scattered power on angle of incidence,

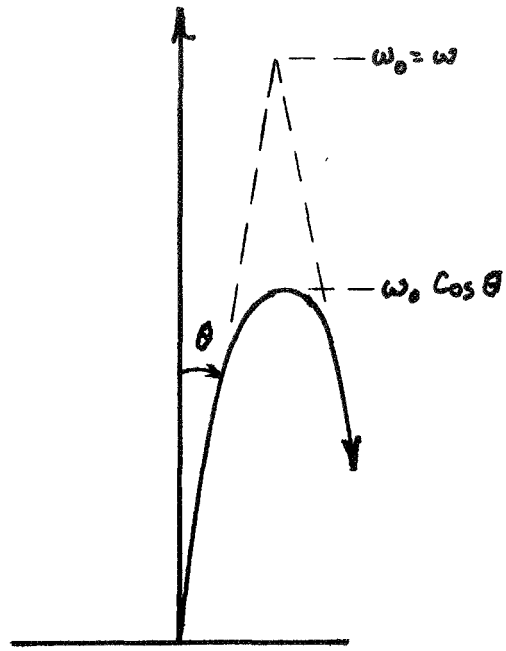

$$P_s \approx \left(\overline{\frac{\Delta\varepsilon}{\varepsilon}}\right)^2 \approx \left(\overline{\frac{\Delta N}{N}}\right)^2 \cot^4\theta.$$

For a given magnitude of fluctuation $\frac{\Delta N}{N}$, therefore, the scattered power due to the wave from a point source should be a very rapid function of distance from the "overhead" location. As shown by the adjacent graph, based upon the above expression, the scattered power varies by 40 db over the outer 90% of the 1st Fresnel zone, assuming a constant value for $\frac{\Delta N}{N}$. Alternatively, if a spectrum of fluctuations $\frac{\Delta N}{N}$ exists, we might expect that even very weak irregularities, (small compared with the 1st Fresnel zone radius (=3.3 km for 1 MHz at 100 km)) could be more effective than much stronger fluctuations beyond.

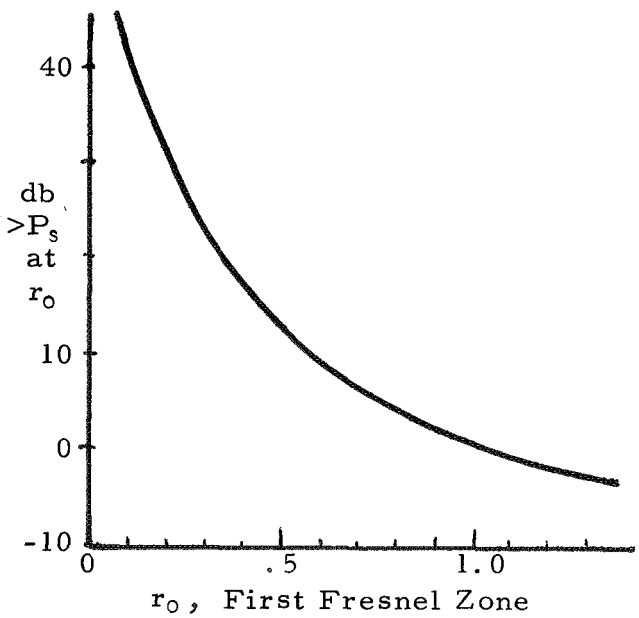

Diffraction: Typically, the diffraction solution describes the relationship to be expected between the phase fluctuations (magnitude $\Delta\varphi$, scale D) attributable to electron density fluctuations (magnitude ΔN, scale d), and the amplitude and phase fluctuations measured at the ground. In our experiment, amplitude (A) and phase (φ) are each measured, and our "Correloid Analysis" separates the mean drift of the diffraction pattern from its random fluctuation, giving also the spatial scales (D) of amplitude and phase in the pattern. In addition, the "scintillation index"

$$S = \sqrt{\frac{\overline{A^4} - \overline{(A^2)}^2}{\overline{(A^2)}^2}}$$

and the variance of the phase,

$$\varphi_o^2 = \overline{(\varphi - \overline{\varphi})^2}$$

may be calculated directly from the Kinesonde observations of A and φ. However, two precautions are necessary, particularly with regard to φ, for the recordings take no measure of the number of phase rotations occurring during the observing interval, but only of the instantanious fractional part of each rotation. By noting the signs of successive phase differences in the recordings, it is possible to reconstruct the number of full rotations occurring during the recording; this has been done in the examples shown in figures 7 and III - 2. Now what diffraction theory relates are the magnitudes of S, $\Delta\varphi$, φ_o, D, d, and distance from the ionosphere (h). If we are to make use of φ_o we must be certain to include in it all of the relevant variations of φ but none of the irrelevant variation as, for example, a doppler shift due to vertical motion of the entire ionosphere, or a phase-path change due to large-scale changes of electron content. The problem is to decide what is relevant: very slow variations of φ, of large magnitude, may be

associated with the smaller-scale fluctuations of amplitude, but the internal evidence alone, in a single example, cannot prove it. A statistical answer will be attempted from the present experiments, to identify which part of the observed phase variation leads on the average to the best adherence to the relationships predicted by diffraction theory.

Analysis of Observations: The procedures we have developed to treat Kinesonde data seem adequate to serve most of the questions presently seen. Although the principal process, Correloid Analysis, is based upon an assumed model for the form of the space-time correlation function, the measurements heavily over-determine the solution, and measures are thereby obtained of the extent to which the observations fit the model. A histogram of the "Root Mean Square Residuals" from 362 independent E-region calculations plus 49 F-region calculations performed to date on Kinesonde recordings made in France, is shown below.

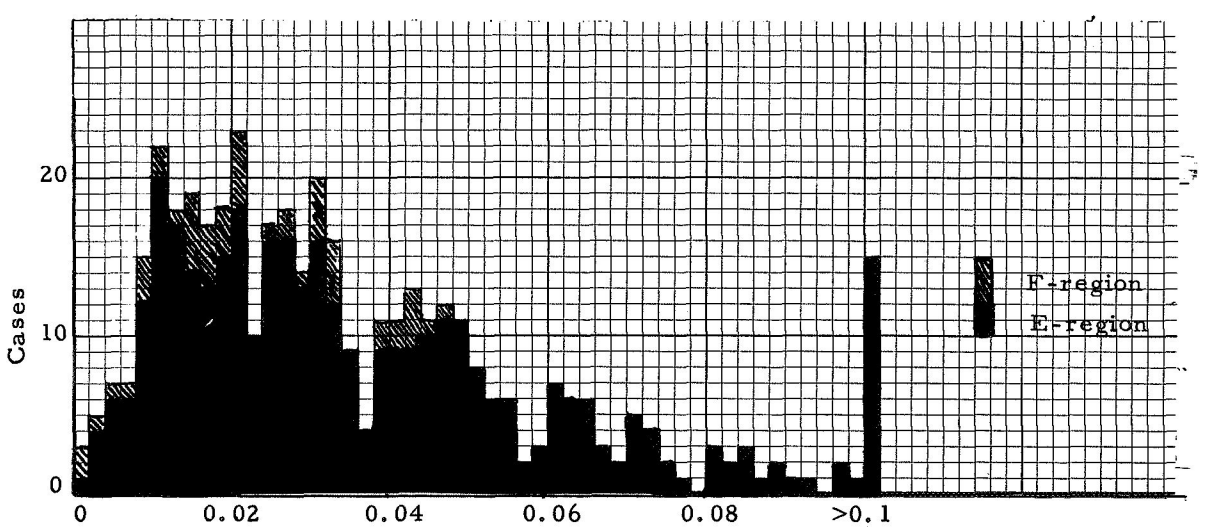

The median RMSR is about 0.03. Examination of the other parameters found during the calculations suggested that the calculated error of velocity, for example, is less than 10% when the RMSR is less than 0.03. The RMSR values larger than about 0.04 are associated with cases of poorly-determined correlations (i.e., when the amplitude fluctuations are slow or shallow), when the correlations are inconsistent, or when the form of the correlation curves is obviously "non-gaussian". The latter situation is most clearly indicative of an unappropriate model; it occurs in less than 1/3 of the E-region cases, and in perhaps half of the F-region calculations.

In an alternative or extension to Correloid Analysis we may examine the phase velocities of the spectral components of the fading separately. This procedure is clearly indicated when periodicities appear in the fading, its spectrum or its correlation function, and may lead to additional parameters when the "phase velocity" varies strongly with frequency.

Ionospheric Irregularity Model: Throughout the main part of the ionosphere (below the F-region peak) the ionization is never as much as 0.1% of the neutral density. This suggests that the principal dynamic processes of the ionosphere have their origin in the dynamics of the neutral air, and it would be observationally convenient if the weak ionization fluctuations by which the Kinesonde measures motions were simply convected by the neutral air motions: This corresponds to invoking "Taylor's Hypothesis" to justify using the ionization fluctuations as tracers. This may yet be justified, at least for the lower altitudes, but there are numerous reasons for not counting on it throughout most of the ionosphere. These reasons are of two basic types: those arising from electrical polarization of the medium (due to differing ion-electron drag against the neutrals in the geomagnetic field), and those arising from the possibility that the "irregularities" are actually associated with atmospheric wave motions so that the

observed velocities are phase velocities rather than those of mass-transport. Neither type of problem has yet a thorough theoretical description, and the possibility that they might occur in combination has received only preliminary treatment. The most comprehensive study of the pecularities of ionized irregularity motion (Dougherty, 1960) is at the same time a treatment most clearly in a form appropriate to interpretation of the Kinesonde experiment. Unfortunately, it concludes that there can be no conclusions, above about 90 km, except that even the motion of "convected turbulence" should uncouple from the neutral air motion in and above the dynamo region. In the upper E and the F regions, the problem becomes dependent upon the processes producing the density fluctuations, which leads to the consideration of atmospheric waves as one plausible source. This has recently been done by Kato, et al. (1970); they reach the significant conclusion that the plasma density irregularity may move with the neutral irregularity under rather general conditions.

The problems are clearly at a stage where theory demands some guidance from experiment -- in fact, they have been there for many years. The critical experimental input to the problems is a series of comparative measurements between the Kinesonde technique and independent measurements of neutral winds and ion drifts; it is additionally required that the measurements extend over a substantial range of altitudes (and that the altitudes be accurately known). These experimental objectives correspond exactly with those of the collaborative measurements made by the Kinesonde, Meteor Radar, and Thomson Scatter systems in France during 1970.

Appendix V. Preliminary List of Addresses of Workers in D and E Region Winds in Europe.

Prof. J. E. Blamont	Institut d'Aeronomie Observatoire de Paris Meudon, S. et O., FRANCE
Prof. W. J. G. Beynon	Department of Physics University of Wales Penglais Aberystwyth/Wales, UNITED KINGDOM
Dr. G. Y. Groves	University College of London Cower Street London W. C. 1, ENGLAND
E. Harnischmacher	Ionosphärenstation Rheintorplatz 2 7814 Breisach, FED. REP. of GERMANY
Dr. A. Haubert	Centre d'Etudes Geophysiques Garchy (Nievre), FRANCE
Prof. A. N. Hunter	Dept. of Environmental Sciences University of Lancaster St. Leonardgate Lancaster, ENGLAND
Dr. A. I. Ivanovsky'	Central Aerological Observatory Hydrometeorological Service of the USSR Ul. Pavlika Morosova 12 Moscow D-376, USSR
Prof. C. de Jager	Laboratorium voor Ruimteonderzoak Huizingalaan 121 Utrecht, NETHERLANDS
Prof. T. R. Kaiser	Department of Physics University of Sheffield Sheffield, ENGLAND
Dr. L. A. Katassav	Institute for Experimental Meteorology Hydrometeorological Service of the USSR Obninsk, Region Kaluga, USSR
Dr. J. V. Kushnerevsky	Institut IZMIRAN Akademgorodok, Region Moscow, USSR

Dr. J. A. Lyssenko	Institute for Experimental Meteorology Hysrometreorogical Service of the USSR Obninsk, Region Kaluga, USSR
Prof. S. F. Mirkotan	Department of Physics Moscow State University Moscow, USSR
Dr. H. G. Müller	Department of Physics University of Sheffield Sheffield, ENGLAND
Dr. R. J. Murgatroyd	Meteorological Office London Road Brackness/Berkshire, UNITED KINGDOM
Dr. J. K. Olesen	Ionospheric Laboratory Technical University of Denmark 2800 Lyngby, DENMARK
Dr. W. R. Piggott	Radio and Space Research Station Ditton Park Slough/Bucks, ENGLAND
Prof. Dr. K. Rawer	Ionosphärenstation Reintorplatz 2 7814 Breisach FED. REP. of GERMANY
Dr. R. Schminder	Geophysikalisches Observatorium Collm DDR 7261 Collmberg, GERMAN DEMOCRATIC REPUBLIC
Dr. A. Spizzichino	C.N.E.T. / R.S.R. 3, Avenue de la Republique 92 Issy-les-Moulineaux, FRANCE


Paris
Nançay
Bierre-lés-Semur
Sens Beaujeu
St. Santin